UNIVERSITÀ DEGLI STUDI DI PALERMO

Information And Communication Technologies
ING-INF/03-Telecomunicazioni
Dipartimento di Ingegneria

Indoor Localization Systems with Bluetooth and Light: Design and Implementation

Ph.D. Candidate
JAGDEEP SINGH

Coordinator
Prof. Ilenia Tinnirello

Supervisor
Dr. Tim Farnham
Bristol Research & Innovation Laboratory,
Toshiba Europe Ltd., UK

Co-Supervisor
Dr. Qing Wang
Delft University of Technology,
Netherlands

XXXIV CYCLE - ACADEMIC YEAR 2020-2023

ABSTRACT

With the advent of creating intelligent indoor spaces across diverse domains such as domestic, retail, industries, and healthcare, there has been an intensified demand for advanced indoor localization systems, especially with the integration of autonomous machinery and robots into daily life. This thesis aims to surpass the limitations of current RF- and Optical-based localization systems by developing more accurate, reliable, energy-efficient, and cost-effective indoor localization systems. These systems are envisioned for services like navigation in autonomous vehicles and asset tracking in industrial settings. The thesis categorizes localization systems into two types: autonomous systems for entities like warehouse robots, and tracking systems for monitoring indoor assets.

Initially, the thesis introduces a Bluetooth Low Energy (BLE)-based autonomous localization system, `BLoB`. This system employs synchronous transmissions for enhanced reliability and energy efficiency, achieving sub-meter-level accuracy with single-antenna BLE devices. `BLoB` capitalizes on a unique beating effect observed in synchronous transmissions, characterized by a sinusoidal pattern of constructive and destructive interference. Utilizing the constant tone extension feature of the BLE 5.1 standard, `BLoB` enables multiple anchors to transmit synchronously, with mobile tags capturing the resulting signal. The identification of peaks in this superimposed signal, combined with signal strength data, empowers `BLoB` to attain sub-meter accuracy in positioning. The efficacy of `BLoB` is validated in various settings, including offices and sports halls, proving its robustness in challenging indoor scenarios.

To further refine BLE localization to centimeter or decimeter levels, the thesis proposes the integration of BLE with precise optical-based localization methods. It introduces `BLELight`, a hybrid autonomous localization system that merges the capabilities of BLE and Visible Light Positioning (VLP) technology through neural network-driven data fusion. The deep neural network model, trained through an incremental learning approach, showcases a substantial improvement in localization accuracy, achieving decimeter-level accuracy.

However, prior to developing this hybrid solution with VLP, the thesis presents an innovative VLP system named HueSense. The system utilizes existing LED lighting infrastructure as transmitters for location beacons. This innovative system requires no modifications to installed LEDs, instead analyzing their intrinsic characteristics for differentiation and location mapping. HueSense employs low-power, off-the-shelf hue sensors to realize this functionality. A prototype using three hue sensors, tested under different lighting environments, demonstrates the system's practicality and accuracy, either as a *standalone* solution or in enhancing BLE-based localization. `BLELight`, by integrating features of both `BLoB` and HueSense, evolves into a comprehensive hybrid autonomous localization system. This system adeptly tackles real-

world challenges such as interference from external ambient light, physical obstructions, and shadows, issues that typically limit VLP efficacy, while also addressing the inherent accuracy constraints of BLE technology.

Further, the thesis explores a tracking system that leverages the new direction-finding techniques of the BLE 5.1 standard, augmented with mmWave radar measurements. This integration, trained jointly in a deep neural network model, addresses the inherent accuracy limitations of BLE. Two variations, BmmW-LITE and BmmW-LITE+, are evaluated. These systems are optimized for single-antenna BLE devices, eliminating the need for bulky multi-antenna arrays and presenting a more compact, cost-effective solution for IoT devices. BmmW-LITE+ extends BmmW-LITE by incorporating semantic capabilities at the edge device, facilitating data transfer from the edge to the cloud, and optimizing bandwidth, power, and memory usage. All systems, tested experimentally, demonstrate decimeter-level localization accuracy and can be easily incorporated into solutions for deployment in real-world indoor environments.

Dedicated to my beloved family and my friends.

ACKNOWLEDGEMENTS

In crafting this acknowledgment, I am reminded of the countless individuals who have illuminated my path toward completing this doctoral journey. Their collective wisdom, support, and inspiration have been the wind beneath my wings, propelling me forward even during the most challenging times.

To Usman Raza, my first supervisor, I owe a profound debt of gratitude for welcoming me into this grand academic and industry endeavor. His guidance, especially in the early, uncertain days marked by the global upheaval of COVID-19, was a guiding star. Usman's insights on the power of presentation have indelibly shaped my approach to academic and professional communication.

Tim Farnham, my supervisor, warrants special thanks for his boundless encouragement and for fostering an environment where my ideas could thrive. His support was a constant beacon of strength and joy.

I am equally indebted to my co-supervisor, Qing Wang, whose assistance has been pivotal to the success of my PhD endeavors. Qing's unwavering support and guidance, coupled with his motivational presence, have inspired me to aim for excellence. His mentorship has been a guiding light throughout this journey. Qing is consistently accessible to me, regardless of the time.

A special note of thanks is extended to Carlo Alberto, from whom I have learned invaluable lessons during my Ph.D. Carlo taught me the complexities of making compelling papers—how to approach them from multiple perspectives, structure the content effectively, and articulate the research problem and solution with clarity and precision. These teachings have been indispensable.

Both Qing and Carlo have been instrumental in securing numerous best paper awards, a testament to their guidance and expertise. This achievement is also a reflection of the significant contributions of all my co-authors. They deserve acknowledgment for their collaborative spirit and significant contributions to our shared work.

My gratitude also extends to Michael Baddley, whose sustained support, especially regarding my work on Bluetooth, culminated in our winning the best paper award—a milestone that I cherish deeply.

Marco Zuniga's mentorship deserves a heartfelt acknowledgment. I have always admired his problem-solving approach and his knack for simplifying complex issues, focusing on what truly matters. The guidance and support from him, Keyarash Ghiasi, and Miguel Chavez during my tenure at TU Delft have been invaluable.

I express my sincere gratitude towards Aleksandar Stanoev, Danielle Puccinelli, and Justin Coon for their guidance and support. Their contributions have immeasurably enriched my doctoral journey.

Special thanks go to my PhD coordinator, Dr. Ilenia Tinnirello, whose support has been instrumental in my journey.

To my friends Arun and Marius, who helped and supported me throughout my PhD, and to ChatGPT and Peizheng Li, whose timely assistance expedited my research, I am profoundly thankful. Peizheng's consistent, patient collaboration and 'let's get it done' attitude were especially commendable.

Acknowledgment is also due to my friends at Toshiba—Marcello Bullo, Adrian—and all BRIL members, administrative staff, and specifically Ruth Wallace, Yichao, Aftab, Magnus, Mahesh, Kohei, and James for their ever-present help and support.

To my friends from India—Varun, Anjali, Vishal x 2, Priyanshu, Harsh, Rohit, Amogh, Anubha, and many more—your unwavering support and cheerful video calls have been a source of happiness and motivation throughout this journey.

I am grateful for the financial assistance provided by ENLIGHT'EM, under the Marie Skłodowska Curie grant agreement No. 814215. The project's efforts in organizing meetings and training schools, along with the coordinators Domenico Giustiniano and Borja Genoves Guzman, have been crucial in providing support and feedback. My sincere appreciation extends to my fellow Early Stage Researchers within the ENLIGHT'EM project for their solidarity and the enriching exchanges we shared. Special mention goes to Omer Dalgic, whose support and the joyous moments we spent together remain unforgettable.

Lastly, my deepest and most heartfelt gratitude is reserved for my family. Their endless love, support, and encouragement have been the foundation of my journey. Words fall short of expressing the depth of my thanks to them, for they have been my unwavering pillar of strength.

Funding

This work was supported by the European Union's Horizon 2020 Marie Skłodowska-Curie grant (Grant Number: 814215).

Team members and collaborators

- **Supervisors**
  - Dr Tim Farnham (Toshiba Europe Limited, BRIL, UK)
  - Dr Qing Wang (Delft University of Technology, The Netherlands)
- **PhD Coordinator**
  - Prof Ilenia Tinnirello
- **Technical Support**
  - Dr. Carlo Alberto Boano (Institute of Technical Informatics of Graz, University of Technology (TU Graz), Austria)
  - Dr. Michael Baddeley (Technology Innovation Institute, Abu Dhabi, United Arab Emirates)
  - Dr. Usman Raza (Waymap Ltd., UK)
  - Dr. Marco Zuniga (Delft University of Technology, The Netherlands)
  - Aleksandar Stanoev (Nordic Semiconductor UK (Bristol))
  - Prof Daniele Puccinelli (University of Applied Sciences and Arts of Southern Switzerland (SUPSI))
  - Prof Justin Coon (Department of Engineering Science, University of Oxford, UK)
- **External Reviewers**
  - Prof. Wasiu O Popoola (The University of Edinburgh, UK)
  - Prof. Petri Mähönen (Aalto University, Finland)

- **Examiners**
  - Prof. Andrew Markham (University of Oxford, UK)
  - Prof. Domenico Giustiniano (IMDEA Networks Institute, Madrid, Spain)
  - Prof. FIlippo D'Ippolito (Università degli Studi di Palermo, Italy)

Institutions

- **BRIL** Bristol Research and Innovation Laboratory, Toshiba Research Europe Ltd., Bristol, UK
- **TU Delft** Embedded Systems Group, Faculty of Electrical Engineering, Mathematics, and Computer Science (EEMCS), Delft University of Technology, The Netherlands
- **SUPSI** Innovative Technologies Department, University of Applied Sciences and Arts of Southern Switzerland

AUTHOR'S DECLARATION

I declare that the work in this dissertation was carried out in accordance with the requirements of the University's Regulations and Code of Practice for Research Degree Programmes and that it has not been submitted for any other academic award. Except where indicated by specific reference in the text, the work is the candidate's own work. Work done in collaboration with, or with the assistance of, others, is indicated as such. Any views expressed in the dissertation are those of the author.

SIGNED: Jagdeep Singh DATE: 14/03/2024

TABLE OF CONTENTS

LIST OF TABLES

LIST OF FIGURES

ACRONYMS

***p*-VLP** . . . . passive-VLP. 10–13, 22, 23, 57–60, 63–68, 83–85, 87, 90–93

AGV . . . . Automated Guided Vehicle. 1, 8, 17–20, 22, 65–68, 127

AMR . . . . Automated Mobile Robot. 1, 8, 17, 20, 127

AoA . . . . Angle Of Arrival. 6–8, 27, 30, 31, 41, 47, 55, 56, 95, 97, 98, 102–105, 109, 110, 113, 125, 128, 130

AoD . . . . Angle Of Departure. 6–8, 27, 41, 55, 95, 103, 104, 128

AR/VR . . . . Augmented/Virtual Reality. 2

B . . . . Blue. 71, 73

BLE . . . . Bluetooth Low Energy. 5–8, 12–15, 17–23, 27, 30–32, 49, 54, 56, 68, 84–93, 95–98, 100–104, 108–115, 118–121, 123–125, 127–132, 134

CDF . . . . Cumulative Distribution Function. xxi, 39, 48, 91, 117, 118, 120

CFO . . . . Carrier Frequency Offset. 29–31, 33, 36, 37, 41–43

CNN . . . . Convolutional Neural Network. 108, 123

CRC . . . . Cyclic Redundancy Check. 43–46

CSI . . . . Channel State Information. 123

CTE . . . . Constant Tone Extension. 6, 28, 30–32, 40, 41, 52, 102, 104, 105, 110, 120, 128, 132

DNN . . . . Deep Neural Network. 22, 86–88, 92, 93, 96, 97, 102, 103, 122, 125, 129, 130

FCN . . . . Fully Connected Network. 108, 109, 111

FFT . . . . Fast Fourier Transform. 34, 36, 54, 105, 107

FL . . . . Fluorescent Lights. 57, 59, 83

FMCW . . . . Frequency Modulated Continuous Wave. 99, 105

FOV . . . . Field Of View. 61, 72, 75, 79, 81, 83

G . . . . Green. 71, 73

GPS . . . . Global Positioning System. 3, 4

I/Q . . . . inphase/quadrature. 30, 41, 45, 54, 97, 102–105, 108–110, 112–115, 125

ID . . . . IDentification. 65–67, 69, 72, 75, 82, 83, 110

IL . . . . Incremental Learning. 87, 88, 92

IMU . . . . inertial measurements unit. 101, 133

IoT . . . . Internet of Things. 1, 2, 5, 9, 12, 15, 16, 19, 68, 69, 72, 73, 84, 96, 101, 123, 128, 132

IR . . . . Infrared. 9, 10

JSAC . . . . Joint Sensing And Communication. 2, 123, 124, 131, 132

LCD . . . . Liquid Crystal Display. 61, 62

LED . . . . Light Emitting Diode. 9–11, 17, 21, 57, 59, 61, 62, 64, 67, 69–84, 89, 90, 93, 128, 132

LiDAR . . . . Light Detection and Ranging. 9

LoS . . . . Line Of Sight. 3, 73

MAE . . . . Mean Absolute Error. 108

MIMO . . . . Multiple Input Multiple Output. 96, 99, 123

ML . . . . Machine Learning. 96, 101

MLE . . . . Mean Localization Error. xxi, 92, 93, 113, 117

mmWave . . . . millimeter wave. 13–15, 18, 19, 22, 23, 95–100, 102, 103, 105–108, 110–115, 118–120, 123, 125, 127, 130, 132

MUSIC . . . . MUltiple SIgnal Classification. 102, 104

NN . . . . Neural Network. 13, 14, 86, 89, 96, 98–100, 105, 106, 108, 109, 111–113, 115, 121, 123–125, 133, 134

PD . . . . PhotoDiode. 9, 11, 57–60, 62, 67–69, 83

R . . . . Red. 71–73

RAN . . . . Radio Access Networks. 123, 132

RF . . . . Radio Frequency. 5, 7, 8, 18, 19, 21, 27, 28, 30, 60, 68, 84, 86, 87, 96, 99, 100, 106, 129

RSS . . . . Received Signal Strength. 4–6, 8, 18, 20, 27, 31, 35, 38, 40, 49, 52, 53, 55, 56, 60, 75, 87, 90, 99, 114, 128

S1 . . . . Sensor 1. 73

S2 . . . . Sensor 2. 73, 75, 76

S3 . . . . Sensor 3. 73, 76

SELU . . . . Scaled Exponential Linear Unit. 89, 111

SemCom . . . . Semantic Communications. 101

SLAM . . . . Simultaneous Localization and Mapping. 9

SOTA . . . . state-of-the-art. 8, 10, 12, 14, 21, 23, 41, 47, 50, 56, 57, 85, 92, 93, 98, 124

ST . . . . Synchronous Transmission. 28, 31–34, 37, 40, 41, 52, 55

TI . . . . Texas Instrument. 99, 105, 110

ToF . . . . Time-Of-Flight. 7, 9

UWB . . . . Ultra-Wideband. 8, 100, 101, 123, 124

VAE . . . . Variational Autoencoder. 103, 108, 109, 111, 119, 120, 124

VLC . . . . Visible Light Communication. 69, 85, 92, 93, 127, 129

VLP . . . . Visible Light Positioning. 9–15, 18, 19, 22, 23, 57–59, 63, 67–71, 83–87, 89, 91, 129

Wi-Fi . . . . Wireless Fidelity. 100, 101, 122, 123

CHAPTER 1

INTRODUCTION

Advancements in the Internet of Things (IoT) are rapidly shaping the smart, digital world around us. An array of sensors and actuators are increasingly becoming an integral part of our daily environments, including homes, retail spaces, factories, and offices [6, 7, 8, 9]. This integration is not only about seamless connectivity but also extends to the incorporation of robots into our daily routines, performing a variety of tasks in diverse settings and significantly enhancing our day-to-day experiences and efficiency. A critical aspect of this integration, especially for Automated Guided Vehicles (AGVs) or Automated Mobile Robots (AMRs), is the necessity of precise location awareness [10, 11, 12, 13]. Moreover, pinpointing their exact location with high accuracy is paramount. In this context, understanding the tasks that require accurate localization versus relative positioning is crucial. For example, navigation and route planning optimization in AGVs demand exact localization for efficient movement and obstacle avoidance [10]. Similarly, accurate localization is vital for asset tracking and stock control, where AGVs need to precisely locate and manage inventory [14]. Conversely, tasks like manipulation rely more on relative positioning, focusing on the AGVs' position in relation to the object it interacts with [15]. The need for precise localization is also evident in applications like geofencing and zone occupancy detection, where AGVs must adhere to specific operational zones to avoid conflicts or congestion [16, 17].

1.1 Motivation

Indoor localization plays a pivotal role in the development of smart indoor environments, with applications ranging from warehouse automation to healthcare. Examples include:

- Within the autonomous sector, these systems are of paramount importance for a wide array of applications, for example, warehouse automation, security, manufacturing and logistics, and Augmented/Virtual Reality (AR/VR), to name a few; significantly enhancing the functionality and efficiency of various technologies within indoor settings [6, 13].

- In industrial settings, such as smart warehouses and workspaces, indoor localization systems prove instrumental in facilitating autonomous robot navigation and asset tracking. By precisely pinpointing the location of valuable resources and devices, organizations can efficiently manage and monitor their operations, leading to increased productivity and reduced operating costs [12, 18].

- Beyond their applications in industrial settings, indoor localization systems hold significant implications for healthcare and assisted living. The ability to accurately track the indoor location of individuals empowers these systems to provide targeted services that greatly improve the quality of life for elderly and vulnerable populations. Furthermore, emergency responders can leverage this technology to swiftly locate individuals in need of assistance, thereby enhancing overall safety and well-being [19, 20].

- In the research realm "Beyond 5G", the concept of Joint Sensing And Communication (JSAC) has been widely discussed [7], with the aim of providing high-quality wireless connectivity and seamless location awareness in both indoor and outdoor environments. The inclusion of these features in readily available IoT devices not only enhances indoor localization capabilities but also paves the way for a variety of location-aware applications. These applications have the potential to bring significant societal benefits, ranging from improving indoor navigation for the visually impaired to optimizing space utilization in crowded indoor areas [21, 22].

- In smart indoor environments, the integration of indoor localization systems fosters the seamless operation of interconnected devices and systems. Such interconnectedness creates intelligent indoor spaces that can dynamically adjust to occupants' needs and preferences, ultimately enhancing user experiences and overall comfort. Examples include personalized climate control in offices, interactive museum exhibits, optimized space management in co-working spaces, and real-time journey updates in public transport hubs [19, 23].

  Figure 1.1 provides a visual depiction of the indoor applications discussed above.

Despite decades of research efforts in developing indoor localization systems that are reliable, cost-effective, power-efficient, and accurate, the quest for a universally applicable solution,

Figure 1.1: Composite view & vision of indoor localization applications.

similar to the Global Positioning System (GPS) used outdoors, remains a challenge [24, 8, 25, 26]. Furthermore, the global Indoor Location Market, valued at $10.9 billion in 2023, is projected to grow about $29.8 billion by 2028, and $52.88 Billion by 2032 [27], experiencing a compound annual growth rate (CAGR) of 23% over the forecast period (according to a report by MarketsandMarkets Research [1]), signifying the increasing demand and potential impact of these technologies.

However, developing effective indoor localization systems poses notable complexities. This complexity arises from the absence of standardized approaches and the difficulty in ensuring compatibility and interoperability between systems. Each technology used for indoor tracking operates on its own unique frequency and communication protocol, each with its own set of limitations. Interestingly, what one technology lacks, another might compensate for. Integrating these diverse technologies into an indoor location solution, be it in industrial spaces or corporate environments, often requires significant updates to the existing infrastructure, including the installation of new servers/firmware and the integration of various systems. This process is further complicated by the intricate indoor location market ecosystem (please see Figure 1.2), which includes technology providers, software developers, and various service providers, all catering to different industries and applications [1, 2, 28].

While indoor localization systems have shown great potential, they face unique challenges not encountered in outdoor environments. The most widely used outdoor navigation system is GPS, which provides highly accurate location information anywhere on or near the Earth when there is an unobstructed Line Of Sight (LoS) to three or more GPS satellites. Global Navi-

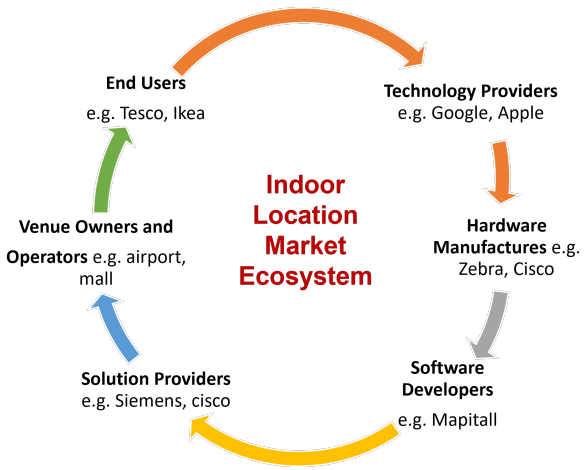

Figure 1.2: Indoor Location Market Ecosystem taken from [1].

gation Satellite System (GLONASS), Galileo, and Compass/BeiDou are other satellite-based systems that provide similar capabilities to GPS [29, 30]. These systems are used primarily for outdoor navigation, but they also have applications in transportation, surveying, and other fields. However, these technologies have limitations in indoor settings, due to the inability of satellite signals to pass through walls, building infrastructure, and other physical obstructions, which hinders their effectiveness indoors [31, 32]. The location information provided by these systems may be inaccurate or unreliable, making them less effective for indoor localization & navigation.

As an alternative, different technologies and methods for indoor localization have been developed. These technologies include Wi-Fi [33, 24, 34] Bluetooth [35, 25], ZigBee [36, 37], RFID [26, 38] and acoustic [39], which use different methods to determine the user's location, such as measuring Received Signal Strength (RSS), triangulating signals from multiple sources, or using proximity-based methods. These technologies can provide more accurate location information in indoor environments than satellite-based systems, but they have their limitations. These are typically susceptible to multipath fading, which limits the achievable ranging accuracy [40, 41].

The principal aim of this thesis is to enhance the precision of these systems and to engineer indoor localization solutions that are not only accurate, but also economically viable and energy-efficient, with cost-effective device implementation and minimal infrastructure and computational requirements.

1.2 BLE Localization

This research opts for Bluetooth Low Energy (BLE) as the primary Radio Frequency (RF) technology to develop indoor localization system, recognizing its role as a leading IoT solution in indoor localization, as highlighted in studies [1, 42]. The decision is reinforced by the widespread availability and cost-effectiveness of BLE hardware [28]. Furthermore, compared to Wi-Fi, BLE is characterized by lower complexity and energy consumption, as well as improved operational efficiency. These attributes make BLE an ideal choice for the development of cost-effective, and smaller-scale devices, thereby facilitating widespread deployment in indoor localization scenarios. The past few years have witnessed a substantial surge in the adoption of BLE tags for various applications. Despite the market contraction experienced during the COVID-19 pandemic, BLE technology has demonstrated robust growth, with annual shipments tripling, according to ABI Research's findings [28]. They also forecast that from 2023 to 2027, the number of shipments will increase by 2.46 times [2]. Please refer to Figure 1.3, for a comprehensive chart.

BLE operating in the low-power 2.4 GHz unlicensed band, initially emerged as a technology tailored for single-hop communication with a focus on low data rate applications, mainly in wearables and multimedia devices. However, the immense popularity of BLE, evidenced by the estimated sale of over 10 billion Bluetooth devices, has spurred interest in extending its use beyond these initial domains [1, 27]. Consequently, the Bluetooth 5.1 standard has introduced direction-finding capabilities into the BLE packet, marking a notable advancement [42]. BLE's versatility is evident in its wide range of applications, including tracking, ranging, data transfer, audio streaming, and location services.

Within the BLE market, location services, with a particular emphasis on indoor navigation, constitute a predominant share. Notably, these services account for 79% of the total Bluetooth location resources, exclusively utilized for indoor navigation purposes [28]. Use cases in location services vary from asset tracking to proximity solutions, but the dominant application remains indoor navigation. The emergence and development of BLE as a market standard in recent years underscore its relevance and potential in shaping the future landscape of indoor localization technologies.

1.2.1 Issues with BLE Localization

Since many years, there have been many BLE devices on the market acting as "low-power beacons", which allow coarse-grained localization of small, cheap, single-antenna tags and these beacon applications typically leverage the *RSS* of packets to estimate the distance between

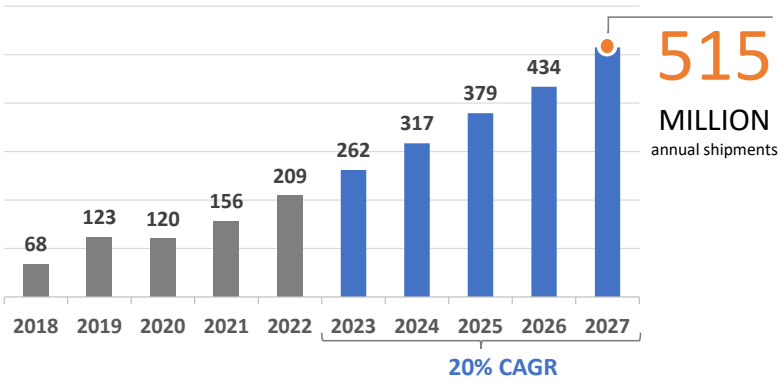

Figure 1.3: Annual Bluetooth location service device shipments (numbers in millions). Data taken from [2].

devices [43, 44, 45], with iBeacon (apple product) [46] and Eddystone (google product) [47] being prominent examples. Battery-operated beacons serve as the fundamental technology for BLE technology. The beacon technology operates by having a proximity-sensing beacon continuously send out a constant signal. When a receiver (e.g. a mobile phone with Bluetooth enabled) comes into its field of effect, the beacon detects the time taken for the broadcast signal to bounce back from the receiver. Using the time measurements, it calculates the distance from the beacon to the receiver to determine its location. Unfortunately, RSS-based localization approaches are known to be brittle and have limited accuracy ($\approx$ 1–2.5 meters), as the RSS can easily be affected by changing environmental conditions and human movements, even when carefully calibrating the reference signal strength [48, 49, 50, 51]. Moreover, the performance of RSS-based approaches is strongly affected by the number of employed anchors (the more, the better) and by their careful deployment, which increases costs [52, 53].

AoA-/AoD-based localization. To counter this, BLE 5.1 introduced direction-finding features that support two methods for determining the direction of a signal: Angle Of Arrival (AoA) and Angle Of Departure (AoD) [42, 54, 55]. These direction-finding features let BLE devices append a *constant tone extension* (CTE) to the transmitted packets, i.e., a sinusoidal waveform with constant amplitude and frequency, as well as continuous phase. A receiver can sample the constant tone and process the in-phase and quadrature-phase (I/Q) components of the received signal, which is then further processed to perform the AoA/AoD localization [42, 4]. Whilst these techniques allow one to achieve a *sub-meter* localization accuracy by leveraging angular information [56, 57], they require the use of bulky *antenna arrays*. According to the standard, it is assumed that only one transmitter is active during the Constant Tone Extension (CTE) phase difference measurement. More precisely, in the AoA technique, the receiver is

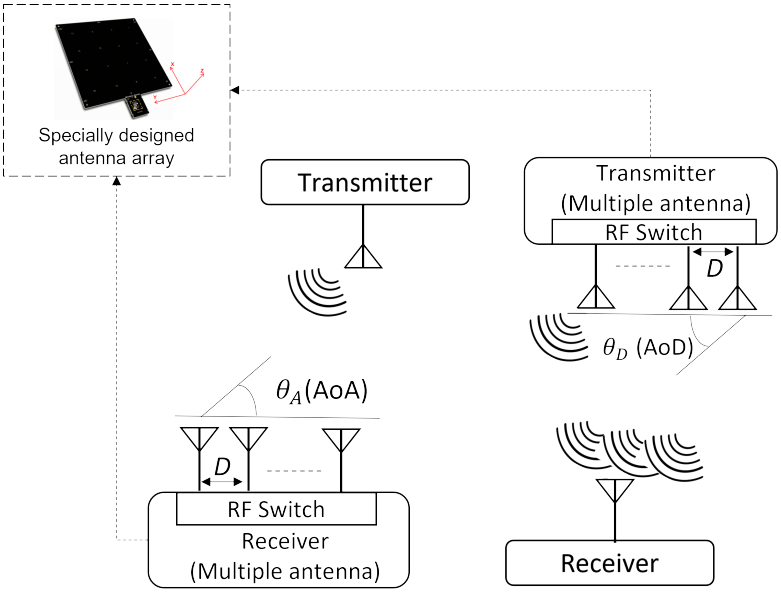

Figure 1.4: BLE 5.1 Direction-Finding Techniques: On the left, Angle of Arrival (AoA) Technique features a receiver with multiple antennas, while the transmitter has a single antenna. On the right, the Angle of Departure (AoD) Technique showcases a transmitter with multiple antennas and a single-antenna receiver.

equipped with multiple antennas controlled using an RF switch. By measuring the phase difference observed at the multiple antennas, the receiver can locate a transmitter's direction. Unlike AoA, in AoD, the transmitter is equipped with multiple antennas. It transmits the signal over multiple antennas in a time-division fashion. The receiver with a single antenna will estimate the transmitter's direction based on this time-multiplexed signal. The two techniques can be realized using a hardware setup shown in Fig. 1.4, in which one side must require an antenna array. Such antenna arrays are often larger than 15 × 15 cm, and hence unpractical for many applications [58]. Moreover, they are costly and hard to design, as the dependence of angular measurements on the antenna separation increases the complexity of the design [59].

Some recent BLE chips claim to provide phase-based Time-Of-Flight (ToF) information also known as Channel Sounding[1], a phase-based ranging approach [60], that promises precise localization. However, this technology is still in its early stage and there are only a limited number of studies on this topic. Furthermore, chipsets supporting this functionality are not yet widely accessible (standardized ToF support is expected in future Bluetooth revisions [61]) [62, 63]). *Consequently, the focus of this thesis is predominantly on utilizing traditional, budget-friendly, off-the-shelf BLE devices that are equipped with single omnidirectional antennas.*

[1] Channel Sounding operates through a phase-based ranging method, where the distance between two radio devices is estimated accurately by analyzing the radio signal's phase [60].

The goal is to maintain the simplicity inherent in single-antenna RSS-based methods, while striving to achieve sub-meter localization accuracy, on par with systems based on AoA/AoD techniques. However, current BLE state-of-the-art (SOTA) solutions has not fully developed or explored the direction-finding enhancements, specifically the AoA/AoD techniques, introduced with BLE 5.1. Therefore, this thesis also aims to assess the accuracy of these advancements and suggest alternative strategies to make these systems more cost-effective and less cumbersome, such as by adopting single-antenna configurations in place of multiple antennas.

However, some indoor scenarios, such as AGVs/AMRs retrieving items from supermarket shelves, as well as the burgeoning requirements of the digital robotics domain, necessitate more precise localization systems capable of delivering decimeter or centimeter-level accuracy. Such a level of accuracy is challenging to achieve with BLE technology alone due to its narrow-band nature, which is further complicated by indoor multipath effects, posing a significant technological hurdle. Therefore, there is a necessity to integrate BLE with other, more accurate technologies, such as optical systems. It is important to acknowledge, however, that while optical systems can offer superior accuracy compared to BLE or RF technologies, they come with their own set of challenges. Retrofitting or replacing existing devices and installations with these more accurate technologies can be a substantial investment and labor-intensive. This is exemplified in the installation of optical systems or the establishment of an anchor infrastructure for Ultra-Wideband (UWB) devices [64, 65]. Although there are cost-effective optical localization methods that provide high accuracy, they often lack reliability. These methods are prone to interference from varying lighting conditions and indoor obstacles, which can considerably restrict their effective localization coverage.

Therefore, despite the wide range of optical and radio frequency (RF) technologies available, achieving centimeter-level accuracy in indoor settings with *minimal costs, reliability* is still a key challenge. One of the primary challenges posed in the indoor environment is the non-uniformity of spaces and the occurrence of multipath fading, making the design of accurate and reliable localization systems all the more essential. Moreover, indoor applications require a more precise location than outdoor applications, a requirement often referred to as the "last meter" problem in localization [66].

1.3 Blending Technological Advantages

One of the possible solutions to address the indoor localization issues, demands and a promising approach, involves the integration of optical and RF technologies to create a hybrid solution [67, 68, 69, 70]. This approach aims to achieve a stable, energy-efficient, and highly accurate system. However, this raises a key question: which optical technologies can be

combined to fulfill the requirements for a highly accurate indoor localization system with centimeter-level precision, while also ensuring energy efficiency, cost-effectiveness, and reliability?

1.3.1 Suitable Optical Technology

To select an effective optical technology method, the following approaches are considered:

- **Visible Light Positioning (VLP)**: VLP utilizes the visible light spectrum (wavelengths between 380-700 nm) to accurately determine the positions of individuals or objects in indoor spaces. The precision of VLP, is attributed to the directional properties of light and the use of Light Emitting Diodes (LEDs) as information sources, which aligns with environmental sustainability goals. VLP operates by wirelessly transmitting data through ubiquitous light sources, typically involving the modulation of light from LEDs. The light variations are detected by devices equipped with light sensors, such as PhotoDiodes (PDs) or cameras [71, 14].

- **Image-based localization**: This method employs cameras to capture environmental images. These images are calibrated with a specific area to identify locations based on visual landmarks. Systems like Optitrack offer millimeter-level accuracy, using multiple specialized cameras and infrared markers in a 3D space, ideal for virtual reality, motion capture, and robotics. Dual-camera systems, relying on stereo vision, are less accurate but have reduced complexity and cost [72, 73].

- **Laser-based localization**: Utilizing Light Detection and Ranging (LiDAR) technology, this method measures distances to objects using laser beams. It's primarily used for creating 3D environmental maps and is often incorporated in Simultaneous Localization and Mapping (SLAM) in robotics [74, 75].

- **Infrared (IR) localization**: These systems use IR sensors and transmitters, determining position through infrared signals, either based on signal strength or ToF measurements [76, 77].

Selection: VLP is highlighted as the most promising for optical localization due to its compatibility with existing lighting infrastructure, high accuracy, cost-effectiveness, and reduced privacy concerns. Camera-based methods, while effective, require significant computing power, making them less suitable for low-power IoT devices. Laser-based systems, although

detailed, are expensive and require sophisticated hardware. IR-based systems offer effectiveness in various light conditions but are limited by range, accuracy, and susceptibility to ambient light interference.

Given the goal of designing a high-accuracy, power-efficient, and low-cost indoor localization system for low-power IoT devices, VLP is identified as the optimal choice. The growing preference for LEDs in lighting, driven by their energy efficiency, cost-effectiveness, durability, and long lifespan, further strengthens VLP's position as a sustainable and progressive localization solution [66, 78, 79].

1.3.2 Issues with VLP

Not all the light sources can be modulated and not all the target objects or humans can carry a a device capable of sensing light [80]. Depending on whether the light sources are modulated or not, VLP systems can be categorized into two main types: active-VLP and passive-VLP (*p*-VLP) systems. In active VLP, light sources actively modulate to transmit data to light sensors. Conversely, in *p*-VLP systems, either the light source or the receiver plays a passive role. This means that in these systems, LEDs are not actively modulated, or the receiver lacks a light sensor, with the target functioning passively. In scenarios where the transmitter is passive, intrinsic characteristics of the light sources are analyzed for light identification and used in localization. Additionally, the *p*-VLP system is divided into sub-categories: passive-source, passive-user, and full-passive. A thorough explanation of these systems, along with an extensive SOTA analysis of *p*-VLP, is presented in the following Chapter 3, offering readers a more comprehensive understanding of VLP systems.

Active-VLP: Existing active VLP systems, despite their potential, face several limitations that have led to limited commercial interest. Some of these limitations include:

- **High infrastructure changes:** On the transmitter side, these systems demand custom-designed light sources with a controller capable of modulating the light. Updating existing light fixtures with these controllers incurs extra cost and deployment effort, making commercialization difficult.

- **Complexity:** Many active VLP systems need to collect different light features and perform extensive signal processing to accurately estimate the position. Complex hardware on both ends of the communication link increases the overall cost.

Additionally, the use of mobile cameras as receivers in certain active VLP systems poses challenges for users, including *high power consumption* and privacy concerns. However, some of these limitations might be addressed by *p*-VLP systems, which are outlined briefly below:

Passive-VLP:

- **Less infrastructure changes:** In *p*-VLP systems, there is no need for specially designed light sources with a controller. The already installed lighting fixtures can be used as a source without any modifications.
- **Energy efficiency:** Most of the *p*-VLP systems capture the light signals using PDs, which consume significantly less power (μW) than cameras. Moreover, in *p*-VLP systems, either the transmitter end or the user is passive resulting in a more energy-efficient design compared to the active systems in which both sides have active elements.
- **Cost-effectiveness:** The use of low-cost PDs and the need for fewer infrastructure changes make *p*-VLP systems cost-effective alternatives to active systems.
- **Device-free localization:** Some *p*-VLP systems enable localization without requiring users to carry any light-sensing device. Light reflection or shadows caused by their body are used for locating them [8].

Difficult commercialization. Since 2015, several companies have begun to commercialize VLP systems, marking a significant advancement in this technology. A notable early adopter was Carrefour in Lille, France, which in 2015, installed Philips's intelligent lighting system [81]. This innovative system was designed not just for illumination but also to assist customers in locating products and accessing available discounts in nearby stores. This installation, however, was not without its challenges. Carrefour had to install 800 LED fixtures across their 7,800 square meter store, a venture that entailed considerable expense [81]. Building on this momentum, Qualcomm, launched its VLP system, named "Lumicast." This system boasted impressive precision, claiming to achieve an accuracy of 5 – 10 cm [82]. Despite these advancements, a critical challenge remained: *both systems required substantial changes to existing lighting infrastructures*. This requirement posed a significant barrier to widespread adoption, as it involved considerable alterations and associated costs. This thesis concentrates on addressing the main challenge in VLP systems: *the necessity of modulating light sources*. Additionally, it aims to enhance power efficiency and reduce both computational complexity and system cost, which could significantly improve the commercial viability of VLP. The research will introduce a new passive-VLP system, specifically the passive-source as detailed in [8]. This system does

not transmit modulated information from the light sources; instead, it analyzes their intrinsic features. A light-sensing device on the target device is used to gather this information and execute localization tasks. In summary, *the thesis has a dual objective when utilizing VLP: Firstly, to develop a p-VLP system that is low-power (utilizing photodiodes), cost-effective, easily integrable, and computationally efficient for IoT devices, thereby providing pervasive location awareness and localization capabilities. Secondly, upon fulfilling this objective, the focus shifts to devising methods by which the VLP system can assist BLE in achieving more precise, decimeter-level localization accuracy. This approach aims to deliver an energy-efficient, reliable, accurate, and cost-effective solution, aligning with the ultimate goal of the thesis.*

Furthermore, from the survey of existing VLP technologies [66, 8, 83], it is found that VLP systems only perform well in some controlled environments, and their performance degrades in real-world situations due to external noise such as ambient light, sensor blockage, and other environmental obstacles. The accuracy of VLP systems tends to diminish in daylight conditions, owing to increased ambient interference. This issue is especially pronounced near wall corners, areas adjacent to them, or around window edges. In such challenging scenarios, no VLP systems have yet managed to reduce positioning errors to the centimeter scale. These limitations persist, largely due to technological constraints and the necessity to keep computational complexity low. A promising strategy, as outlined in the objectives of this thesis, is to enhance the accuracy of BLE systems. In doing so, the existing challenges associated with VLP could be effectively tackled through the integration of VLP and BLE-based localization systems, creating a more precise and robust solution.

1.3.3 Integrating RF with Optical Technology

In response to the technological bottleneck of both technologies BLE & VLP and the need for low computational complexity, this thesis advocates a hybrid solution that combines BLE with VLP. This strategy is designed to offset the low accuracy of BLE against the limited range of VLP, leveraging the strengths of both technologies to create an indoor localization system that is highly accurate, low computational-cost, and energy-efficient, thus fitting for practical applications. The focus is on developing innovative techniques to address the unique challenges of BLE and VLP to facilitate effective real-world deployment. The goal extends beyond merely merging these technologies; it encompasses first resolving inherent issues in each technology, presenting novel solutions that surpass the current SOTA in localization accuracy, cost, and power efficiency. Subsequently, a hybrid solution is designed, aiming to outperform the capabilities of both individual systems.

However, achieving decimeter-level accuracy in tracking systems, with smooth and con-

tinuous motion, poses another significant challenges, particularly when striving to avoid the addition of extra sensor units for passive object tracking. While BLE technology alone falls short in meeting this level of accuracy, the incorporation of VLP introduces its own set of challenges. Notably, *p*-VLP faces difficulties in continuous tracking in environments with numerous light sources and often requires supplementary sensor units. Therefore, to resolve these issues, this thesis proposes the integration of BLE technology with millimeter wave (mmWave)[2] radar measurements as a viable solution to enhance the accuracy of BLE tracking systems, thereby eliminating the need for extra sensing units on the target device.

Moreover, in addressing these tracking challenges, the thesis sets out to fulfill its objective of thoroughly exploring the new direction-finding techniques introduced in the BLE 5.1 standard. These techniques, designed for asset tracking solutions, have yet to be fully explored in terms of their capabilities. The research aims to bridge this gap by comprehensively assessing and utilizing these advanced techniques. However, this integration is not without its challenges. mmWave radar technology is hindered by rapid signal loss over distances and reduced effectiveness in environments with stationary targets or multiple objects [5, 84]. Consequently, this research delves into developing a strategy that effectively combines the strengths of both BLE and mmWave radar technologies. The aim is to overcome their individual limitations and establish a more efficient and dependable tracking system.

It is important to note that the superiority of a hybrid solutions doesn't imply it is always the optimal choice. The selection of a localization system should be tailored to specific application requirements. Further details and insights will be explored as the thesis progresses.

1.3.4 Advanced Techniques in Cross-Technology Data Fusion

Data fusion, a critical process in combining and integrating data from diverse sources, aims to enhance the correlation, accuracy, and utility of the resulting information beyond what any single data source or technology can offer [85, 86, 87]. This technique finds its applications in various fields including health monitoring, localization, and multimedia processing [88, 89]. For example, a healthcare-focused sensor data fusion system is detailed in [90], and a multimodal fusion module for speaker separation, integrating audio, video, and speaker embedding streams, is proposed in [91]. Furthermore, the emergence of machine learning has led to the rising prominence of Neural Network (NN)-based data fusion methods, particularly in complex localization tasks [92, 93, 94]. These NN approaches, as discussed in [95], often surpass traditional data fusion algorithms such as Kalman Filters, Bayesian methods, or rule-based

[2]This research is focused exclusively on BLE technology and encompasses mmWave radar methods that have been developed through a collaborative effort with a fellow researcher.

systems in terms of versatility and accuracy. This is especially evident in environments where sensor data and its geographic correlation are complex. Michelsanti *et al.* [96] provide an overview of NN-based fusion techniques used in audio-visual systems, such as concatenation, addition, and product-based methods. These techniques, based on similar NN design principles, are adaptable for fusing radio features in localization tasks.

Utilizing NNs for data fusion in localization, especially when integrating technologies like BLE, VLP, and mmWave radar, presents substantial benefits over conventional methods. Each technology possesses unique characteristics and limitations, and NNs, with their design flexibility, are adept at harnessing these diverse strengths to significantly enhance the accuracy and robustness of localization systems. NNs are particularly effective in noise reduction and signal enhancement, learning to disregard non-essential data variations, like random noise, while concentrating on patterns essential for accurate localization.

SOTA NN architectures, designed for efficient real-time data processing, are vital for numerous real-time indoor localization applications [92, 93, 97]. The NN model is also adopted in this thesis to fuse data from different technologies, demonstrating its versatility and effectiveness in integrating diverse data sources for enhanced localization accuracy. However, it is important to acknowledge that the effectiveness of NN-based methodologies heavily relies on the presence of high-quality training data that accurately reflects the operational environment and conditions. In this thesis, special focus is placed on extracting various types of valuable data, which can more effectively represent the relationship between data and location, thereby enhancing the learning capability of the NN model.

In the following section, a concise formalization of the localization challenges & opportunities outlined in this section will be presented.

1.4 Challenges and Opportunities

This thesis distinguishes two principal categories of localization systems. The first category includes autonomous localization systems, in which the target, such as a warehouse robot or an individual in a shopping mall, autonomously determines its position and navigates on its own. The second category covers tracking systems, primarily used for monitoring purposes, like tracking asset locations in a warehouse.

1.4.1 Challenges

The focus of this thesis is on addressing three key challenges in the development of autonomous indoor localization systems, outlined below. For in-depth information on each

challenge, readers are directed to the corresponding chapters, identified with a 'CHx' index. This 'x' in the 'CH 'index refers to the chapter number in the thesis, with each challenge directly related to a specific chapter.

CH2 **Developing accurate and cost-effective BLE localization systems**: The challenge lies in enhancing the accuracy of BLE-based location systems in indoor settings, where multipath effects and signal fading present significant difficulties. Solutions using advanced methods with multiple antennas, while effective, tend to be bulky and costly. The goal is to maintain the simplicity and affordability of BLE devices, such as those with a single antenna, while achieving sub-meter accuracy and overcoming channel effects. The question is how to attain such precision with BLE technology.

CH4 **Cost & infrastructure changes**: A significant challenge for VLP is the necessity to modify existing lighting systems for location signaling. Such modifications can incur substantial costs, and there is often reluctance from companies to make these investments. Furthermore, the dependency on power-intensive cameras for light detection limits VLP's suitability for low-power IoT devices.

CH5 **Enhancing VLP systems for real-world use**: Existing VLP systems perform well only in controlled environments. In real-world scenarios, factors like external ambient light sources, obstacles, and shadows, decline localization performance, ultimately restricting the effective localization areas. The key challenge is to adapt and improve VLP systems so they can perform well in these everyday environments and also expand their range of operations.

CH6 **High-Accuracy Tracking**: The challenge involves enhancing BLE tracking by integrating it with mmWave radar technology to achieve high-precision tracking. This enhancement seeks to compensate for the shortcomings of VLP systems, particularly their inability to provide continuous tracking without additional sensors.

Ultimately, this research seeks to provide a solution for achieving decimetre-level localization accuracy in large public spaces, catering to the needs of smart factories and work-spaces.

In addition to defining key challenges, this thesis also sets forth various hypotheses related to these challenges and details the specific goals of the research. The aim is to address these challenges, test the hypotheses, and meet the objectives, thereby contributing fresh insights and solutions in the areas of Visible Light Communication, and Bluetooth Low Energy.

1.5 Research Context

The research presented in this thesis closely aligns with the goals of the ENLIGHT'EM project, an innovative initiative that seeks to harness the potential of LEDs as a sustainable and energy-efficient lighting technology. This project opens up new avenues for emerging IoT services while capitalizing on the inherent advantages of LED technology. Supported by the European Union's Horizon 2020 research and innovation program under the Marie Skłodowska-Curie grant agreement No. 814215, ENLIGHT'EM places a strong emphasis on training early-stage researchers (ESRs). These ESRs make significant contributions at both technical and scientific levels, engaging in diverse activities, including disseminating research findings, participating in Ph.D. programs, and attending network-sponsored tutorials and workshops. The consortium behind ENLIGHT'EM includes industrial partners who blend theoretical knowledge with practical expertise, offering ESRs invaluable technical training opportunities. The research within ENLIGHT'EM is organized into three distinct technical work packages (WPs): WP1 focuses on Low-energy Technologies, WP2 explores Intelligent Algorithms and RF Integration, and WP3 is dedicated to Applications and Services. Specifically, this thesis aligns with the work of ESR11, situated within WP3. ESR11's primary objective is to develop a hybrid indoor localization system by integrating radio frequency technologies like Bluetooth Low Energy with Optical Technology, such as Visible Light Communication. This integration aims to achieve a highly accurate, energy-efficient, and cost-effective indoor localization solution.

This study is conducted at the Bristol Research & Innovation Laboratory (BRIL), a division of Toshiba Europe Limited in Bristol, United Kingdom, as well as in collaboration with the Delft University of Technology (TU Delft) in the Netherlands. This research partnership also extends to the University of Applied Sciences and Arts of Southern Switzerland (SUPSI) and the University of Palermo (UniPA) in Italy.

1.6 Research Questions and Hypotheses

The thesis is structured around specific research questions, followed by hypotheses formulated in response to these questions, as detailed below::

RQ1 **Is sub-meter accuracy achievable with single-antenna BLE devices? How does exploiting the beating effect—a by-product of synchronous transmission protocols — alongside the unique carrier frequency offsets caused by hardware discrepancies, contribute to advancing single-antenna BLE technology in tag localization? Moreover,**

can the reliable identification of BLE nodes be ensured without the need for frequency tuning?

H1 The research posits that by harnessing the 'beating effect'—an outcome of the simultaneous transmissions from multiple transmitters inherent to the synchronous transmission protocol—it is feasible to localize a tag with accuracy at the sub-meter level using *single-antenna* BLE devices and reduced **channel occupancy** within the BLE technology framework.

H2 Furthermore, the hypothesis suggests that the identification of individual anchor nodes, as delineated in hypothesis H1, can be efficiently conducted through the analysis of carrier frequency offset, which arises due to hardware discrepancies. This approach circumvents the necessity for frequency-tuning adjustments.

RQ2 How can the intrinsic characteristics of LEDs be optimized for enhancing Visible Light Positioning systems in mobile objects such as AGVs/AMRs, ensuring system viability without modifying existing lighting infrastructure, and addressing challenges of identification overlap, environmental variables, and the quest for centimeter-level accuracy?

H3 The hypothesis posits that by extracting the intrinsic properties of LEDs, such as their dominant color composition, these light sources can be uniquely identified. This identification process can then be utilized to provide location services to mobile objects, achieving an accuracy level down to the centimetre.

RQ3 How can the integration of optical and RF technologies enhance the accuracy and precision of indoor localization systems, and what methodologies and feature selection criteria are essential for effectively merging different modalities data and addressing the inherent limitations of each technology to improve overall localization performance?

H4 The research hypothesizes that integrating optical and RF technologies for localization purposes can significantly improve the precision and accuracy of such systems to decimeter-level, thereby mitigating the inherent limitations associated with each technology when used independently.

H5 Furthermore, it is proposed that leveraging machine learning methods, particularly through the application of incremental learning techniques, for the integration of these diverse modalities could enhance the process of feature fusion from

both technologies. This integrated approach is anticipated to yield localization systems that are not only reliable but also exhibit high levels of accuracy, reaching down to the decimeter scale.

1.7 Research Objectives

The primary goal of this thesis is to develop innovative indoor localization systems that are both accurate and precise. The thesis categorize these systems into two types: autonomous systems and tracking systems. The required level of accuracy varies depending on the intended application. For instance, AGVs in supermarkets need sub-meter accuracy for navigating to specific sections. Achieving closer proximity to a particular shelf demands even greater precision, potentially at the decimeter level. In the healthcare sector, where robots might be employed for transporting patients, the necessity for high accuracy and reliability in tracking becomes paramount. However, designing a reliable and universally effective indoor localization system is complex due to the irregular nature of indoor spaces, effects like multipath fading, the movement of targets, and the lack of standardized technologies. To create a stable, energy-efficient, and highly accurate system, it is necessary to integrate various technologies.

> *The goal of this thesis is to exploit the complementary properties of optical and RF technologies. By integrating both, the aim is to provide the best trade-off for each technology in terms of location accuracy, cost, and energy consumption, thereby designing more efficient indoor localization systems...*

The initial aim of this thesis is the development of a hybrid autonomous localization system, integrating BLE and VLP technologies. The subsequent phase of our research focuses on the creation of advanced tracking systems, amalgamating BLE technology with mmWave radar technology. The essence of this work is to synergistically blend these technologies, thereby enhancing the efficacy and performance in applications of both autonomous localization and tracking. The objectives are outlined as follows:

Objective 1 Develop innovative methods to enhance the performance of RSS-based BLE localization techniques. Investigate how single-antenna BLE devices can be optimized to achieve sub-meter level accuracy. Furthermore, pioneer methods to integrate the use of the Constant Tone Extension feature from the BLE 5.1 standard into RSS-based localization methods.

- To evaluate the robustness of the developed localization method in dynamic, multipath-rich environments.

- To investigate how to maintain consistent localization performance as the testing area increases.
- To explore whether RSSI-based approaches can be enhanced to match the performance of AoA-based techniques.
- To examine the use of BLE protocols, like synchronous transmission, for effective localization services.

Objective 2 Design a low-power, cost-efficient, easily integrable, and computationally modest passive VLP system, specifically for IoT devices, to facilitate ubiquitous location awareness and tracking capabilities. Additionally, develop methodologies and techniques to significantly reduce the infrastructure requirements and the initial investment necessary to support indoor VLP services.

Objective 3 Engineer novel fusion approaches such as utilizing machine learning techniques to integrate optical and RF features for the development of a hybrid localization system. This system should be highly accurate, aiming for precision at the decimeter level, and reliable. This involves addressing the individual limitations of each technology and then synergizing them to construct a reliable and precise indoor localization system.

Objective 4 Develop innovate methods to reduce the cost of developing BLE multi-antenna array angle techniques for tracking systems. Investigate the capabilities of the latest BLE 5.1 direction-finding standard and suggest innovative ideas to enhance the accuracy of these systems to the decimeter level. These techniques would fuse BLE features with more accurate tracking technologies, such as mmWave radar systems.

For all the objectives stated, the overarching aim is to develop the necessary software and hardware toolchains. These toolchains will demonstrate the viability and real-world application potential of all the systems developed.

1.8 Thesis Novel Contributions

The core contributions of this research are twofold. Firstly, it focuses on the design of innovative autonomous indoor localization systems, which could significantly benefit AGVs in warehouses or similar indoor settings, enhancing their location awareness and enabling autonomous navigation in smart environments. Secondly, the thesis presents the development

of a tracking solution, tailored for the healthcare sector, asset tracking in industrial settings, aligning with the advancements of Industry 4.0.

To tackle the challenges outlined in Section 1.4 and achieve the goals set forth in Section 1.7, this thesis has devised **four innovative localization systems**. Among these, three pertain to autonomous localization, wherein the target can autonomously determine its own location, while the fourth solution focuses on tracking. The subsequent section offers concise overviews of these novel solutions, highlighting their unique contributions. Before delving into these descriptions, the section first elaborates on the technological innovations this thesis contributes to the development of these solutions.

1.8.1 Technology Contributions

To the best of the author's knowledge,

1. the thesis presents a pioneering narrowband localization system that relies on a synchronous transmission protocol, designed to **minimize wireless channel occupancy**. This innovative approach enables accurate RSS-based BLE localization for devices equipped with a **single-antenna**. The thesis introduces signal processing techniques to exploit the 'beating' spectrum that can be performed on mobile tags (such as AGV/AMR) to make them spatially aware and intelligent enough to make location-dependent decisions. The approach facilitates **very high-resolution tracking**, not yet possible with any conventional Bluetooth-based localization system. Relying on the latest standardized advances in Bluetooth 5.1 specifications (such as **Constant Tone Extension**) and exploiting these in novel ways different from their intended use, makes the thesis approach radically different from the state-of-the-art approaches.

2. the thesis presents the first **passive** visible light positioning system that relies on **single-pixel colour sensors** to extract the light's hue-spectrum. By leveraging these sensors, it can provide location awareness services and accurate localization, **without requiring any modifications** to the existing lighting infrastructure- offering a **cost-effective & power-efficient** solution. This approach marks a significant advancement in the field of VLP, making it more accessible and feasible for widespread implementation. Additionally, the thesis posits that the integration of these passively gathered light characteristics with RF-based technologies (such as BLE, as discussed in this thesis) could notably augment their localization precision. It proposes an incremental learning framework to merge data from both technologies, overcoming the limitations of each technology individually and delivering a reliable and accurate localization system.

3. the thesis presents the pioneering experimental exploration of **Bluetooth 5.1 direction-finding** techniques especially the angle-of-arrival techniques, to achieve **sub-meter** level precision in tracking mobile objects through the use of multi-antenna arrays. It further offers a **single-antenna** based tracking system that maintains similar sub-meter accuracy while avoiding the use of bulky, costly antenna array. Moreover, the thesis introduces the integration of this advanced BLE-based tracking system with mmWave radar technology utilizing DNN-based techniques to offer a decimeter-level tracking accuracy. This integration effectively overcomes the limitations inherent in each technology.

1.8.2 Contributions

Contribution 1: BLoB

The first contribution of this thesis is the creation of a novel BLE localization system based on beating, named **BLoB**. This system fulfills the objective of designing an accurate yet cost-effective RF-based localization method. It utilizes synchronous transmission protocols in low-power wireless communication, where the resulting beating effect—a sinusoidal pattern of constructive and destructive interference in the received signal—plays a crucial role. This research use this effect innovatively for localization, marking a departure from traditional methods. A distinctive feature of BLoB is its reliance on single-antenna configurations for both anchors and tags. This contrasts with the current SOTA localization systems that typically require complex and expensive antenna arrays for sub-meter accuracy. BLoB is implemented on standard BLE devices and its effectiveness is rigorously tested in various settings, including static and mobile scenarios across different environments like office rooms, libraries, meeting rooms, and sports halls. Comprehensive details of this system and its performance evaluation are provided in Chapter 2. This development is instrumental in validating the hypothesis outlined as H1, and H2 in the thesis.

Contribution 2: HueSense

The second key contribution of this thesis is the development of an innovative passive visible light positioning system, named **HueSense**. This system is based on the observation that LEDs emit slightly different colour spectra, which are indistinguishable to the human eye but can be detected by colour sensors. This unique characteristic allows for the identification of each light source by its spectrum, without the need for modulation or alteration. This approach eliminates the necessity of modifying existing lighting infrastruc-

ture, relying instead on cost-effective and energy-efficient off-the-shelf hue sensors for location awareness services in AGVs. Detailed discussions and findings on this system are presented in Chapters 3 and 4. This objective is designed to validate the hypotheses outlined as H3 in the thesis.

Contribution 3: BLELight

The third contribution of this thesis is the development of a hybrid system, **BLELight**, which is a Deep Neural Network (DNN)-based localization system combining *p*-VLP and BLE technologies. This system aims to achieve stable, energy-efficient, and accurate indoor localization. To effectively integrate the diverse features from both *p*-VLP and BLE, an incremental learning approach is proposed for training the Deep Neural Network (DNN). This method allows for the fusion of data from visible light and BLE, addressing their individual limitations and attaining decimeter-level accuracy. Incremental learning is used to minimize feature interference from different sources, ensuring that model learning at each stage is influenced primarily by one signal feature. The core premise of this approach is the belief that both RF and optical (VLP) modalities, despite their differences, provide valuable insights into the signal-location relationship in indoor environments. This confirms the fourth hypothesis- H4, presented in this study.

Contribution 4: BmmW

The fourth key contribution of this thesis is the development of **BmmW**, an advanced tracking system that combines BLE technology and mmWave radar. This system enhances BLE 5.1's constant tone extension feature with mmWave radar data to enable real-time 3D tracking of a mobile tag with decimeter-level precision. A unique aspect of BmmW is its integration of a DNN trained with data from both BLE and mmWave measurements. This integration capitalizes on the strengths of each technology, addressing the challenges of BLE's limited accuracy and the signal attenuation and multiple object identification issues of mmWave radar. Additionally, to further optimize cost-efficiency, the system introduces BmmW-LITE, tailored for single-antenna BLE devices, thus eliminating the need for more complex and expensive multi-antenna arrays. A detailed discussion and analysis of this system are provided in Chapter 6.

1.9 Thesis Structure

The structure of this thesis is organized as follows: Chapter 2 presents the developed BLE-based localization system, which is founded on a synchronous transmission protocol. Initially, the chapter presents an overview of the current SOTA in BLE technology, then it details the protocol and provides a thorough technical overview of the technique used to construct BLoB, a BLE-based system. Moreover, this chapter includes experimental validations of the system conducted in a variety of environments.

Chapter 3 offers a comprehensive overview of VLP systems, with a particular focus on the emerging *p*-VLP systems. The chapter develops a taxonomy to categorize *p*-VLP systems and delve into the challenges they face for wider acceptance in commercial environments. Following this, Chapter 4 introduces the developed novel *p*-VLP system. This chapter not only discusses the underlying principles of the system but also showcases a prototype, which is analyzed for its applicability in real-world scenarios, particularly in uncontrolled lighting environments. This analysis is supported by various experiments to validate the system's effectiveness.

Chapter 5, demonstrates the hybrid localization system. This system is developed by integrating the key features from both the *p*-VLP system introduced in Chapter 4 and the BLE system from Chapter 2. The development methods discussed in this chapter are heavily based on machine learning techniques.

Chapter 6 presents the tracking system, which is a fusion of BLE technology and mmWave radar. This chapter starts by reviewing the SOTA tracking solutions for both these technologies and discusses various techniques for their integration. It provides a complete description of the proposed fusion technique for tracking systems, along with experimental validations to support its efficacy.

Finally, Chapter 7 concludes the thesis. It discusses the key findings from this research and draws conclusions. Additionally, this chapter looks forward to future research possibilities, offering recommendations for further work in this area.

Figure 1.5 offers a clear overview of the thesis's organization, detailing the progression from one chapter to the next and emphasizing the unique topic and research focus of each chapter. This visual guide aids in understanding the logical sequence and specific areas of study covered in the research.

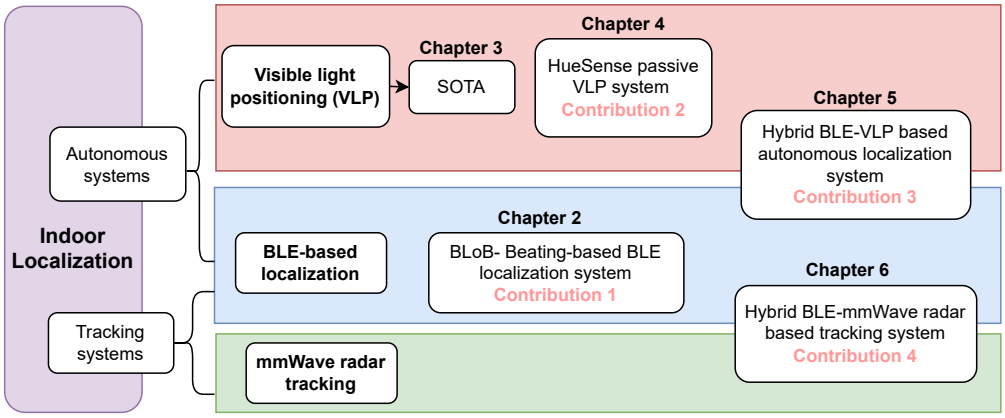

Figure 1.5: Illustrating the sequential structure and key focus areas, contributions of the thesis.

1.10 List of Publications

The research conducted in this thesis has resulted in two USA patent applications, the submission of two articles in indexed journals, and five published conference proceedings. Additionally, the author has collaborated with other researchers on two conference proceedings. The following sections provide a list of all these articles.

1.10.1 Patent Applications

This section presents a list of patents that have emerged from this research. It should be noted that while one of these patents is publicly accessible and included in this document, the other patent is not yet publicly available. Consequently, it is not shared here, respecting the considerations of intellectual property rights.

- J. Singh and P. Li, “Method and system for optical localisation,” 2023. US Patent App. 18/352,987.

- U. Raza, J. Singh, A. Stanoev, and V. Marot, “Method and system for wireless localisation,” May 4 2023. US Patent App. 17/453,386.

1.10.2 Conference Proceedings

This section presents a list of conference proceedings as part of the outcomes of the research conducted in this thesis.

- J. Singh, Q. Wang, M. Zuniga, and T. Farnham, "Huesense: Featuring LED Lights Through Hue Sensing," in Proceedings of the 1st ACM Workshop on AI Empowered Mobile and Wireless Sensing, pp. 19–24, 2022. **[Best Paper Award]**

- J. Singh, M. Baddeley, C. A. Boano, A. Stanoev, Z. Chai, T. Farnham, Q. Wang, and U. Raza, "BLoB: Beating-based Localization for Single-antenna BLE Devices," in Proceedings of the 20th International Conference on Embedded Wireless Systems and Networks (EWSN), ACM, Sept. 2023. **[Best Paper Award]**

- P. Li*, J. Singh*, H. Cui, and C. A. Boano, "BmmW: A DNN-Based Joint BLE and mmWave Radar System for Accurate 3D Localization," in 19th International Conference on Distributed Computing in Smart Systems and the Internet of Things (DCOSS-IoT), pp. 47–54, IEEE, 2023 (*Contributed equally to the research). **[Best Paper Award]**

- J. Singh, T. Farnham, and Q. Wang, "When BLE Meets Light: Multi-modal Fusion for Enhanced Indoor Localization," in Proceedings of the 29th Annual Interna- tional Conference on Mobile Computing and Networking, pp. 1–3, 2023. **[Qualified for the Student Research Competition at ACM MobiCom 2023.]**

- J. Singh and U. Raza, "Passive visible light positioning systems: An overview," in Proceedings of the Workshop on Light Up the IoT, pp. 48–53, 2020. **[Survey paper]**

1.10.3 Journal Articles

This section provides a list of journal articles resulting from the research conducted in this thesis. Please note these articles are submitted and currently under review.

- P. Li*, J. Singh*, H. Cui, and C. A. Boano, "BmmW+: A DNN-based Joint BLE and mmWave Radar System for Accurate 3D Localization with Goal-oriented Communication," in Pervasive and Mobile Computing, 2023 (*Contributed equally to the research). **[Special Issue Invited Paper]**

- J. Singh, M. Zuniga, T. Farnham and Q. Wang, "HueLoc: Localization through LED's Hue Spectrum," in IEEE Internet of Things Journal, 2024.

1.10.4 Collaborations

This section provides a list of publications in which the author has participated as a collaborator and the material is not included in the thesis.

- J. Singh*, D. Watkinson*, T. Farnham, and D. Puccinelli, “Detecting and Con- trolling Smart Lights with Litalk,” in Proceedings of the 1st ACM Workshop on AI Empowered Mobile and Wireless Sensing, pp. 13–18, 2022 (*Contributed equally to the research).
- O. Dalgic, J. Singh, T. Farnham, and D. Puccinelli, “Augmenting a Smartphone Camera with a Telephoto Lens for Enhanced LED-to-Camera Communication,” in 2023 IEEE Wireless Communications and Networking Conference (WCNC), pp. 1–6, IEEE, 2023.

CHAPTER 2

BLoB: Beating-based Localization for Single-antenna BLE Devices

This chapter introduces BLoB, a BLE-based scalable localization solution for the ubiquitous BLE Devices. Initially, the functioning of BLoB is explained, followed by a demonstration of its effectiveness in various real-world settings.

2.1 Introduction

BLE is another key technology for accurate indoor localization, characterized by its *ubiquitous nature* and *low power consumption* [35]. This chapter explores the method of preserving the inherent simplicity in *single-antenna* BLE devices and RSS-based approaches, while still achieving *sub-meter* localization accuracy, comparable with AoA/AoD-based systems. Specifically, RSS-based localization systems can attain high accuracy, even within sub-meter ranges, by gathering distance measurements from multiple anchors using different frequency channels in a sequential time-division manner. However, this approach leads to a significant use of communication channels, making it less scalable and limiting the update rates. Moreover, the 2.4 GHz band is prone to RF interference, affecting some transmitted packets. To mitigate these issues, the implementation of synchronous transmission protocols is proposed, where all anchor nodes transmit simultaneously [98]. This method lessens channel congestion, enhances scalability and update rates, and reduces the time the radios need to be active. The subsequent sections will explain how synchronous transmission elevates localization performance and improves channel occupancy.

The structure of this chapter is as follows: Background information about Synchronous Transmission (ST), beating, and the CTE feature is presented in Section 2.2. An overview of BLoB, including its design and hardware implementation, is detailed in Section 2.4. The experimental evaluation of BLoB's performance is conducted in Section 2.6, and its limitations and potential future enhancements are discussed in Section 2.7.

2.2 Preliminaries

This section describes how synchronous transmissions can lead to beating effect (Section 2.2.1) before introducing necessary background information on the BLE 5.1 CTE feature (Section 2.2.2).

2.2.1 Synchronous Transmissions and Beating

Flooding protocols based on ST have been extremely popular within the low-power wireless community as a means of providing highly reliable multi-hop communications [99]. In contrast to traditional RF communication practices, transmitting nodes in ST-based communications *intentionally* send packets at the same time as their neighbors. While this may seem counter-intuitive (as one would assume the competing signals would collide at the receiver) a high degree of synchronization between nodes and certain physical layer (PHY) aspects of low-power narrowband communications allow successful demodulation of the overlapping signals, specifically *capture effect*[1] and *non-destructive interference* [100].

Particularly in IEEE 802.15.4-based ST and the coded BLE 5 PHYs, the capture effect plays a significant role, allowing successful reception from nodes simultaneously sending *different* data [101]. However, when sending the *same* data (i.e., precisely the same packet or bit sequence, such as a constant tone), successful reception is largely dependent on frequency synchronization between the transmitting nodes [3]. While perfect synchronization would produce constructive interference across the packet and an overall power gain, *small manufacturing imperfections* result in marginally different carrier frequency offsets. This leads to *non-destructive* interference consisting of sinusoidal periods of *both* constructive and destructive interference across the packet, known as the *beating effect*. Figure 2.1 shows an example of *simple* sinusoidal beating pattern created by two synchronous transmitters, and how *complex* beating patterns are created when an additional transmitter is overlapped. Recent literature has explored how this beating effect impacts ST performance. Importantly, Baddeley et al. [3]

[1]The capture effect enables the RF receiver to pick up one of the colliding packets in a ST, given that the incoming RF signal meets certain power and timing constraints [99, 98].

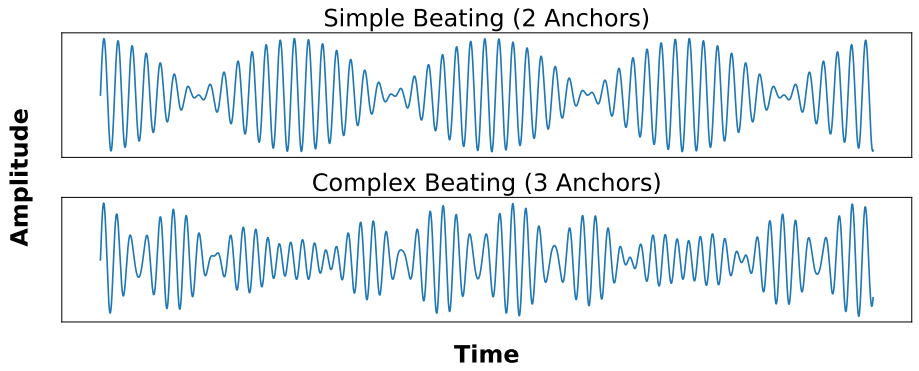

Figure 2.1: Sinusoidal interference patterns created by *simple* (2 anchors) and *complex* (> 2 anchors) beating [3].

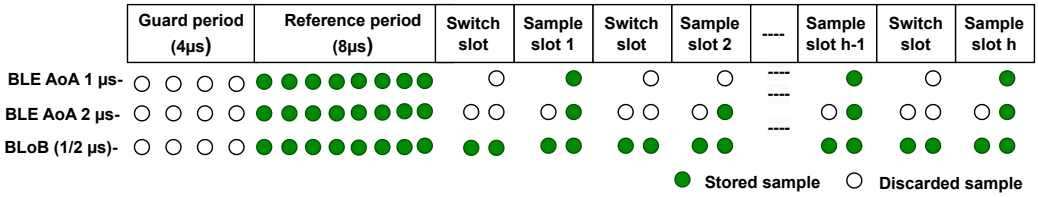

Figure 2.2: Overview of *CTone* sampling and of the stored I/Q samples at the receiver. Classical systems (e.g., AoA-based [4]) store $h = 74$ or $h = 37$ I/Q samples when using 1 μs- or 2 μs-long antenna-switching and sampling slots. In contrast, BLoB uses a *single antenna* and leverages the antenna-switching slot for extra I/Q sampling, which results in up to $h = 148$ collected samples.

demonstrated the existence of beating over synchronous transmissions (with an increasing number of nodes) by evaluating errors across a large number of randomly-generated packets, *resulting in clear beating patterns across a histogram of bit errors*. Notably, this study showed that not only is the beating frequency consistent across different PHYs (for the same nodes), but that *different pairs of transmitters produce a frequency that is significantly dissimilar*, due to relative Carrier Frequency Offset (CFO) between devices. Moreover, subsequent studies have shown that the relative CFO between synchronously transmitting devices can be predictably modelled and estimated despite temperature variations [98]. This thesis research will reveal experimentally that the beating pattern is influenced not only by the quantity of transmitters but also by the geographical distribution of the transmitting nodes. Furthermore, the research will experimentally demonstrate that minor manufacturing imperfections in the hardware, resulting in varying carrier offsets, generate a signal magnitude that fluctuates between valleys and peaks, which is commonly referred to as a "*beating signal*."

2.2.2 Constant Tone Extension in BLE

BLoB leverages the beating signal to capture the relative CFO between devices (anchor nodes) and identify the devices themselves by exploiting the CTE feature in BLE 5.1. The latter allows to append to a BLE packet a constant-frequency signal consisting of unwhitened and constant 1 digits, whose length can vary between 16 μs and 160 μs [42]. The purpose of the CTE is to provide a constant wavelength signal (*CTone*) that can be sampled by a receiver, which then processes its inphase/quadrature (I/Q) components to derive polar coordinates yielding the phase angle and the amplitude value [55].
The CTE can be divided into several sub-fields, as illustrated in Figure 2.2, starting from a guard band of 4 μs followed by a reference period of 8 μs. The rest of the CTE field is then divided into slots for antenna switching and sampling. The switching and sampling slots can either be 1 μs or 2 μs long: this allows, for example, AoA implementations to choose between a finer localization (faster switching) and a higher energy efficiency, or a simplified antenna design (slower switching) [4]. Moreover, 2 μs-long slots make it possible to use a cheaper RFswitch between the antennas that has a longer transition time. The CTE field contains $h = 74$ and $h = 37$ samples when using 1 and 2 μs-long switching and sampling slots, respectively. On the BLE receiver side, while receiving a packet (composed of a preamble, access address, protocol data unit, cyclic redundancy check, and CTE), the radio also samples the I/Q components of the baseband signal at 1 μs frequency. In BLoB, as only single-antenna devices are used, also the I/Q samples in the antenna switching slots can be leveraged, which results in up to $h = 148$ collected samples during the sample slots. The additional number of samples allows the receiver to more effectively separate and decode the individual signals being transmitted and reliably detect beating patterns across all BLE 5 PHY configurations, which makes our approach independent of the underlying PHY. Please note that the CTE field consists of only 1s with no information attached: there is hence no requirement to demodulate the *CTone* at the receiver.

2.3 BLoB: Beating-based Localization

BLoB lets off-the-shelf single-antenna BLE tags to examine the *beating patterns* across a CTE signal received when multiple single-antenna anchors transmit data simultaneously. It is demonstrated that the relative CFO between devices transmitting simultaneously can be extracted from the received beating pattern, which allows for reliable identification of anchors. Exploiting this information and analyzing the peaks in the beating and signal spectrum enables the identification of anchor nodes that strongly contribute to the beating and are hence located

nearby the receiving tag. These observations facilitate the refinement of location estimates and significantly enhance the accuracy of an RSS-based localization system operating on single-antenna BLE devices.

Contributions Building upon these principles, this chapter presents BLoB, a novel BLE-based localization system capable of achieving sub-meter accuracy with the use of small and inexpensive *single-antenna* devices, and without relying on any angular information. In BLoB, multiple anchors transmit packets synchronously using the CTE, while mobile tags extract the signal characteristics – particularly the beating profile – from the superimposed signal resulting from the synchronous transmissions, enabling accurate location determination. This chapter made the following contributions with BLoB:

i) Introduction of signal processing techniques for the identification of relevant anchor nodes based on the CFO detected within the beating pattern.

ii) A method is showcased to determine the contribution from a pair of *dominant* anchor nodes within the received beating pattern (i.e., nodes that strongly contribute to the beating and are hence located nearby the receiver), which allows for the refinement of the location estimate.

iii) The design of BLoB, an indoor localization system that integrates the aforementioned solutions and leverages ST and BLE's CTE feature to achieve accurate localization using *single-antenna* devices only, is presented.

iv) Implementation of a prototype of BLoB on off-the-shelf Nordic Semiconductor nRF52833 boards with a single PCB antenna is described. BLoB only requires support for the CTE feature, and it can hence run on any off-the-shelf device compliant to BLE 5.1 and above.

v) The performance of BLoB is experimentally evaluated in several indoor environments, ranging from large public spaces (e.g., tennis hall) to office rooms. The results in both static and mobile settings demonstrate that BLoB retains sub-meter localization accuracy even in multipath-rich environments. Such performance is superior to classical RSS-based approaches and is comparable to that of AoA-based systems, which is remarkable considering that BLoB operates on *single-antenna* devices and does not utilize any angular information.

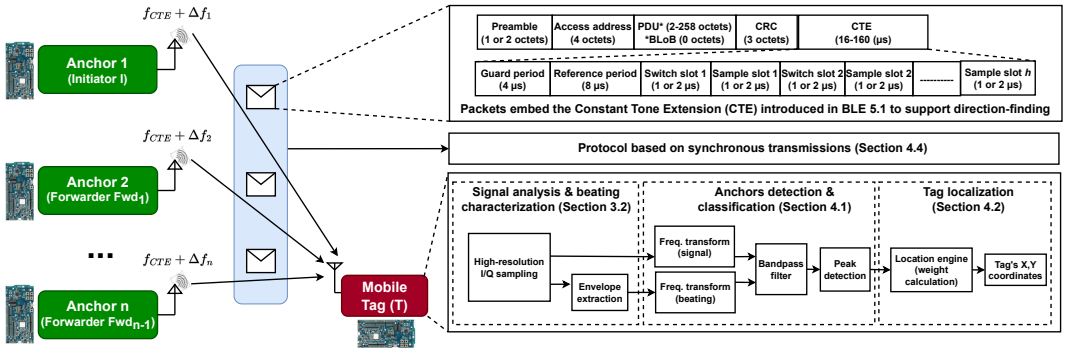

Figure 2.3: Overview of BLoB, a localization system that uses up to n spatially-separated *single-antenna* anchors synchronously transmitting packets embedding the CTE to localize *single-antenna* mobile tags by examining the beating characteristics across the received signal. One of the anchors acts as initiator (I) and is responsible for time-synchronizing all network operations.

The core idea of this chapter has been patented (please refer [102]), and the results were showcased at the prestigious 20^{th} International Conference on Embedded Wireless Systems and Networks (EWSN) in 2022, where they were honored with the 'Best Paper Award'.

2.4 BLoB: High-level Overview

This section provides a high-level overview of BLoB (Section 2.4.1), and a detailed description on how ST-induced beating using the *CTone* helps localization of single-antenna BLE mobile tags (Section 2.4.2).

2.4.1 System Overview

Figure 2.3 illustrates BLoB's architecture at-a-glance. In BLoB, spatially-distributed anchors equipped with a *single antenna* synchronously transmit identical packets with empty payload and CTE appended, following a ST-based flooding protocol (detailed in Section 2.5.4). Due to the presence of inherently imperfect crystal oscillators, the *CTone* signals are sent at slightly different frequencies from the intended center frequency by each anchor (Δf_i). Surrounding tags, also equipped with a single antenna, receive the superimposed *CTone* signal resulting from the synchronous transmissions and perform high-resolution I/Q sampling using up to $h = 148$ samples, as shown in Figure 2.2. Signal analysis and beating characterization is then performed on the collected I/Q samples (Section 2.4.2). This serves as input to anchor detection and classification (Section 2.5.1), and subsequently to tag localization (Section 2.5.2).

Table 2.1: Comparison of BLE-based localization techniques.

Method	Anchor(s)	Tag(s)	Operation
AoA	Single-antenna device transmits packets embedding the CTE	Multiple-antenna device captures the I/Q data of the CTE by switching between antennas	Receiving devices track other objects by measuring the phase difference of the received waveform at different antennas
AoD	Multiple-antenna devices transmit a packet embedding the CTE while switching through multiple antennas	Single-antenna device captures the I/Q data of the CTE	Receiving devices track their own positions by measuring the phase difference of the received waveform from different antennas
RF	Single-antenna device transmits packets that do not embed the CTE	Single-antenna device measures signal strength	Receiving devices track their own positions by estimating the distance based on the received signal strength and a reference signal strength
BLoB	Single-antenna devices synchronously transmit packets embedding the CTE	Single-antenna device captures the I/Q data of the CTE	Receiving devices track their own positions by analyzing the received signal strength at beating and signal frequencies

Hence, BLoB is fundamentally different from other BLE-based localization approaches, as summarized in Table 2.1.

2.4.2 Leveraging Beating for Localization

In BLoB, n anchor nodes synchronously transmit sufficiently-long (160 μs) *CTone* signals with frequencies $(\omega_1, \omega_2, \ldots, \omega_n)$ to produce beating, as shown in Figure 2.3. Mathematically, consider the *CTone* signals from n spatially-distributed anchors, represented as:

$$a_1 \cos(\omega_1 t), \ldots, a_n \cos(\omega_n t) \text{ and } CTone_i = a_i \cos(2\pi f_i t), \tag{2.1}$$

where ω is the angular frequency of the signal in radians and a_i is the amplitude of the i^{th} transmitted signal.

For beating to occur, the *CTone* frequencies $f_1, \ldots, f_n$ should not be equal to each other, and the separation between any two frequencies must not be equal, e.g., the *CTone* frequency can be chosen as:

$$f_i = f_{\text{CTE}} + \Delta f \quad \text{with} \quad \Delta f = (m * f_s)/L, \tag{2.2}$$

where f_{CTE} equals to 250 kHz, Δf is the frequency offset, f_s is the sampling rate, and L is the length of the *CTone* signal. The parameter m is an integer value, provided f_i should fall in receiver bandwidth. The frequency offset can be deliberately chosen using Eq. 2.2 to avoid side lobes interference; however, *the inherent CFO caused by the inaccuracy of crystal oscillators is sufficient to analyze beating in BLoB.*

The tag receives the superimposed *CTone* signal (SICT) resulting from the ST. Ignoring any channel impairments for simplicity, such a superimposed signal can be described as:

$$SICT = \sum_{i=1}^{n} A_i \cos(2\pi f_i t), \tag{2.3}$$

where $A_1, A_2, \ldots, A_n$ are the amplitudes of individual *CTone* signals after attenuation and as received at the mobile tag. To obtain the amplitude of the transmitted CTone signal frequencies, the receiver can use the Fast Fourier Transform (FFT) to analyze the signal spectrum of the received or beating signal. However, the method for extracting the pairwise contribution of the CTone signals in beating will be explained in the following section.

2.4.2.1 Envelope Extraction of the Beating Signal

To extract and analyze the pairwise contributions of anchors' amplitudes in the received beating signal, the tag extracts the *squared* envelop of the received superimposed ST-signal by taking the squared value of the Hilbert transform [103], which can be expressed as

$$\left| \text{Hilbert}\left(\sum_{i=1}^{n} A_i \cos(2\pi f_i t) \right) \right|^2 . \tag{2.4}$$

By applying an FFT on the envelope obtained with Eq. 2.4, one can characterize the resulting amplitude of beating frequencies and their corresponding power amplitudes, as sketched in Figure 2.4. Within the beating spectrum, one can identify a number of peaks, representing the contribution in beating from each pair of anchor nodes. Such contribution is strongly dependent on the tag's position: if the tag is closer to a given anchor, the amplitude of the peaks involving this anchor will be higher: `BLoB` call such an anchor a *dominant* anchor (or the corresponding beating frequency a *dominant* frequency). The maximum number of peaks in the beating spectrum is $\binom{n}{2}$. These peaks will be used together with the amplitude of the transmitted *CTone* signal frequencies for localizing a tag's position (see Section 2.4.2.2).

2.4.2.2 High-Resolution Tracking

The frequency power spectrum of the squared envelope of the received analytic signal can be expressed as (a comprehensive derivation is available in Appendix 8):

$$\begin{aligned} S_n(\omega) &= 2\pi \sum_{i=1}^{n} a_i^2 \delta(\omega) \\ &\quad + 2\pi \sum_{k>l} a_k a_l \left[\delta(\omega - \omega_k + \omega_l) + \delta(\omega - \omega_k - \omega_l) \right]. \end{aligned} \tag{2.5}$$

where k and l vary between 1 and n. S_n is the frequency power spectrum received from the transmitters, whereas $\delta(\omega)$ is a Dirac delta function at the frequency ω.

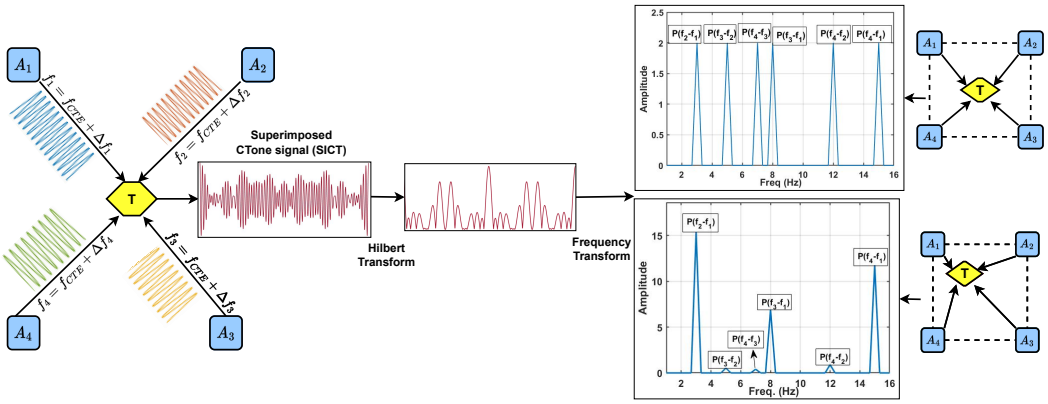

Figure 2.4: Principle behind beating-based localization- A *single-antenna* tag extracts the squared envelope of the received superimposed signal (i.e., deriving from the *synchronous transmissions* of anchors A_1, A_2, A_3, A_4 embedding a *CTone* sent at frequency f_1, f_2, f_3, f_4). This allows the tag to determine the contribution of the dominant anchors (by analyzing the highest peaks in the beating spectrum). The top-right figure depicts the case in which there is no dominant frequency in the beating spectrum (in fact, the tag is located at the same distance from all anchors). The bottom-right figure depicts a beating spectrum with a clearly dominant frequency, i.e., that of anchor A_1.

In BLoB, by examining the peak amplitudes of beating frequencies at $|\omega_k - \omega_l|$ (along with the signal frequencies ω_k, ω_l that capture the RSS information from the anchors), one can obtain additional information compared to classical RSS-based localization approaches (which only leverage RSS information without beating), and hence increase the accuracy of the localization system. In other words, the computation of the envelope and the extraction of the beating frequencies and amplitudes enables a tag to use additional $N(N-1)/2$ observations (on top of the N observations from the signal spectrum), resulting in a finer location estimate. Notably, the larger number of observations does *not* result in any additional traffic nor higher channel occupancy, and only leads to a negligibly larger expense in terms of signal processing. Section 2.5.1 details how to extract the dominant/true peaks reflecting the signal and beating amplitudes information.

2.4.2.3 BLoB in Principle

Consider $n = 4$ transmitted *CTone* signals with unit amplitude, represented as $\cos(2\pi f_1 t)$, $\cos(2\pi f_2 t)$, $\cos(2\pi f_3 t)$, $\cos(2\pi f_4 t)$ with *CTone* frequencies $f_1 = 2$, $f_2 = 5$, $f_3 = 10$, $f_4 = 17$ Hz. The tag receives a superimposed signal (Eq. 2.3) and performs the steps described in Section 2.4.2.1 to extract the amplitude of the signal at the beating frequencies and transmitted *CTone* frequencies. These steps are implemented in Matlab assuming a path-loss channel

model [104], and derive the illustration shown in Figure 2.4.

Specifically, Figure 2.4 (top-right) shows the single-sided power spectrum of the squared envelope of the received signal representing the frequency on the x-axis and the received power at those frequencies on the y-axis. A total of six peaks can be identified, i.e., $\binom{n}{2}$, corresponding to the absolute numerical difference between *CTone* frequencies. Moreover, the input CTone signals can be extracted directly from the signal spectrum i.e. by applying an FFT on the received signal.

This example assumes uniform power of all transmitted *CTone* signals. For this reason, in Figure 2.4 (top-right), where the tag is located exactly at the same distance from all anchors, the peaks corresponding to the six beating frequencies have the same amplitude. A change in the tag's position is reflected as a change in the peak amplitude of the beating frequencies. Figure 2.4 (bottom-right) shows an example where the tag moves closer to anchor A_1: in this case, the peaks related to A_1 are clearly dominant (i.e., their amplitude is higher). Note that this example assumed a perfect channel model with no impairments. In real environments, due to channel noise and multipath effects, there will be many other peaks in the received spectrum other than those at the anchor nodes' frequency. A method is therefore introduced to determine the true dominant peaks in the spectrum, followed by a section on performing localization using this approach.

2.5 BLoB: Design & Implementation

Next, the design and implementation of BLoB are detailed in this section, with an emphasis on anchor detection and classification in real-world systems (Section 2.5.1) and on tag localization (Section 2.5.2). Additionally, this section includes a modeling of BLoB and an analysis of its performance in Matlab (Section 2.5.3). Lastly, the ST communication primitive of BLoB (Section 2.5.4), which is utilized in the evaluation experiments detailed in Section 2.6, is presented.

2.5.1 Anchor Detection and Classification

The example in Section 2.4.2 assumes a perfect channel model with no impairments. In real environments, due to channel noise and multipath effects, there will be many other peaks in the extracted beating and signal spectrum other than those at the anchor nodes' frequency. Moreover, as BLoB exploits the CFO and does not tune the anchors' clocks, side lobe interference creates more challenges to detect the true peaks in the spectrum. A method

is thus derived that enables BLoB to determine the true dominant peaks in the beating and signal spectrum, effective in real-world environments.

2.5.1.1 Peak Searching

To determine the peaks in the beating and signal spectrum (which helps determine the number of anchors present in an ST-based network), BLoB performs the following steps:

(i) Determine all the local maxima values $L_{\max}$ and their neighbor local minima values $L_{\min_1}$, $L_{\min_2}$ in the received beating and signal spectrum. In the case of the signal spectrum (provided the transmitted *CTone* frequencies are known), the frequency corresponding to local maxima and minima should satisfy the condition:

$$|f_{L_{\max}} - f_{L_{\min_i}}| < \Delta f_{\min}\,, \tag{2.6}$$

where $f_{L_{\max}}$ and $f_{L_{\min_i}}$ are the signal frequencies corresponding to the local maxima sample point and nearest minima sample point to local maxima, respectively. $\Delta f_{\min}$ is the minimum CFO in the transmitted signal frequencies.

(ii) The local maxima found in step (i) should have amplitudes greater than a threshold T_1, which is empirically chosen (verified experimentally in Section 2.6) to be equal to 1/5 of the maximum received power in the signal spectrum. By setting this threshold, the unwanted spectral peaks and channel noise are eliminated.

2.5.1.2 Anchor Detection

BLoB exploits *both* the beating *and* the signal spectrum to determine the dominant number of anchors present in the network. Firstly, it finds the peaks in the unfiltered signal and beating spectrum and then configures the cutoff frequency of a fixed impulse response (FIR) filter based on the found peaks. The cutoff frequency for the FIR filter is calculated as follows:

$$f_{\text{lower}} = f_1 * \alpha_1, \quad f_{\text{upper}} = f_2 * \alpha_2, \tag{2.7}$$

where f_1, f_2 are the frequencies corresponding to the first and the last peak found in the spectrum, respectively, whereas α_1, α_2 are the redundancy coefficients [105]. Next, again search the peaks in the filtered spectrum. A decision about the total number of anchors present is made based on the peaks found in the filtered signal spectrum *and* in the beating spectrum. This method is called as `blended approach` (M_B), as it uses *both* beating *and* signal spectrum. For comparison, an alternative approach is explored that relies *solely* on the

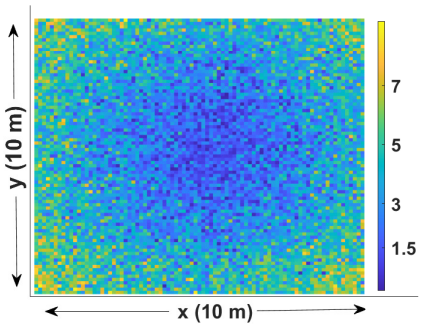

(a) Loc error using `freq approach` (M_F)

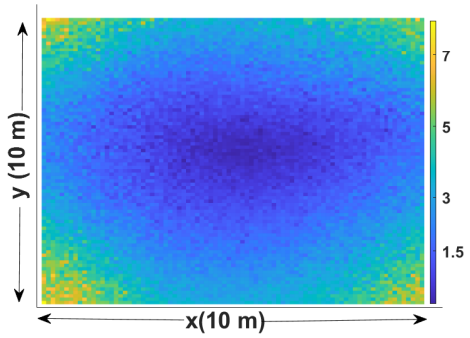

(b) Loc error using `blended approach` (M_B)

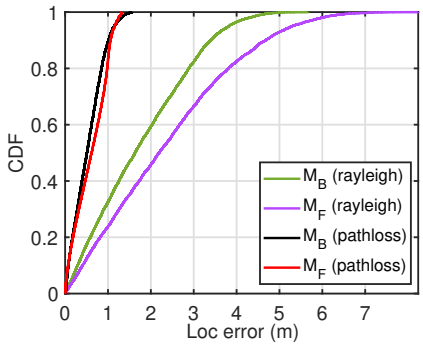

(c) CDF of the Loc error

Figure 2.5: Analyzing BLoB's localization performance under different channel models in a Matlab environment. The colour bars in Figures 2.5a and 2.5b represent the localization error in meters.

signal spectrum, specifically using only the amplitude at CTone frequency signals, without incorporating any information about the pairwise amplitude contributions from the beating spectrum. This method, akin to classical RSS methods, is termed as `freq approach` (M_F). In this approach, the peaks identified in the filtered signal spectrum are interpreted as the number of dominant anchors present.

2.5.2 Tag Localization

BLoB, calculates the tag's coordinates based on the amplitude of the received signals at the beating *and* signal frequencies from multiple anchors. Specifically, it uses a *weighted centroid approach* to determine the tag position, as BLoB has access to the amplitudes of individual anchor nodes and the contribution of pairs of anchor nodes.

Step 1 (weights calculation). Calculate the weights (W) corresponding to each dominant

synchronous transmitter using the peak amplitude (denoted as P) at beating and signal frequencies and assign the weights for the `blended approach`:

$$W(i) = \sum_{i,j=1,i\neq j}^{n} P|\omega_i - \omega_j| + P(\omega_i). \tag{2.8}$$

Step 2 (2D localization). The weighted 2D coordinates x_r, y_r of the mobile tag are computed as:

$$x_r = \frac{\sum_{i=1}^{n}(W(i) * x_t(i))}{\sum_{i=1}^{n} W(i)}, \quad y_r = \frac{\sum_{i=1}^{n}(W(i) * y_t(i))}{\sum_{i=1}^{n} W(i)}, \tag{2.9}$$

where $x_t(i), y_t(i)$ are the known coordinates of anchor A_i.

2.5.3 Preliminary Results from Simulation

To validate the algorithms presented in Section 2.5.1 and 2.5.2 as well as to further investigate how different profiles of beating and signal frequency amplitude affect the location estimates provided by the proposed approach, assume a 2D plane of 10×10 m^2 with 4 anchor nodes (A_1, A_2, A_3, A_4) at the four corners of the square plane. These anchors operate at 250 kHz, 257.69 kHz, 269.23 kHz, and 273.08 kHz *CTone* frequencies, respectively, chosen to satisfy Eq. 2.2. The length of the CTE packet used is 160 μs with a sampling rate of 8 Msps. The BLE packets embedding a CTE are generated in a Matlab-based BLE 5.1 simulator [106].

The tag captures the raw I/Q samples of the BLE packet, including the payload and CTE. The processing of the received signal to derive power amplitudes at beating and signal frequencies involves discarding the payload and focusing *only* on the CTE field in the packet for location estimation, meaning there is no requirement for payload data in `BLoB` (Section 2.5.4). Simulation of hundreds of tag locations is conducted to determine the location based on the proposed approach, taking into account the path loss [104] and Rayleigh fading channel model [107].

Figures 2.5a and 2.5b display the calculated Euclidean localization error (defined as $Er_i(i) = |l_k - l_{cal}|$, where l_k, l_{cal} are the known and calculated tag's position, respectively). These errors are calculated for the x, y coordinates of the tag at different positions using the `freq approach` and the `blended approach`, respectively. In the `freq approach` (*only* the signal frequency spectrum), the weight is assigned as: $W(i) = P(\omega_i)$.

The CDF derived over the Er_i of all location estimates for both methods is shown in Figure 2.5c under the path loss and Rayleigh fading channel models. Both methods perform well when the tag is located at the centre and receives equal power from all transmitters. However, the `blended approach` performs better when the receiver moves away from the centre

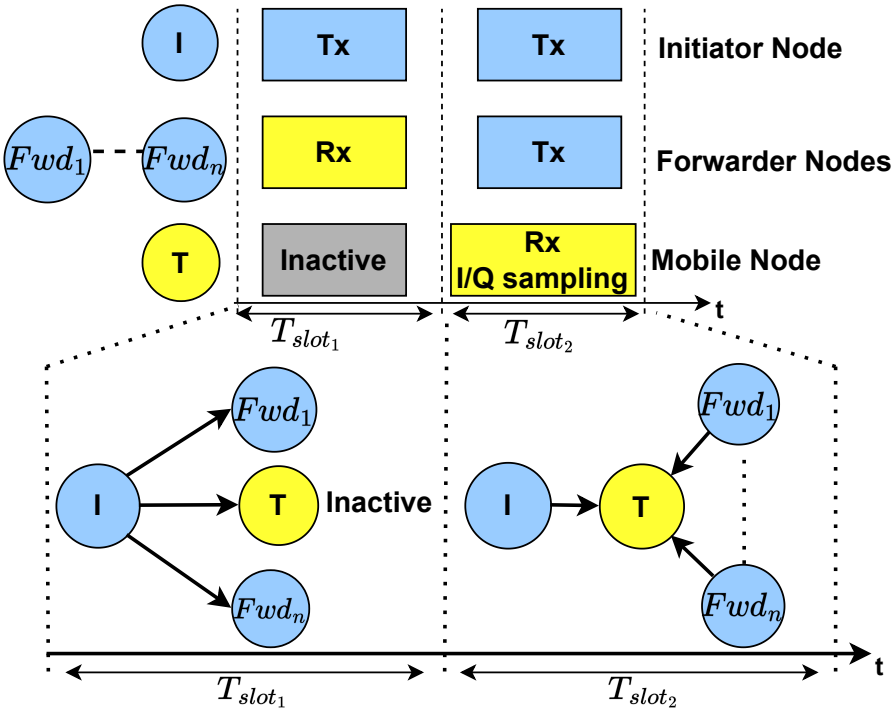

Figure 2.6: ST-based protocol used in BLoB. The tag (T) syncs on the first timeslot then localizes on the second.

position. The calculated mean localization error is 0.6 m and 3.6 m, for the `freq approach`, whereas it is 0.53 m and 2.3 m for the `blended approach`, under the path loss and Rayleigh fading channel models, respectively. This means that the additional information derived by considering the beating characteristics (pairwise contribution of each anchor's power) in the `blended approach` improves the localization performance *by up to 36%* compared to the `freq approach` (which is equivalent to conventional RSS-based localization).

The results mentioned above are obtained through simulation. To examine BLoB's performance in real-world conditions, an ST-based protocol is implemented on off-the-shelf BLE devices, as detailed in the following section.

2.5.4 ST-based Communication Primitive

Figure 2.6 illustrates the adaptation of an ST communication primitive to facilitate CTE-based analysis of the beating effect. Utilizing the direction-finding radio extension within the ST protocol, packets embedding a *CTone* are generated and received. In the initial time slot,

forwarders[2] serve as receivers for time synchronization; subsequently, in the next time slot, they begin synchronous transmission of *CTone* signals, with the receiver conducting I/Q sampling. The Nordic Semiconductors `nRF52833` SoC [108] has been enhanced to enable the radio's I/Q sampling capability, essential for obtaining raw baseband samples for signal beating analysis.

As antenna switching is *not required* in neither transmitters nor receivers, each device role is configured to expect its peer to be responsible for switching. As such, the transmitters are configured for AoA mode, while the receiver is configured for AoD mode. Other radio peripheral features leveraged include the ability to capture I/Q samples throughout the entire received packet, not just the CTE extension, and the option to over-sample with a 125 ns interval between samples [108]. It is important to note that while the `BLoB` concept primarily focuses on localization (using an empty payload), it can also support *simultaneous* communication and localization in an ST-based network, as long as the protocol allows for the *CTone* signals from different anchors to overlap.

Moreover, with an appropriate CTE length, beating detection across all BLE 5 PHY configurations is feasible, rendering the approach independent of the physical layer [3].

2.6 Experimental Evaluation

The performance of `BLoB` is experimentally evaluated, initially focusing on the accuracy of detecting and classifying dominant anchors (Section 2.6.1). Subsequently, the localization accuracy of `BLoB` in various environments is quantified, along with a performance comparison to the SOTA AoA technique (Section 2.6.2).

2.6.1 Detection of Dominant Anchors

The evaluation begins by examining the accuracy of `BLoB` in detecting and classifying dominant anchors. The evaluation seeks quantitative answers to these questions:

- Is the inherent CFO caused by the inaccuracy of crystal oscillators sufficient to discern anchors? (Section 2.6.1.2)

- Can dominant anchors present in the network be detected by leveraging the beating induced by the CFO? Do packet loss and antenna polarization affect the anchor detection accuracy? (Section 2.6.1.3)

[2] Within Nordic Framework transmitters other than initiator are called 'Forwarder' [108].

2.6.1.1 Experimental Setup

Experiments are conducted using Nordic Semiconductors `nRF52833-DK` boards in an office room, as depicted in Figure 2.7, with up to 7 anchors. To test `BLoB`'s anchor detection accuracy, four scenarios are considered:

(S1) Anchors and tag are in the same plane (as in Figure 2.7a) with the same antenna polarization;

(S2) Anchors and tag are in the same plane (as in Figure 2.7a) with different antenna polarization;

(S3) Anchors and tag are in a different plane (as in Figure 2.7b) with the same antenna polarization;

(S4) Anchors and tag are in a different plane (as in Figure 2.7b) with different antenna polarization.

2.6.1.2 Inherent CFO Detection

The study begins by investigating whether the inherent CFO, resulting from the inaccuracy of crystal oscillators, is adequate for differentiating between anchors in real-world settings. For this purpose, the *CTone* frequency shift due to CFO is measured and compared for several `nRF52833-DK` boards. Operating at a carrier frequency of 2.4 GHz, the expected baseband *CTone* signal spectrum should peak at f_{CTE}=250 kHz [42]. However, in practice, deviations occur, as shown in Table 2.2, with the CFO varying up to 11.69 kHz from the nominal *CTone* frequency of 250 kHz. These findings confirm the feasibility of distinguishing anchors based on their CFO in real-world settings. The CFO present across different anchors can be determined by following the below steps in `BLoB` and described in the Algorithm 1.

i. Turn on the initiator and follow the steps described in Sect. 2.5.1.1 to find the dominant peak in the signal spectrum. Assume that f_1 is the *CTone* frequency corresponding to the detected peak. As only the initiator is active, only one dominant peak should exist in the signal spectrum, and no beating should occur. If the detected peak does not correspond to f_{CTE}, CFO is present and equals $f_{CTE} - f_1$. Consider f_1 as the true *CTone* frequency.

ii. Determine the *CTone* frequency of each forwarder by keeping the initiator on and by activating one forwarder at a time, e.g., activate Fwd_1. Then, determine the dominant peaks in the signal spectrum. If two peaks are detected, the frequency corresponding to the new detected peak should be the *CTone* frequency of the considered forwarder (e.g., f_2 for Fwd_1).

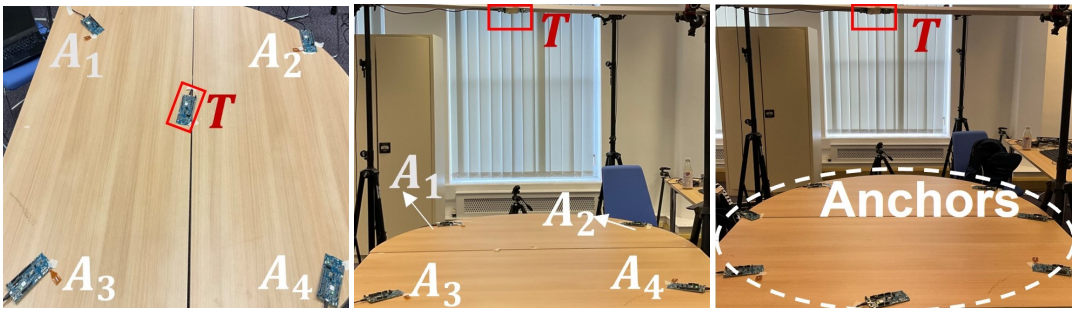

(a) Same plane (b) Different plane (c) Up to 7 anchors

Figure 2.7: Experimental setup used in Section 2.6.1.

If only one dominant peak is detected in the signal spectrum, then the beating spectrum is observed.

If the beating does not occur, then the considered forwarder shares the same *CTone* frequency with the initiator. If beating occurs, this implies that the difference between the frequency of the initiator (f_1) and of the forwarder (e.g., f_2 for Fwd_1) is too small to be distinguished in the signal spectrum. We then determine the dominant peak in the beating spectrum. Assuming the frequency corresponding to the detected dominant peak is Δf_{12}, the *CTone* frequency f_2 for Fwd_1 is calculated as $f_2 = f_1 \pm \Delta f_{12}$ with two possible values (e.g., 252 kHz or 248 kHz when Δf_{12}=2 kHz and f_1=250 kHz). To resolve the ambiguity, we can add a new forwarder: if the frequency of the latter is 255 kHz, then in the beating spectrum we will either find a peak at (255-252)=3 kHz or at (255-248)=7 kHz.

Importantly, while CFO is a property of the radio oscillator and is thus sensitive to environmental factors such as temperature variations, recent work has demonstrated that the relative CFO between synchronously transmitting devices can be predictably modeled and estimated as a function of temperature [98]. This supports the practicality of the proposed approach in harsh environmental conditions.

2.6.1.3 Anchor Detection

Next, task is to test BLoB's anchor detection accuracy based on the detection of dominant peaks which facilitate localization. Three configurations are considered for this purpose:

- *With CRC*: Only the CRC passed packets are considered and CRC failed packets are discarded.
- *Without (W/O) CRC*: Only failed CRC packets are used.

Algorithm 1 To examine CFO across anchors in BLoB

Require: Extracted Signal & Beating spectrum
Ensure: CFO for each anchor
1: Turn on initiator and find dominant peak f_1 using peak search algorithm described in § 2.5.1.1
2: **if** Detected peak is not f_{CTE} **then**
3: Set CFO as $f_{\text{CTE}} - f_1$
4: Set f_1 as the true *CTone* frequency
5: **for** each forwarder Fwd_i **do**
6: Keep initiator on and activate Fwd_i
7: Find dominant peaks in the signal spectrum
8: **if** two peaks are detected **then**
9: Set f_2 as the frequency corresponding to the new detected peak
10: Set f_2 as the *CTone* frequency of Fwd_i
11: **else if** only one dominant peak is detected **then**
12: Observe beating spectrum
13: **if** no beating occurs **then**
14: Fwd_i shares the same *CTone* frequency with the initiator
15: **else**
16: Identify dominant beating peak & assign its frequency as Δf_{12}
17: Calculate f_2 for Fwd_i as $f_2 = f_1 \pm \Delta f_{12}$ with two values
18: Resolve ambiguity by adding a new forwarder and observing the beating spectrum to determine the correct f_2

Table 2.2: Observed CFO on different nRF52833 boards. Device 685508885 (underlined) acts as initiator. Δf represents the detected CFO compared to the nominal 250 kHz value, whilst Δ_{init} captures the frequency delta w.r.t. the initiator.

Device ID	**Detected *CTone* freq. (kHz)**	Δf **(kHz)**	Δ_{init} **(kHz)**
685508885	252.453	+2.453	0
685557904	244.756	-5.244	-7.697
685939208	250.910	+0.910	+1.543
685695561	246.295	-3.705	-6.158
685435368	238.600	-11.40	-13.853
685083356	261.690	+11.69	-9.237
685465122	255.532	+5.532	+3.079

- *Both*: Both failed and successful CRC packets are used.

Four anchors are considered to simultaneously transmit *CTone* signals (as depicted in Figure,2.7a), with tags detecting dominant peaks in both the beating and signal spectrum. The analysis is conducted under two approaches: the *average peak* and the *average packet* approach. For the *average peak* approach, anchor detection accuracy is determined by the

Table 2.3: Anchor detection accuracy for *avg. peak* and *avg. packet* methods with four anchors with `freq` and `blended` approach.

Method	Scenario	With Cyclic Redundancy Check (CRC) (freq)	With CRC (blended)	W/O CRC (freq)	W/O CRC (blended)	Both (freq)	Both (blended)
Avg. Peak	S1	21.90%	99.42%	11.11%	100 %	18.65%	100%
	S2	19%	100%	20.66%	100 %	24.45%	99.18%
	S3	21.93%	98.83%	30.56%	100 %	18.21%	98.55%
	S4	20.94%	86.91%	31.93%	99.16 %	12.50%	89.17%
Avg. Packet	S1	25%	100%	75%	100 %	75%	100%
	S2	75%	100%	100%	100 %	75%	100%
	S3	100%	100%	100%	100 %	75%	100%
	S4	100%	100%	75%	100 %	75%	100%

Table 2.4: Anchor detection accuracy using *average peak* and *average packet* methods.

		Nodes						
		1	2	3	4	5	6	7
Avg. Peak	`Freq`	100%	19%	20.66%	24.45 %	3.47%	1.37%	0%
	`Hybrid`	100%	100%	100%	99.18 %	87.28%	84.96%	87.96%
Avg. Packet	`Freq`	100%	100%	100%	75 %	60%	33.33%	57.14%
	`Hybrid`	100%	100%	100%	100 %	100%	100%	57.14%

ratio of the total number of true dominant peaks detected in each received packet to the total number of anchors present. In the *average packet* approach, I/Q samples are averaged over 20 packets (Empirical Statistical Optimization) before determining the true dominant peaks. Table 2.3 presents the anchor detection accuracy (quantified as the number of times the detected peaks correspond to the actual number of anchors) from several hundred runs. The *average packet* approach proves more efficient as averaging reduces the impact of channel noise.

Corrupted packets. The beating effect may result in packet loss in a communication link [3]. Although, intuitively, this is undesirable, `BLoB`'s performance actually increases when considering the failed CRC packets, as the beating pattern will be more complex – hence leading to a higher detection accuracy, as confirmed from the results in Table 2.3.

Antenna polarization. Further, analysis reveals that changing antenna direction increases the number of CRC failed packets received at the tag (W/O CRC configuration). This results in more complex beating patterns, enhancing accuracy, as evident in Table 2.3. Furthermore, the results demonstrate that employing `BLoB` can achieve 100% anchor detection accuracy in most cases.

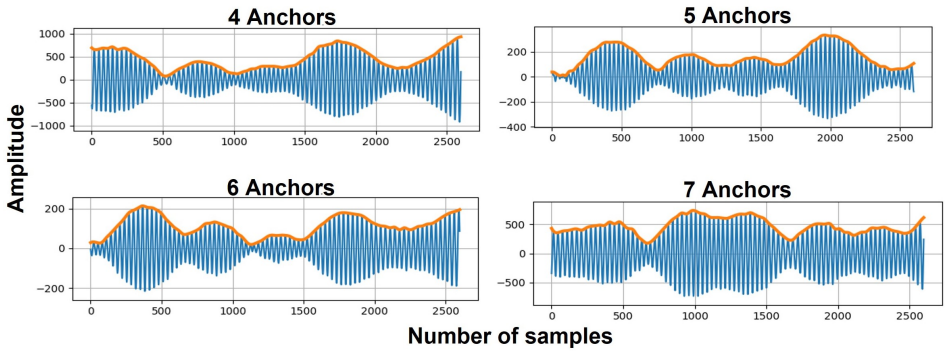

Figure 2.8: CTE-derived beating patterns at the receiver.

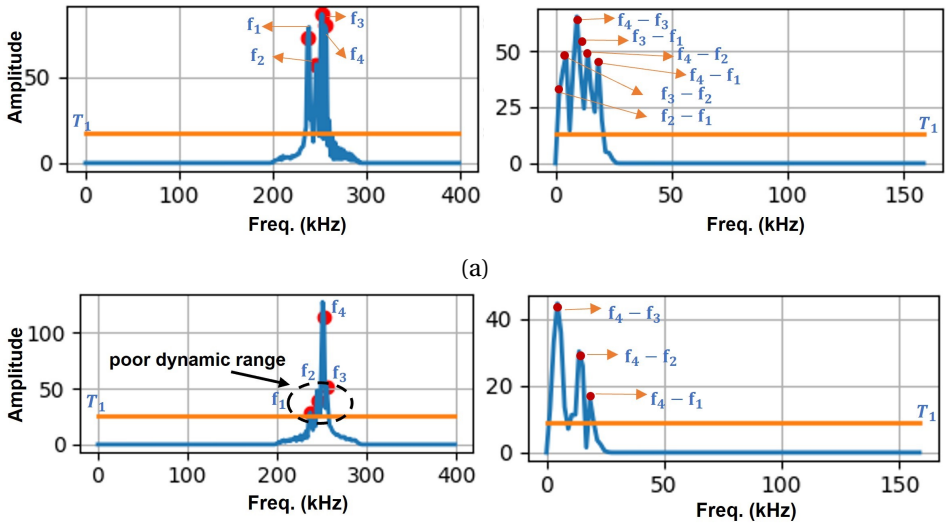

(a)

(b)

Figure 2.9: Office 1: Real-time received signal spectrum (left) as well as received beating spectrum (right) with 4 anchor nodes. Figure (a) refers to a tag placed in the middle of four anchors; Figure (b) refers to a tag is in close proximity to anchor A_4.

Maximum number of detectable anchors. The maximum number of nodes detectable with BLoB and the effects of adding more anchors on the beating signal are tested. The *Both* configuration (utilizing both failed and successful CRC packets) is considered in the S3 scenario. In this setup, node detection accuracy reached 100% for both the average peak and packet methods, as indicated in Table 2.3. To determine the maximum number of detectable anchors, the density of anchors in the network is incrementally increased by adding a new anchor in each successive run, as illustrated in Figure 2.7b. Each new anchor is positioned at an equal distance from the tag, with Figure 2.7c depicting the setup with seven anchor nodes. The introduction of each new anchor alters the beating pattern (refer to Figure 2.8), which impacts

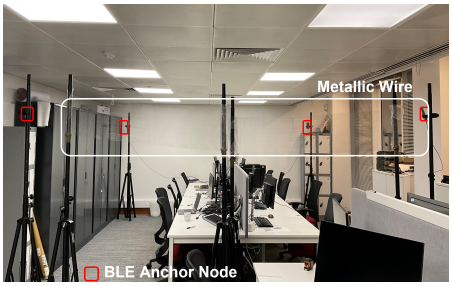

(a) Office 1 (metallic wire in x-direction, D_x)

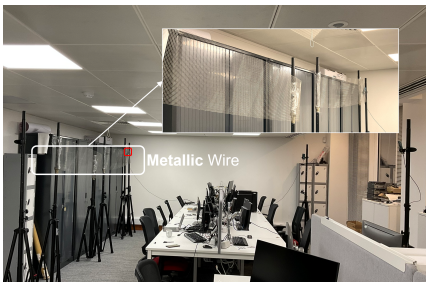

(b) Office 1 (metallic wire in y-direction, D_y)

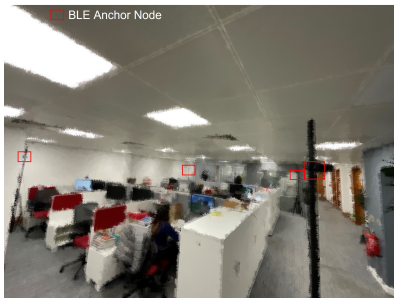

(c) Office 2

(d) Library

(e) Meeting room

(f) Sports hall

Figure 2.10: Environments used in the experiments in Section 2.6.2.

the accuracy of anchor detection. An analysis reveals that as the number of anchors increases, more peaks of varying amplitudes appear, and the intervals between valleys in the beating patterns decrease. Consequently, peaks begin to merge in the frequency spectrum, leading to reduced anchor detection accuracy. However, as shown in Table 2.4, BLoB successfully detects up to 6 anchors with an accuracy of 100% in the experiments conducted.

2.6.2 BLoB's Localization Performance

The evaluation of BLoB proceeds with an analysis of its localization performance, focusing on accuracy, robustness to harsh environments, and a comparison with the SOTA AoA approach.

The results provide quantitative answers to the following questions:

- How robust is BLoB localization in dynamic and multipath-rich environments? (Section 2.6.2.2 and Section 2.6.2.3)
- Does BLoB's performance remain consistent as the testing area increased? (Section 2.6.2.4)
- How does BLoB perform in mobile settings? (Section 2.6.2.5)
- Can BLoB achieve a performance that is comparable to AoA-based solutions even though it does not explore phase information? (Section 2.6.2.6)

2.6.2.1 Experimental Setup

To evaluate the localization performance of BLoB in realistic scenarios, various dynamic multipath-rich environments are being considered, listed in Table 2.5. These environments include offices, sports halls, libraries, and meeting rooms, each of which contains a variety of reflective and scattering objects such as chairs, desks, monitors, wardrobes, and RF-operated equipment, creating a *multipath-rich* environment. Four anchor nodes are placed in a square formation on tripods at a height of 1.8 m in the offices and sports hall, and on a table at a height of 1 m in the library and meeting room, respectively (see Figure 2.10). The tag is placed at randomly-distributed testing positions (denoted as N_{TL}) with varying amounts based on the environment being tested (as summarized in Table 2.5). At least 150 packets are collected at each position and the absolute error at each N_{TL} is calculated as the Euclidean localization error (E_r). Results are presented by averaging multiple combinations over time of 10 packets each and computing the CDF over E_r. It is important to note that all presented results are raw measurements only, without the use of any filtering techniques such as Kalman or particle filters.

2.6.2.2 Results in Static Multipath-rich Environments

The localization performance of BLoB is evaluated first in Office 1 without the addition of reflective objects. The real-time beating and signal spectrum with four active anchor nodes are visible in Figure 2.9a, with the localization performance test results presented in Figure 2.11a.

Role of antenna orientation. The robustness of BLoB is tested by evaluating its localization performance with different antenna polarizations in an office environment. As indicated in Figure 2.11a, the majority of errors (90%) remain below 1 m, with mean localization errors for horizontal (A_h) and vertical (A_v) antenna polarizations being 87.55 cm and 107.3 cm,

respectively. While antenna orientation typically impacts localization performance significantly [109], in BLoB, this impact is minimized due to the use of superimposed CTone signals to create beating – less affected by antenna polarization [110].

Addition of metallic wire. To further assess BLoB's performance in complex reflective environments, a dense/thick metallic wire is added at the same height as the anchor nodes in Office 1. Whilst not a full metal sheet, the fence is more than just a simple wire and adds significant reflections. Different placements of the metallic wire are tested: one in the x-direction (Figure,2.10a) and another in the y-direction (Figure,2.10b) relative to the setup. Figures,2.11b and,2.11c demonstrate that BLoB maintains sub-meter accuracy even in highly-reflective environments. Contrary to other BLE localization methods that rely on angular information or RSS [57], BLoB is capable of handling both low and high reflection environments by exploiting more sampling points and the beating effect.

Performance in the proximity of an anchor. The simultaneous ranging approaches are susceptible to *dynamic range* problems, as highlighted by [64, 65], particularly when the tag is in close proximity to the anchor node. To evaluate BLoB's performance in such scenarios, measurements are taken near the anchor A_4 (f_4) within a 1 m radius. Although the amplitudes of signals from other anchor nodes transmitting at CTone frequencies f_1, f_2, and f_3 in the signal spectrum are relatively low, the analysis of the beating spectrum (shown in Figure 2.9b) helps BLoB to determine the pairwise contribution of each anchor's power. As a result, an accuracy of 0.93 m is achieved, which is only 0.07% less than the mean average error obtained in this area.

Table 2.5: Mean BLoB localization error in different scenarios.

Environment		**Office 1**			**Office 2**	**Library**	**Meeting Room**	**Sports Hall**
		W/o metallic wire	Metallic wire	Blockage				
Area (m^2), Testing Loc. (N_{TL})		20, 52	20, 52	20, 20	15, 15	15, 20	10, 30	90, 30
Mean Loc. Error (cm)	`freq`	101.57	94.10	84.51	106.86	138.41	78.04	154.37
	`blended`	87.55	91.47	70.25	72.06	93.43	50.84	116.18

2.6.2.3 Dynamic Environment

Following promising results in Office 1, BLoB is evaluated in three additional dynamic environments with anchors placed at *different heights*: Office 2, a Library, and a Meeting Room, as depicted in Figure 2.10. The results[3], shown in Figure 2.11d, reveal that the Library environment exhibits more localization error (93.43 cm) compared to the others, attributed to the presence of multiple book racks and a metallic down-ceiling causing increased multipath.

[3]All presented results are averaged over different antenna configurations.

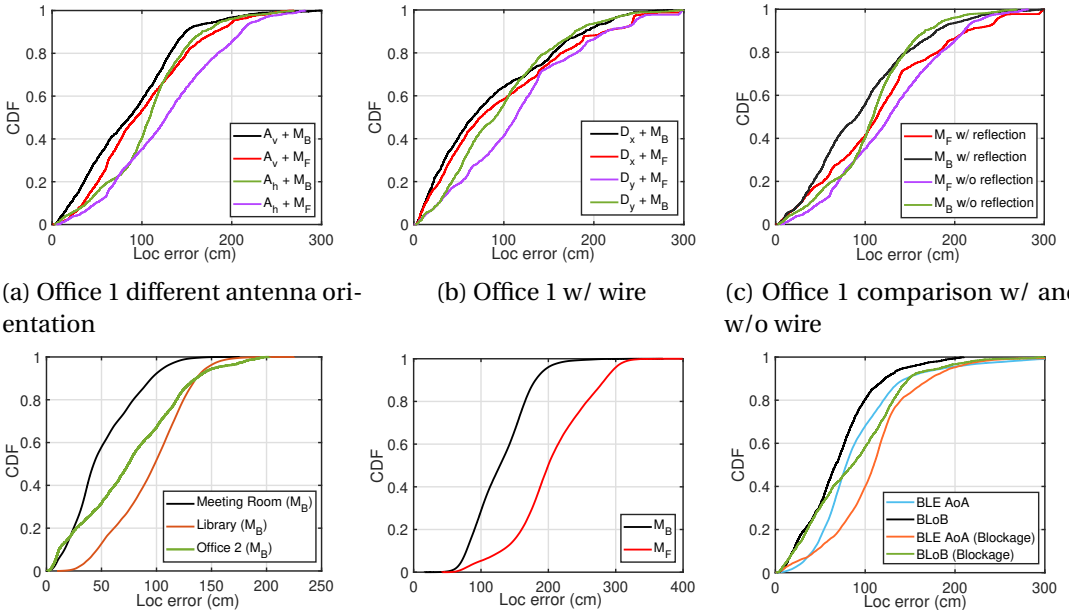

(a) Office 1 different antenna orientation

(b) Office 1 w/ wire

(c) Office 1 comparison w/ and w/o wire

(d) Different indoor environments

(e) Large environment

(f) BLoB vs BLE AoA

Figure 2.11: CDF of the localization error in different multipath environments. Office 1: different transmitter antenna polarization (A_v: vertical, A_h: horizontal) w/o metallic wire **(a)**, a metallic wire placed at different positions **(b)**, comparison of Loc. error of setup- with and w/o metallic wire placement **(c)**, Dynamic environment (considering `blended approach`): Library, Office 2, Meeting Room **(d)**, Large indoor tennis hall **(e)**, BLoB's localization performance compared to BLE's AoA technique. The latter uses bulky multiple-antenna arrays and yet achieves a comparable performance to BLoB, which is a single-antenna system **(f)**.

However, BLoB still achieves sub-meter accuracy. A performance comparison of BLoB with the SOTA solutions that utilize a constant tone is detailed in Table 2.6.

2.6.2.4 Large Environment

BLoB is further evaluated in a large sports hall, covering an area of $90m^2$, where it is being tested in one court while the adjacent courts are in use. Ground truth locations of the tag are provided by the highly-accurate Optitrack system [111]. Eight Flex13 motion capture camera systems are deployed as shown in Figure 2.10f. The Optitrack system, which can be calibrated within minutes, offers mm-level accuracy without requiring manual marking of fixed positions. Calibration is performed during the initial 5 minutes of the experiments, achieving a localization accuracy of 0.401 mm, significantly finer than what BLE typically achieves. The localization accuracy results for BLoB, illustrated in Figure 2.11e, demonstrate

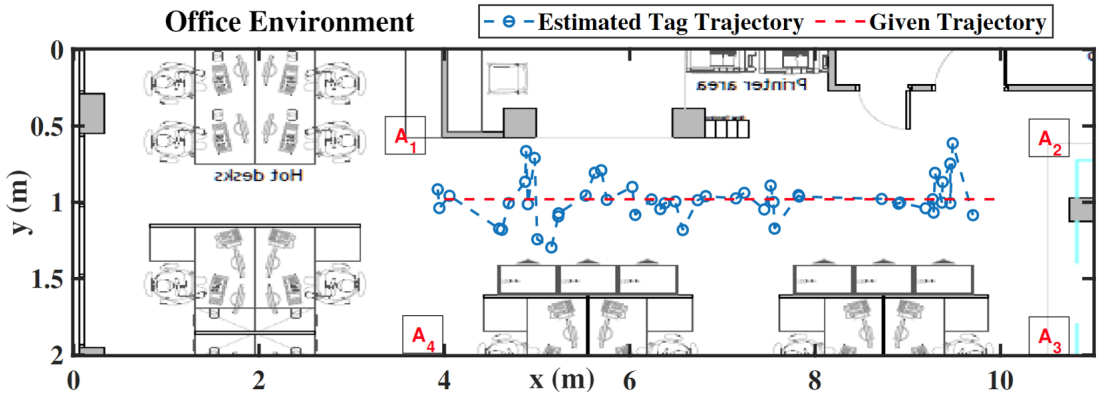

Figure 2.12: Mobility experiment in the Office 2 environment.

that 90% of localization errors are under 1.5 m, with a mean average localization error of 116 cm. These results validate the feasibility of using BLoB in large indoor public spaces.

2.6.2.5 Mobile Scenarios

To validate BLoB's performance in mobile scenarios, it is tested with a mobile target in the multipath-rich Office 2 environment during normal office hours (thereby introducing mild RF interference across the 2.4 GHz spectrum in the form of everyday office activities). As shown in Figure 2.12, anchors were placed at A_1 to A_4, creating a 7 m by 1.5 m arena, while the tag was placed on an autonomous robot which moved 6 m along a predefined linear trajectory (this indicates by the red dashed line) from right to left across the middle of the arena. The estimated tag trajectory from BLoB is shown in blue, and from 45 samples the mean estimated localization error obtained with the mobile target was 96.58 cm. While this does not represent a full study of BLoB's performance in mobility conditions, this indicated the viability of BLoB's sub-meter localization accuracy in real-world mobile scenarios.

2.6.2.6 BLoB vs. AoA-/AoD-based systems

The localization performance of BLoB is now demonstrated to be comparable with AoA-based direction finding solutions, *despite* its reliance solely on single antennas and the consequent non-utilization of angular information. When using AoA, a tag is equipped with multiple antennas controlled using an RF switch. By measuring the phase difference observed at the multiple antennas, the tag can locate a transmitter's direction, and perform trilateration to find its position coordinates. If the separation between antennas is known, the AoA is computed

Table 2.6: Comparison of localization error in SOTA.

SOTA	Technique	Multi-Array / Single Antenna	Mean Error
Farnham [114]	AoA	Multi	2.5m
Qian et al. [57]	AoA	Multi	$> 10^{\circ}$
Rinaldi et al. [115]	AoA	Multi	$> 20^{\circ}$
He et al. [116]	AoA	Multi	$> 5^{\circ}$
Cominelli et al. [40]	AoA	Multi	0.85m
Pau et al. [56]	AoA & RSS	Multi	0.70m
BLoB	RSS-CT	Single	0.55m

using Eq. 2.10:

$$\theta_A = \arccos((\phi\lambda)/(2\pi D)), \tag{2.10}$$

where λ is the wavelength, ϕ is the phase difference, and D is the distance between adjacent antennas in the antenna array. To evaluate AoA's performance, four multiple-antenna arrays are used in Office 1, placing the tag in identical locations where BLoB was tested, using Silabs EFR32xG22 boards [58] and Silabs' AoA implementation [4, 112, 113]. Figure 2.11f presents the results: BLoB achieves a comparable localization performance to that obtained using AoA, also in challenging *non-line-of-sight* (NLOS) conditions (the tag is getting obstructed from two anchors due to the boundary between two tables, see Figure 2.10a). Specifically, BLoB exhibits a 50% error of 87.55 cm, whereas AoA-based localization exhibits an error of 95.72 cm. In NLOS conditions, the difference in error is $\approx$ 18.66 cm in favor of BLoB.

2.7 Discussions & Limitations

This section discusses additional features and benefits of BLoB, along with its main limitations.

Minimizing channel occupancy. The use of ST reduces the number of transmissions over the air and thus reduces signaling overhead incurred system, *minimizing* channel occupancy. This is a key advantage of BLoB in comparison to classical systems which rely *only* on RSS: the latter require individual responses from each anchor, whereas in BLoB all anchors synchronously transmit a response embedding a CTE, pictorially represented in Figure 2.13.

Example: How BLoB scheme compares against legacy schemes from an operation point of view and key performance metrics such as latency and radio resource utilization can be elaborated with a simple example setup consisting of 4 anchors (A_1, A_2, A_3, A_4) and 1 mobile tag.

RSS based localization: This requires many transmissions at various times. These include:

- Request from T to anchor A_1, Response from A_1 to T, T records the RSS

- Request from T to anchor A_2, Response from A_2 to T, T records the RSS
- Request from T to anchor A_3, Response from A_3 to T, T records the RSS
- Request from T to anchor A_4, Response from A_4 to T, T records the RSS

T process all the RSS and coordinates of anchors to estimate its position. The process concludes in time at least long enough to complete eight over-the air transmissions.
BLoB localization:

- Either T or a dedicated anchor A_i sends a CTE request
- All anchors on receiving it transmit a CTE response concurrently
- Mobile tag T receives the concurrent CTE response and applies the signal processing, and estimates its coordinates

The process is concluded in the time needed to complete two over-the-air transmissions over a single channel. The RF footprint in time (channel occupancy) is short to complete such transaction even on the congested Bluetooth advertising channels, the three special ones out of 40 channels.

Frequency diversity. *BLoB can localize an unlimited number of devices in an extremely short time while benefitting from the frequency diversity over a single narrowband channel.* This diversity is extracted from the frequency spectrum, providing diversity in frequencies denoted as $f_1, \ldots, f_n$. Additionally, the beating spectrum contributes to even more diversity, resulting in a total of $N + (N \cdot (N-1)/2)$ frequency components, all within a single 2 MHz channel. This comprehensive frequency diversity leads to enhanced localization accuracy. Furthermore, when employing multiple concurrent transceivers with frequency diversity, BLoB exhibits resilience against Wi-Fi interference. The frequency diversity continues to increase as the number of anchors increases, as demonstrated in Figure 2.14. This increase will not occur without the beating spectrum exploration.

Scalable and privacy-preserving localization. Similar to GNSS-based systems, in BLoB mobile tags are not actively involved in the communication and hence do not disclose their presence. In other words, BLoB enables *fully-passive* localization that preserves the user's privacy and allows to potentially support countless tags. Moreover, BLoB does not suffer from the disadvantages of AoA/AoD-based systems, where it is challenging to verify the truthfulness of transmitted CTones in such systems, a change in phase introduced by an attacker can cause a significant shift in the AoA [40].

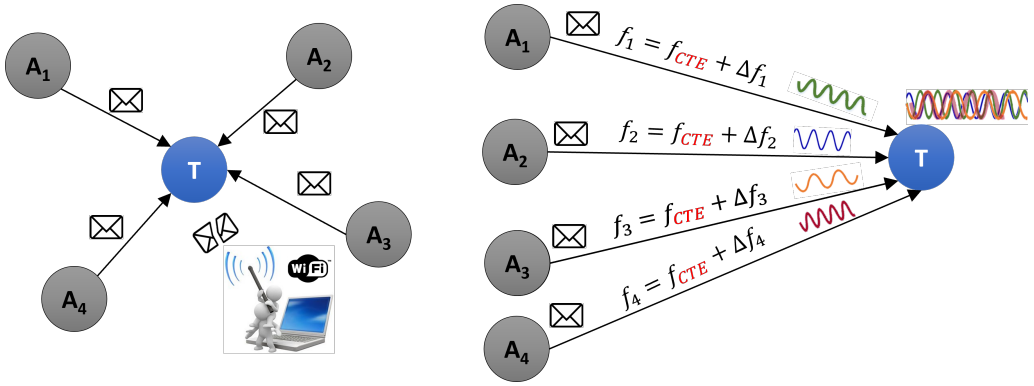

Figure 2.13: Comparison of TDMA and BLoB localization Approaches: On the left, each anchor uses different frequency channels and transmits sequentially in a time-division manner. On the right, all anchor nodes transmit synchronously with inherited CFO from each other.

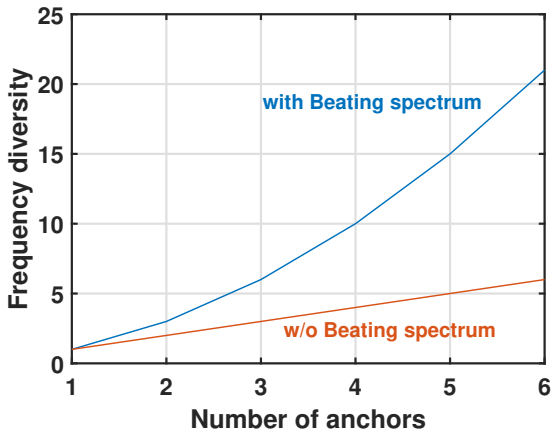

Figure 2.14: Frequency Diversity in BLoB as the Number of Anchors increases within a single narrowband channel.

Channel hopping to improve performance. In BLoB's implementation, channel hopping is employed to average out I/Q performance across multiple fading scenarios. Since the beating spectrum depends on the carrier frequency of all transmitters, averaging out I/Q samples taken across multiple channels enhances the likelihood of sampling a combination that yields larger beating amplitudes.

Computational complexity. Currently, the signal processing in BLoB is carried out on MATLAB based on the traces obtained with the actual BLE boards. However, the signal processing algorithms employed by BLoB are relatively lightweight, and can be implemented on dual-core BLE-based SoCs such as the nRF5340 by utilizing the second core and the ARM CMSIS-DSP accelerated library to perform the FFT operations required for the algorithm. Such an

embedded prototype of BLoB will be implemented in future work.

Dynamic range. The beating amplitudes extracted at the $|\omega_k - \omega_l|$ frequencies can be useful in addressing the dynamic range issue in ST-based localization methods [64, 65]. This issue occurs when the signal strength from one anchor node is much higher than that of other sources, resulting in signal clipping and making it challenging to accurately measure the RSS or the time difference of arrival between the signals. By using beating extraction in BLoB, the pairwise contribution of each anchor's power can be determined, aiding in the calculation of the received power of every anchor node.

2.8 Related Work

BLE-based localization. In the pioneer study of BLE 5.1 AoA [40], the authors successfully demonstrated the effectiveness of the technique on USRPs, achieving sub-meter accuracy. However, the testbed scenario was limited to an outdoor environment with few multipath reflections, and the accuracy was calculated by averaging over a large number of packets (1200 phase delay points), resulting in high computational complexity and difficulty in reproducing real-time results. Another experimental demonstration of AoA using SiLabs boards [58, 113] was performed in [56], where the authors reported an average distance error of $0.7m$ using a hybrid solution based on RSS and AoA. However, this study was limited to only *eight* static locations, positions were averaged over 48 packets, and the tests were conducted in a single controlled environment with no consideration for multipath interference. A study by Rinaldi et al. [115] examined the effect of distance on AoA direction-finding techniques for localization in industrial environments. It was found that the angular error increases with distance (even beyond 10 degrees), and that it largely depends on the polarization of the antenna array. Shuai et al. [116] studied the impact of multipath, noise, and antenna switching on AoA calculations, finding an angular error of 12.1 degrees. To mitigate this, two algorithms based on non-linear recursive least square and unscented Kalman filter were proposed, resulting in an improvement of 7.1 degrees for line-of-sight. Finally, it has been observed that direction-finding techniques are highly impacted by channel selection [57, 117]. For instance, [40] studied the impact of channel hopping on AoA and found that the angular error spreads more at lower frequencies. In this context, BLoB, overcomes the current hardware restrictions of AoA/AoD techniques, and has been thoroughly tested in multipath-rich environments with both static and mobile targets, where it sustains sub-meter accuracy.

UWB-based localization. Ultra-wideband (UWB) systems are known to achieve a high localization accuracy thanks to their fine-grained timing resolution [64, 118, 119, 120]. UWB

radios can in fact process ultra-narrow impulses of 2 ns and precisely estimate the channel impulse response (CIR). By applying signal processing on the CIR, a mobile tag can extract ToA information, which – combined with the known coordinates of the anchors – allows to estimate its position with cm-level accuracy. Unfortunately, narrowband systems such as those based on BLE do not benefit from the fine time resolution and the advanced hardware features present in UWB radios. Nevertheless, BLoB achieves sub-meter localization using BLE, a far more ubiquitous technology than UWB.

Other wireless localization technologies. Wi-Fi can provide high-resolution indoor localization systems [33, 24]. However, its high power consumption and the need of special chips for beamforming and time-of-arrival analysis limits its wide adoption [121]. The performance of LoRa for localization is heavily affected by the signal configuration and the environment [122, 123]. Simka et al. [124] reported that the localization error increases by 1.23 m using low-bandwidth signal configurations. Moreover, LoRa's localization performance degrades for short distances and in indoor applications, making it unsuitable for indoor localization at sub-meter accuracy [125, 126].

2.9 Concluding Remarks

This chapter has capitalized on BLE's constant tone extension feature and the beating effect from synchronous transmissions to develop BLoB, a novel BLE-based localization system that can localize mobile tags with sub-meter accuracy using small, inexpensive *single-antenna* devices, without the need for angular information. BLoB has been assessed through simulation and real-world experiments in various indoor settings, including multipath-rich environments, and in both static and mobile contexts. The research findings indicate that BLoB's performance surpasses traditional RSS-based methods and is on par with AoA-based systems, which depend on more complex, costly multi-antenna arrays. Therefore, BLoB is a practical solution for many IoT use-cases where bulky multi-array antennas are impractical. However, certain applications require decimeter-level precision, a level of accuracy challenging to achieve with BLE technology, whether through RSS or angle-based methods. The intrinsic operating frequency of BLE, increased vulnerability to multipath interference, and hardware clock limitations are significant barriers to such precision. To overcome these challenges, combining BLE with another technology that inherently mitigates these issues is a promising approach. The upcoming chapters of the thesis are dedicated to explaining optical localization solutions, specifically designed to enhance BLE localization with the goal of achieving decimeter-level accuracy. To ensure a thorough understanding, the next chapter offers a detailed background on this optical technology, presenting the current SOTA.

CHAPTER 3

EMERGING PASSIVE VLP SYSTEMS

This chapter provides a comprehensive overview of emerging passive Visible Light Positioning (VLP) systems, with a special emphasis on passive-VLP to enhance the reader's understanding. It begins with a classification of *p*-VLP systems as detailed in Section 3.2. This classification, based on the types of passive elements and receivers, draws from the framework proposed by Wang et al. [80]. Following this, there is an extensive survey of the most recent advancements in *p*-VLP systems, categorized according to this established classification. The focus then shifts in Section 3.3 to explore various commercially significant applications. This section examines how the SOTA *p*-VLP systems are tailored to fulfill the requirements of these applications. Additionally, Section 3.4 presents a comparative analysis of different passive positioning systems, highlighting their performance based on real-world system implementations, to offer a practical perspective of these technologies. The chapter concludes by addressing the ongoing challenges that *p*-VLP systems face in gaining wider commercial acceptance. The outcome of this chapter are published and presented at the ACM Workshop on Light Up the IoT, co-located with ACM MobiCom 2021.

3.1 Introduction

VLP is a technology that can accurately locate people and objects using light. It works by using common light sources like LEDs or Fluorescent Lightss (FLs) to send data and location information through visible light. To do this, the light from these sources is modulated to carry location signals. On the receiving end, a device sensitive to light, such as a PD or a camera,

detects these changes in light to determine the location.

However, not all light sources are suitable for modulation. VLP systems that use actively modulated light sources to send data to light sensors are called active VLP systems. Despite their potential, active VLP systems face a few challenges that have limited their commercial interest. Some of these limitations are:

- **High infrastructure changes:** On the transmitter side, these systems demand custom-designed light sources with a controller capable of modulating the light. Updating existing light fixtures with these controllers incurs extra cost and deployment effort, making commercialization difficult.

- **Complexity:** Many active VLP systems need to collect different light features and perform extensive signal processing to accurately estimate the position. Complex hardware on both ends of communication link increases the overall cost.

- **The burden on the user:** The users of an active VLP system require carrying an optical sensing unit for positioning. Although mobile phone cameras are pervasive and abundant, users are confronted with their high power consumption and privacy concerns. Furthermore, the requirement of holding the mobile in the direction of light sources to receive location estimates is a cumbersome task. This limitation also exists in *p*-VLP mainly where the receiver is an active device, more details are provided in Section 3.2.

In *p*-VLP information can be sent even without modulating the light source and the user may or may not have to carry a light-sensing device for receiving the location beacons. The *p*-VLP systems offer the following benefits:

- **Device-free localization:** *p*-VLP systems enable localization without requiring users to carry any light sensing device. Light reflection or shadows caused by their body are used for locating them.

- **Security:** In passive user systems, there is no need for users to keep personal gadgets like mobile phones for estimating their position.

- **Energy efficiency:** Most of the *p*-VLP systems capture the light signals using PDs, which consume significantly less power (μW) than cameras. Moreover, in *p*-VLP systems either the transmitter end or the user is passive resulting in more energy-efficient design compared to the active systems in which both sides have active elements.

- **Less infrastructure changes:** In *p*-VLP systems, there is no need for specially designed light sources with a controller. The already installed lighting fixtures can be used as a source without any modifications.
- **Cost-effectiveness:** The use of low-cost PDs and the need for fewer infrastructure changes make *p*-VLP systems cost-effective alternatives to active systems.

3.2 Architecture and Taxonomy of passive-VLP Systems

3.2.1 Architecture

The architecture of *p*-VLP systems consists mainly of three components: a light source, user, and receiver. The light source can be man-made like incumbent FLs, LEDs or natural light sources like the sun. The receiver is a light-sensing device usually a PD or camera referred to as 'Rx' in this chapter. The user can be a human, robot, or any object like a carton box in a warehouse, etc.

3.2.2 Taxonomy

p-VLP systems are classified based on types of transmitter and users' involvement into three categories: passive source, passive user and fully *p*-VLP systems as shown in Figure 3.1. Like the work presented in [80], a light source is defined as *passive* if it only provides illumination and *active* if it *also* modulates data. The user is considered active if it carries a light-sensing device and passive otherwise [1]. Figure 3.1 (a) represents an active VLP system in which the user is localized with the help of one or multiple deployed active light sources and an active light sensing device carried by the user. Based on the received modulated information, the user locates its position. On the other side, *p*-VLP systems do not always need an active light source. The light operation and user involvement solely depend upon the type of *p*-VLP system. Furthermore, *p*-VLP systems are classified into types of receivers namely PD-based systems and camera-based systems as shown in Figure 3.2. The next section briefly describes each type of *p*-VLP system with examples from the research literature.

3.2.2.1 Fully Passive

In fully passive systems, neither the light fixtures modulate the location beacons nor users carry any photosensor. Instead, typical unmodulated light sources present in indoor spaces such as bulbs and sunlight from windows, etc, are used for positioning purposes. As a user

[1] Passive user localization is also synonymous to *device-free localization* or *non-cooperative localization.*

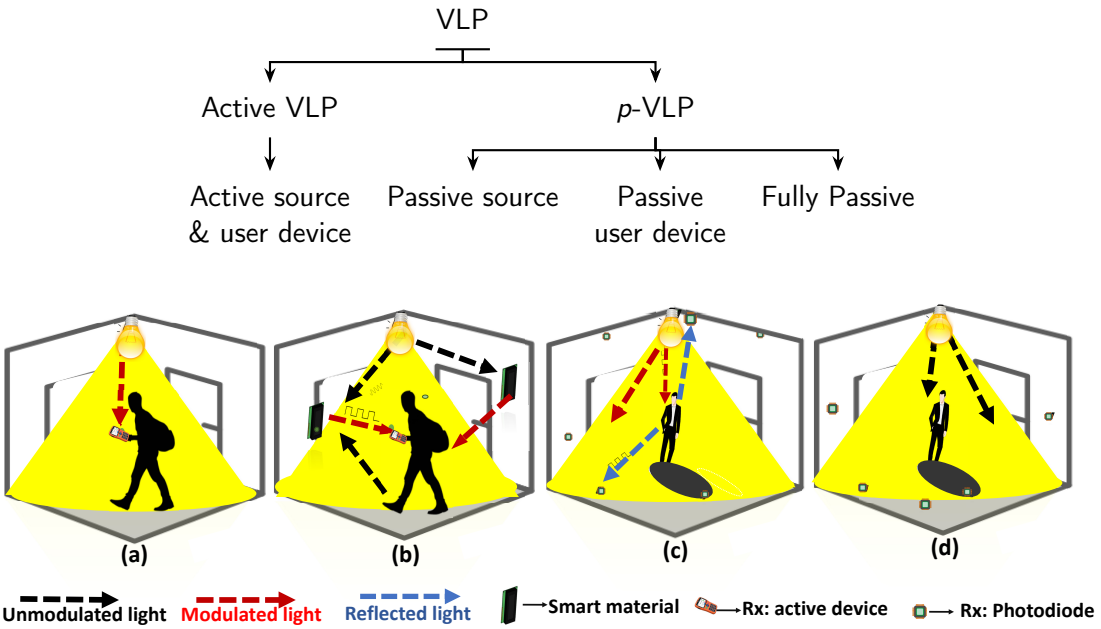

Figure 3.1: Different classes of VLP systems: (a) *Active VLP* systems require active modulated light sources and an active user device. (b) *Passive source* systems employ unmodulated light sources but rely on intelligent materials/devices to modulate the light sources. (c) *Passive user* systems do not require a target to carry an active user device and monitor the shadow of the target using modulated light sources and ambient photosensors for localization. (d) *Fully passive* systems neither require modulated light sources nor active user devices to track the target, albeit through ambient photosensors.

moves around, it blocks the light and produces a shadow. The shadows of the users are of varying intensity. This causes a change in the light intensity at different points in the room. The light sensors placed in the room measure these changes and estimate the user's actual position and/or room occupancy status. Such light sensors can be placed at different places in the room.

Systems: LocaLight [127] is a fully passive localization system that embeds co-located PDs and RFID sensors on strategic points on the floor to localize users using their shadows. The receivers are battery-free and harvest energy intermittently from the incident RF signals generated by RFID readers. Due to a lack of continuous energy supply real-time positioning is not possible. For the same reason, the performance of successfully detecting a target depends on its speed. SmartWall [128] also exploits shadows but embeds PDs on the wall to estimate the user's location based on a fingerprinting technique and machine learning. Specifically, Weighted k Nearest Neighbor (WKNN) classification is employed on the RSS values to predict real user position at the inference stage. The system only locates the objects and is further

extended in WoW [129] to track moving targets. However, both systems require extensive manual effort on fingerprinting. To reduce the dependency on labeled training data and fingerprinting, FieldLight [130] makes use of artificial potential fields along with light sensors to localize the target. While all the above systems exploit shadows other fully passive systems use reflections. CeilingSee [131] converts the ceiling LEDs so that these can also sense energy reflected back from the targets. Variance in diffuse reflection only helps the LEDs to detect occupancy but not estimate the target location. The presence of multiple targets under Field Of View (FOV) of light causes interference and thus can degrade the detection of occupancy.

3.2.2.2 Passive User

In passive user systems, the user is not equipped with any light-sensing device. The user's involvement in locating its position and occurrence is passive. However, the light source modulates the data and transmits positioning beacons. The light reflections and shadows caused by the user's body are used to locate its position. Compared to the fully passive systems, the passive user systems dominantly exploit reflections. The reflected received data is decoded by the receiver circuitry to retrieve the user position. The receiving sensors can be placed anywhere in the targeting area similar to fully-passive systems.

Systems: The work done in [132] is an example of a passive user system which modifies the light driver circuit to send a time-multiplexed signal to recognize the source of reflected light at each sensing device and based on a threshold user occupancy is detected. Similarly, EyeLight [133] sends on-off modulated data through the lighting device to check if the target has crossed the light barrier or not. Instead of modulating the one LED, the StarLight [134] approach modulates each LED in a custom-designed light panel and embed the sensing device on the floor. Based on the shadow it measures the frequency power changes, based on which the user's movement and gesture are detected.

3.2.2.3 Passive Source

In passive source systems, the light sources do not modulate the positioning beacons instead, an intelligent or smart material chip is placed in an environment to modulate the light. The smart material can be made of a polarizer, Liquid Crystal Display (LCD) and birefringence material [135], etc. As light passes through these materials it changes the light properties such as polarization, etc. These changes although unperceived by humans are then detected by active receivers to estimate their position. The chip can be placed at suitable locations in the room to modulate room light and even close to a window to modulate the natural sunlight. System performance not only depends on the reflection or blockage of light but

is also sensitive to user device handling dynamics related to its alignment and orientation towards smart material chips.

Systems: RainbowLight [135] and PIXEL [78] are two pioneer passive source systems. Both use polarization-based modulation. PIXEL exploits a mobile camera as a sensing unit and an LCD-based smart chip to do a binary color shift keying modulation. However, to detect the color light changes a polarizer is also placed in front of the camera. On the other side, RainbowLight's modulating chip consists of a birefringence and polarizer material which produce a specific interference pattern of the light spectrum at different directions to the chip when light passes through it. An initial mapping between chip direction and received light spectrum by a mobile camera at various positions of a mobile device is built. This procedure is done once for every chip and compared with these initial mapping values, the users' 2D position is estimated. Further, to improve the initial mapping an interpolation-based method is proposed. For the 3D position calculation of the device, an intersection-based method is developed which makes use of 3 chips to locate the device. The above two systems are camera-based approaches that need to put a special material in front of the camera. To overcome this limitation PD-based receivers are used in other passive source systems such as CELLI [136]. CELLI uses the principle of spatial resolution to find the position of a mobile device. It sends parallel interference-free polarized beams through the LCD pixels to different spatial cells. The transmitted beams are unique to the projected cell. The user in the projected cell carries a PD-based receiver to recover its unique cell coordinates. However, with this, the user does not know its actual position for calculating the actual position a two-lens strategy is used which makes this system a complex one.

Alternative passive source systems exist that do not require the placement of intelligent surfaces or materials in the environment. Instead, these systems utilize the unique intrinsic features of light sources for identification, aiding in localization. The effectiveness of such systems hinges on the distinctiveness of the extracted features. However, there can be challenges, as multiple light sources may share similar intrinsic features.

Systems: LiTell [137] identifies a unique 'light fingerprint' by capturing high-frequency signals from the ballast (a device placed in series with a load to limit the current driving the light source) of fluorescent bulbs, known as their characteristic frequency. This process requires high-resolution cameras, leading to high power consumption. On the other hand, Pulsar [138] employs the characteristic frequency of LEDs but uses a different approach. Instead of cameras, it employs an intricate setup involving several PDs, which, while avoiding cameras, results in significant computational demands. Another method, iLAMP [139], distinguishes light sources through their spatial-radiation pattern, essentially the pattern of light intensity distribution. This technique also depends on power-intensive cameras and ambient light

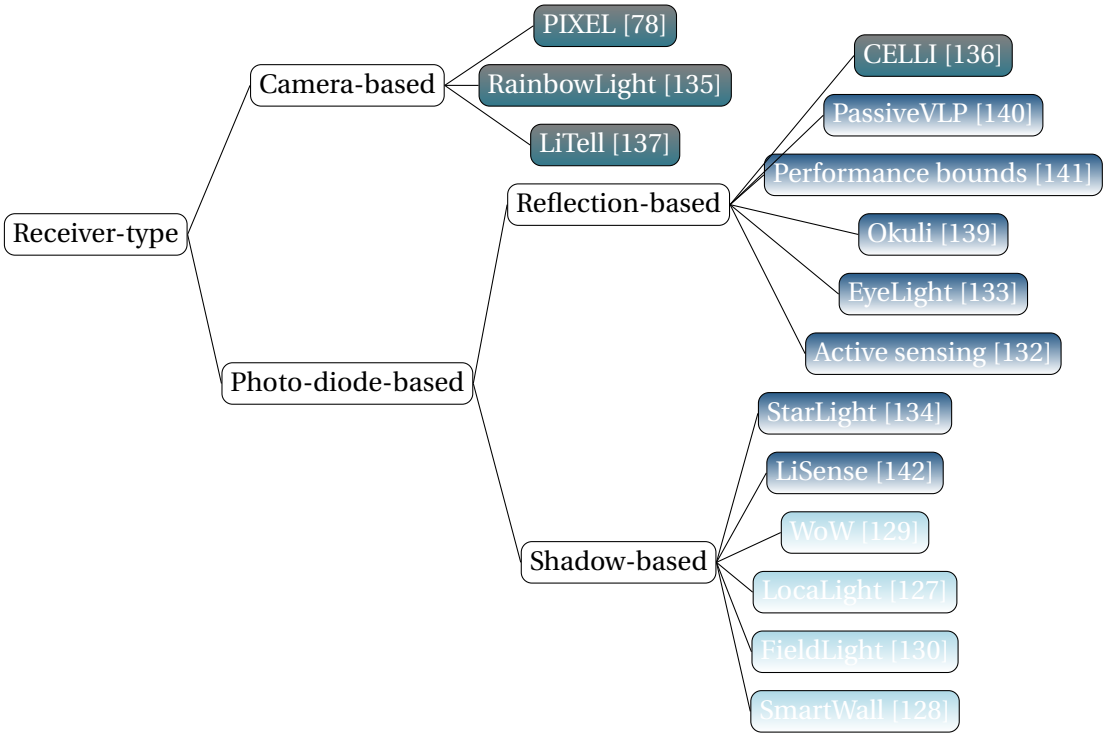

Figure 3.2: Classification of positioning systems by receiver type and passive components.

sensors, contributing to its complexity as a passive VLP system.

3.3 Applications of passive-VLP Technologies

VLP positioning has a wide variety of applications such as asset tracking, autonomous robot navigation, human localization, to name a few. This section provides an overview of the different applications of the *p*-VLP system, categorized based on the classification defined in this chapter and aligned with corresponding research in these domains.

3.3.1 Occupancy Management

Passive user and fully passive systems can be used for occupancy measurement in an indoor space. Occupancy measurement plays a significant role in Smart-building management, e.g., based on occupancy count regulation of heating and cooling in a room can be achieved which will optimize power consumption. Moreover, in shopping malls, and retail stores with occupancy measurement, one can predict which location has attracted the most customers.

Table 3.1: Summary of recent passive VLP systems.

System	Design goal	Key techniques	Testing environment				Performance	Remarks
			Area	Noise	LEDs	PD		
Okuli [139]	Locate finger on a keypad	On-off, RSS	$9x7cm^2$	Y	1	2 along with LED on dedicated 3D printed shroud	median error 0.7 cm, 1.43 cm (90 % cases)	More infrastructure changes as it needs dedicated hardware & can only track human finger
LiSense [142]	Construct 3D human skeleton	FDM, RSS	$3x3m^2$	Y	5	324 on floor	10 degree mean angular error	Overhead of light sensors deployment and more changes in luminarie design
Starlight [134]	Construct & locate 3D human skeleton	FDM, RSS	$3.6x4.8m^2$	Y	20	20 on floor	10 degree mean angular error, 9.7 cm (95 % cases)	Need to attach laser pen on object for calibration and PD deployment overhead
Eyelight [133]	Detect room occupancy,activity & location	On-off, TDM	$7.5x6m^2$	N	6	24 on ceiling	median error 0.89m, 93.70%	Occupancy detection & work in controlled lighting conditions only
Ceiling-based sensing [132]	Detect occupancy & motion	On-off,TDM, RSS	$2ft$ distance	N	7	3 on ceiling	12%	Do not localize the target only checks if the door has opened or not
Performance bounds [141]	3D Localization	Model object impulse response, Reflection based	$5x5m^2$	N	9	9 on ceiling	RMSE < 10 cm	Model depends upon physical geometry of the room, simulated work only
p-VLP [140]	Identify objects & locate 1D position	Tailored modulation, TDM	$2.5m$ distance b/w nodes	N	6	Shine+ board, ceiling	avg. error 0.97 cm, max. 5.3 cm	Can only track few points in a path
WoW [129]	2D localization	shadow based-RSS	$2x3.6m^2$	N	NA	14 on wall	7 and 13cm for stationary and mobile target	Need high Fingerprinting & PD deployment overhead
Localight [127]	1D Positioning	Shadow based-RSS	$1.53m^2$ circular	N	NA	5 on floor	NA	Only identifies the person movement static or walking
Fieldlight [130]	2D localization	shadow based-RSS	$4.8x9.6m^2$	N	NA	14 on wall	68 cm (corridor), 84 cm (lab), 120 cm (foyer)	Assumes constant background ambient light, overhead of PDs deployment
Smart wall [128]	2D localization	shadow based-RSS	$3.4x2.2m^2$	N	NA	7 on wall	7.9 cm	Need extensive fingerprinting & can only locate the target
CeilingSee [131]	Detect occupancy	Reflection based	$5x6m^2$	N	16	16 on ceiling	> 90%	Need more changes in the installed lighting fixtures
RainbowLight [135]	2/3D localization	Mapping & Trilateration	$3m$ link	NA	NA	mobile device in user's hand	avg. 3.3 cm in 2D, 9.6 cm in 3D	Initial mapping, 3 chips should be in Rx FoV for 3D localization
LiTell [137]	2D localization	Intrinsic characteristic freq. of CFLs	$2m$ link	NA	NA	mobile device in user's hand	90.30%	Works only when light is on,temp. dependent performance
PIXEL [78]	2D localization	AoA	$2.4x1.8m^2$	NA	NA	mobile device in user's hand	<30 cm in 90% cases	Power inefficient receiver
CELLI [136]	2/3D localization	PPM, spatial modulation, RSS	$2.5m$ link	NA	NA	mobile device with PD module	1.59 cm (2D), 2.65 cm (3D)	Complex design and need of guiding lenses b/w Tx & Rx makes it less suitable for large deployment

Systems: EyeLight [133] can measure the occupancy by measuring the deviation in the average received power from the base light level (calculated when the room is empty) and it achieved a 93.7% accurate occupancy count. Another fully *p*-VLP system CeilingSee [131] has achieved > 90% occupancy inference performance.

3.3.2 Human Gesture Monitoring and Communication

Gesture monitoring benefits those living in assisted environments, for valuable emergency evacuations & aids for visually impaired persons, and communicating through gestures is helpful in providing virtual keyboard writing, handwriting-based input for smartphones or smartwatches, virtual-gaming, etc. Due to the light reflection phenomenon and shadow property, *p*-VLP is a boon for human gesture monitoring.

Systems: Okuli [139] develops a passive user-based system to detect the movement and track a human's finger in a defined work-space. It utilizes the fact that fingers are round and good reflectors of light to build a model-driven solution. With a workspace of 9 x 7 cm, Okuli can detect and localize a random finger's positioning with an error of 1.43 cm in 90% cases and a median error of 0.7 cm. Another work, LiSense [142] a shadow-based human sensing system that reconstructs 3D human skeleton postures. It uses 324 floor-mounted lighting sensors and modulated lighting sources to reconstruct five main body joints with a mean angular error of 10 degrees. StarLight [134] the extended work of this system reduces the number of receivers used to 20 but with a higher error of 13.5 degrees. The above-discussed examples are passive user system based. Recently, researchers have investigated fully passive systems for localization which can also be used for human gesture monitoring and communication through them e.g. WoW [129] and SmartWall [128]. The systems have achieved a high localization accuracy of 7 cm and 7.9 cm, respectively. However, such systems require extensive fingerprinting and labeled training limiting their application usage.

3.3.3 Automated Industry 4.0

In a factory, any item with a reflective surface can be tracked and monitored through *p*-VLP. Even robots can be tracked and navigate through *p*-VLP. Not only device-free tracking but device IDentification (ID) is also possible. However, for decoding ID the device/object should have a smart reflecting material or visible-light-based barcodes on its surface. Furthermore, passive source systems can be utilized to provide location awareness and navigation for AGVs. These systems generate unique light signatures throughout a designated area, which can be correlated with a map of light installations relative to that area. AGVs can store this information

for enhanced location awareness. Additionally, by integrating sensor fusion technology, AGVs can accurately determine their precise location within the area.

Systems: In their study, [140] adapted the external surface of a toy aluminum car, a type of passive user system, to enable localization, tracking, and identification of its ID. This modification resulted in an average localization error of just 0.97 cm, along with successful decoding of the object's ID.

Additionally, LiTell [137], another passive source project, demonstrated remarkable accuracy. It achieved a 10 cm accuracy in 90% of cases when a phone was stationary and level, and a median accuracy of 15 cm with 90% reliability at 25 cm when the phone was carried by someone walking. Pulsar [138], a similar system, attained a median localization error of 0.6 meters and a heading direction error of 4 degrees while in motion. However, the prototype of Pulsar showed a response latency of 840 ms, posing a challenge for real-time application suitability.

3.3.4 Advertising

Location-based services have gained significant popularity, particularly in the retail industry. In shopping centers, custom chips designed for passive source systems can be strategically placed throughout the facility. Users with mobile devices can then receive information about promotions, discounts, and other offers from various vendors based on their specific location. Additionally, in grocery stores, details such as product descriptions and pricing can be conveniently provided to shoppers via these passive source system-equipped custom chips.

Systems: PIXEL and RainbowLight are the two passive source works in this category that can be used for this application by employing their polarizer-based smart chips. Among different systems, the RainbowLight has achieved a localization accuracy of 3.3 cm and the PIXEL system has a $< 3cm$ accuracy for 90% cases, when the receiving device is placed at 3m.

3.4 Comparative Analysis of passive-VLP Systems

By now, the description of existing *p*-VLP systems according to the proposed taxonomy has made it evident that the design goals of different *p*-VLP systems vary significantly from each other. Furthermore, it should also be noted that the unique peculiarities of these systems and a lack of common benchmarks, led system designers to test such systems under radically different environments. Table 3.1 presents a summary of design goals, methods, testing environment, and reported performance of *p*-VLP systems discussed above. The reader can find information about the deployment or testing setup which includes area, the number, and

arrangement of LEDs and PDs, as well as whether the effect of ambient noise is considered or not. All these factors matter a lot when comparing the accuracy of VLP systems.

It is concluded that the fully *p*-VLP systems are cost-effective due to their inexpensive receivers and minimal infrastructure modifications, though this is largely dependent on the specific application (and not applicable for autonomous system applications). Moreover, it is noted that most of these systems heavily depend on fingerprinting, which can be a labor-intensive process. A model-driven training method can be employed to reduce the dependence on fingerprinting as proposed in FieldLight [130]. Shadow-based systems achieve higher accuracy than reflection-based systems provided that the cost of deploying a large number of light sensors can be afforded. Until now, the designed systems have been tested in controlled environments only. The performance of reflection-based methods can be improved by putting reflective material on the surface of objects. However, whether a reflective material can be used depends on the application.

The designed passive user systems are mostly application-dependent. It is indeed not easy to find a one-size-fits-all solution. Okuli [139] provides minimum error but its usage scope is limited to extremely small areas. PassiveVLP [140] is the only VLP solution that has decoded the object ID passively while performing localization. Compared to the active VLP system, passive solutions are energy-efficient, cost-effective and less disruptive to previously deployed infrastructure. This makes their commercialization case stronger. However, it is a research area in its infancy and still requires a huge effort from the industry and standardization bodies to push their commercialization.

Passive source VLP systems can be deployed in areas where the light source cannot be easily modulated and the user wants to retrieve information about the environment. The smart material chips can be easily deployed there and the user can use a mobile phone as a receiver. These chips can be powered by photovoltaic cells. However, the power inefficiency of a mobile device is still a problem. Moreover, the passive source offers great potential for autonomous systems (e.g. to provide location services to AGVs).

3.5 Concluding Remarks and Open Research Problems

Recent years have witnessed a burgeoning interest in the field of passive VLP, as evidenced by the substantial increase in research activities. This chapter provides a concise review of contemporary *p*-VLP systems. A taxonomy is proposed, under which the characteristics of each system are analyzed and discussed. Additionally, this section highlights instances where *p*-VLP systems offer distinct advantages over their active VLP counterparts. It is anticipated that with the escalating demand for cost-efficient and energy-saving positioning solutions,

p-VLP will emerge as an increasingly crucial technology. *p*-VLP represents a novel research domain, ripe with a multitude of untapped opportunities. Concurrently, the development of *p*-VLP is confronted with several unresolved challenges, some of which are outlined in the following sections:

Deployment overhead of light sensors: In shadow-based *p*-VLP systems the localization accuracy depends on the characteristics of the shadow cast by a user. As the user moves, shadow also moves which necessitates the deployment of a large number of light sensors. A careful and smart way of deployment should be adopted to reduce the number of light sensors while getting maximum accuracy.

To get enough received reflected light: The amount of the reflected light from the surface of a target depends on the shape, size, posture and color of the reflecting surface. Therefore, reflected light is often weak and is also subjected to environmental noise. These factors degrade system performance. There is a need to train machine learning models based on the reflectivity of particular shapes.

Localizing multiple targets passively: Until now, the designed *p*-VLP systems work only for a single user. However, in real-world environments, this is not usually the case.

Design of a more robust and flexible receiver: Because *p*-VLP systems enjoy less control over the environmental light conditions and interference, there is a need to design more sophisticated receivers.

Power Consumption: While camera-based *p*-VLP systems provide more reliable solutions, they also incur higher power and computational costs. Therefore, there is a need to develop lightweight algorithms and integrate sensor fusion to reduce the constant reliance on cameras during the localization process.

Low Light Conditions and Blockage: The current *p*-VLP systems have been tested in controlled settings with manageable ambient light and minimal sensor obstruction. Given that these issues are prevalent in VLP, integrating VLP with other technologies is essential to ensure continuous location services under various conditions.

Research Goal. Section 3.3 explores various potential applications of *p*-VLP systems. The research in this thesis will be primarily centered on leveraging *p*-VLP systems for providing location services to AGVs. A major objective is to reduce costs by avoiding modifications to the existing lighting infrastructure, such as employing passive source systems, and by enhancing power efficiency using energy-efficient PDs. These PDs are specifically designed for seamless integration with low-power IoT devices. Moreover, the research is focused on reducing the computational complexity of the associated algorithms. Efforts are also made to tackle challenges like low light conditions and sensor blockage, aiming to integrate technologies from other RF domains, such as BLE, to develop a more robust and efficient system.

CHAPTER 4

HUESENSE: FEATURING LED LIGHTS THROUGH HUE SENSING

This chapter introduces HueSense, a localization system developed using Visible Light Communication (VLC) technology. The initial sections will detail the workings and development of the HueSense prototype, followed by demonstrations of its real-world effectiveness.

4.1 System Overview

HueSense is a novel passive VLP system, leveraging off-the-shelf, power-efficient color sensors to provide localization for low-power IoT devices. It uniquely employs existing LED lights, unmodified and unmodulated, as anchors, which addresses commercialization challenges in VLP systems. The system aims to offer a cost-effective, low-power, and computationally light solution for ubiquitous location awareness and tracking in IoT devices. *The key innovation lies in the ability of color sensors to detect subtle differences in LED spectra, imperceptible to the human eye, allowing for the unique identification of light sources without the need for modifying their spectrum.* Figure 4.1 showcases HueSense's motivation. While the implementation could use PDs, it would require multiple PDs with spectral sensitivity tailored to the light source's dominant colors.

In HueSense, reliance is placed solely on *single-pixel* color sensors to extract the light hue-spectrum. The primary challenge is to distinguish among unmodulated lights efficiently and effectively without the need for additional ID information. This is achieved by employing power-efficient and cost-effective single-pixel light color sensors as detectors. However, the use of single-pixel digital detector modules and the extraction of spectral information present a

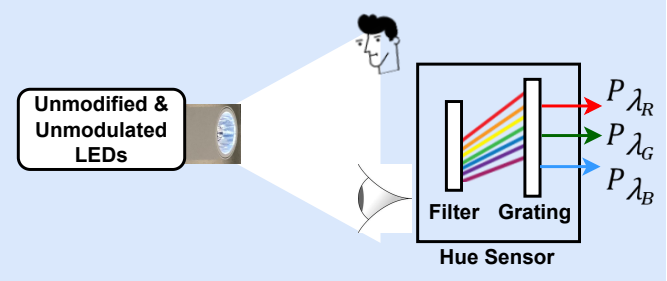

*Detected wavelength (λ_m) at the maximum spectral power in the wavelength range of 400-500 nm for four commodity LEDs of the **same model and brand**.*

LED	L1	L2	L3	L4
$\boldsymbol{\lambda_m}$ **(nm)**	448.0312	455.2858	450.2281	456.1662

Figure 4.1: Motivation of HueSense: LEDs have slightly different colour spectrum that human eyes cannot distinguish. Still, the differences can be detected by colour sensors, indicating that an LED can be uniquely identified by its spectrum without the need to modulate it.

challenge in employing common localization methods such as channel-based or angle-based techniques, referenced in sources like Luxapose [79] and Pixel [78]. The determination of distance or angle using the classical channel model may be inaccurate, as the received power at a specific wavelength varies for different distances/angles relative to an LEDs and differs among LEDs. To address this, a regression-based learning method is proposed to understand the behavior of power at specific wavelengths for varying distances/angles under different LEDs, thus enabling accurate localization.

To the best of current knowledge, HueSense is the first passive VLP system using single-pixel color sensors for extracting the light hue-spectrum and employing both classical and machine learning techniques for light mapping and location services. The contributions of this chapter are summarized as follows.

1. A novel power-efficient and cost-effective approach for *passive* light feature extraction, utilizing *single-pixel colour sensors* to determine the power of dominant wavelengths in white LEDs.

2. Application of this technique to differentiate between unmodified and unmodulated white LED light sources, crucial for enabling spatial awareness services.

3. Development of a dual-phase localization system that merges classical mathematical methods with a learning-based regression approach to localize mobile targets.

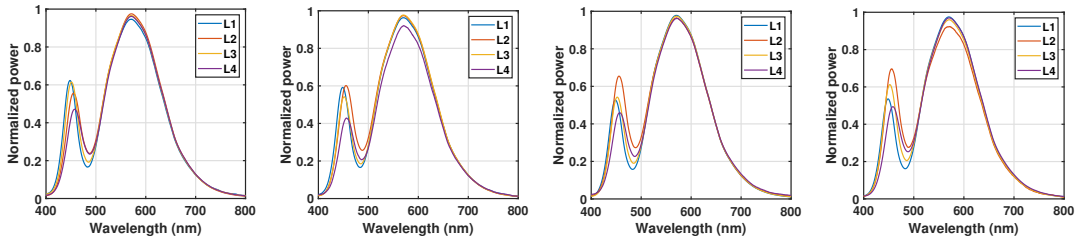

(a) $\theta = -45°$ (b) $\theta = -30°$ (c) $\theta = 30°$ (d) $\theta = 45°$

Figure 4.2: Detected LED spectrum using high-spectrum resolution spectrometer at different incident angle (θ).

4. Experimental validation of HueSense, implemented on Arduino boards for light identification and location services for mobile targets. Tested in a real-world scenario within a dense VLP network of area $25m^2$, it demonstrates 100% identification precision with moving targets and achieves decimeter-level localization accuracy.

The core concept and light identification analysis of HueSense have been published in the Proceedings of the 1st ACM Workshop on AI Empowered Mobile and Wireless Sensing, associated with ACM MobiCom 2022. This work was honored with the **Best Paper Award** at the workshop.

4.2 Design

This section initially introduces the principle of the proposed passive light identification method, addressing how to effectively differentiate between unmodulated LED light sources. Following this, the technique for extracting and analyzing those hidden discriminating features, referred to as *light ID* in this chapter, using cost-effective color sensors, is presented.

4.2.1 Preliminary

Motivation. The wavelength of light emitted by LEDs, and thus its colour, depends on the materials forming the LED chip. Due to unavoidable manufacturing imperfections, e.g., the variations in the phosphor coating thickness and the non-uniformity, different optical properties of the light originate such as the change in radiant flux and colour temperature. These imperfections make LEDs' radiated power for particular wavelengths different, which motivates the design of HueSense.

In the case of white LED light, the three dominant emitted wavelengths are λ_R, λ_G, and λ_B at Red (R), Green (G), and Blue (B) channels, with a greater contribution from B and G

Table 4.1: Performed t-test on LED L1 spectrum with other LEDs (L2, L3) obtained at different spectrometer positions (P1-P5) within the FOV of the LEDs.

Position, LEDs	P1, L1-L2	P1, L1-L3	P2, L1-L2	P2, L1-L3	P3, L1-L2	P3, L1-L3	P4, L1-L2	P4, L1-L3	P5, L1-L2	P5, L1-L3
h-value	0	1	1	1	1	1	1	1	1	1
p-value	0.4914	3.6448e-05	1.1421e-05	5.9617e-10	2.8785e-36	0.0024	3.4147e-281	4.0482e-289	5.0735e-101	3.0002e-06

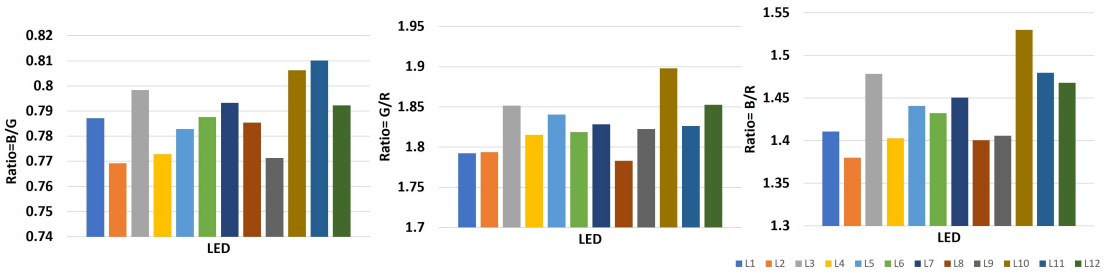

Figure 4.3: RGB power ratio comparison among 12 commodity LEDs of the same model & brand.

channels compared to the R channel. To generalize this property, a spectrometer[1] is used to extract the LED light spectrum from four different white LED lights in a room. The resultant spectrum is displayed in Figure 4.2, showing the moving average of intensity to mitigate peaks/intensity fluctuations due to ambient noise. The spectrum for different LEDs within their FOV is captured, revealing that each LED possesses a unique hue-spectrum, and the spectrum properties remain consistent at various positions.

Moreover, to statistically affirm that the spectrum series are distinct, a t-test[2] is performed on the L1's spectrum mean with zero mean difference as the null hypothesis. The results, displayed in Table 4.1, confirm the statistical significance, validating the principle of HueSense.

Additionally, more variations in the light spectrum are noticeable around the 450 nm wavelength. The emitted wavelength corresponding to the maximum power peak in the 400-500 nm range varies for different lights. Figure 4.1 depicts the maximum power peak wavelengths for four lights in this wavelength range (the maximum power variation region), serving as a potential ID for LED lights. However, spectrum extraction is only feasible using a spectrometer, an expensive and impractical solution for small IoT devices.

The following section introduces an alternative, cost-effective approach to realize the hue properties of LED lights using off-the-shelf hue sensors.

[1] `https://www.thorlabs.com/newgrouppage9.cfm?objectgroup_id=3482`

[2] A t-test is an inferential statistic used to determine if there is a significant difference between the means of two groups, which may be related in certain features.

4.2.2 Light ID: Distinguishing LEDs Through Their Hidden Colour Features

An important hidden feature, which can be derived from Figure 4.2, is that the ratio of power at dominant wavelengths (i.e., λ_R, λ_G, and λ_B, in case of the white LED lights) at different positions remains constant. The principle of HueSense is to extract the power around the dominant wavelengths present in the unmodulated white LED bulbs and use this hidden feature as a discriminative feature among lights. To obtain this hidden feature, small off-the-shelf hue sensor[3] can be used to extract the spectral power at λ_R, λ_G, and λ_B wavelengths. This type of sensor can be easily deployed into the tiniest IoT devices, and they can directly extract the dominant wavelengths of white lights from LED bulbs. For example, Figure 4.3 shows the obtained power ratios for 12 LEDs under LoS scenarios in a lab environment.

Proposed LED's light ID. Based on the captured power ratio values, the construction of the ID L_i for the ith LED is proposed using the following tuple:

$$L_i : \langle \frac{P_{B_i}}{P_{G_i}}, \frac{P_{G_i}}{P_{R_i}}, \frac{P_{B_i}}{P_{R_i}} \rangle \tag{4.1}$$

where $i = \{1, \cdots, N\}$, N is the total number of LEDs; P_{R_i}, P_{G_i}, and P_{B_i} are the received spectral power at R, G, and B channels, respectively. In reality, these IDs can be calculated from the measurements of the LEDs and are stored in a database for future light identification during testing.

Light identification with multiple sensors. The sensor module can be placed on top of robots with the stored LED ID database information that can estimate their locations in a room, i.e., under which LEDs they are moving. This estimation can be done by finding the minimum Euclidean error between the stored LED ID values and newly measured power ratios at dominant wavelengths, denoted as $\tilde{L}$.

However, *how can differentiation be made between light sources with the same power ratios of R, G, and B channels or approximately negligible difference between the power ratios?* To eliminate this problem, employ *multiple sensors with different incident angles*. This approach facilitates the sensor modules to have the information of neighbouring LEDs that will help with the light identification. The design is shown in top part of Figure 4.6, where Sensor 2 (S2) and Sensor 3 (S3) are inclined at 45-degree angles with respect to the centre Sensor 1 (S1). The optimum inclination angle can be found based on the separation between different light sources and link distance. However, with HueSense, the goal is to create a versatile solution that can be applied to various illumination infrastructures. The inclination angle of 45 degrees is selected since the minimum separation between light sources in various indoor settings is

[3]https://www.hamamatsu.com/eu/en/product/optical-sensors/photo-ic/color-sensor/rgb-color-sensor.html

Algorithm 2 Light identification with multiple sensors.

procedure LED LIGHT ID ASSIGNMENT
For each sensor $S_j, j \in \{1,2,3\}$, extract the power at R, G, B wavelengths for each light $L_i, i \in \{1,2,\cdots,N\}$ in the database as $P_{R_{ij}}$, $P_{G_{ij}}$, $P_{B_{ij}}$, and store the ID as

$$L_{ij} : \langle \frac{P_{B_{ij}}}{P_{G_{ij}}}, \frac{P_{G_{ij}}}{P_{R_{ij}}}, \frac{P_{B_{ij}}}{P_{R_{ij}}} \rangle$$

procedure LIGHT IDENTIFICATION
Let $\tilde{L}_{kj}$ denote the measured ID values at location k.
At current location k, calculate the Euclidean error as
$E^i_{kj} = \sqrt{(L_{ij}[1] - \tilde{L}_{kj}[1])^2 + (L_{ij}[2] - \tilde{L}_{kj}[2])^2 + (L_{ij}[3] - \tilde{L}_{kj}[3])^2}$
Find the minimum error value for each sensor as

$$D_{kj} = \min_i E^i_{kj}$$

and store the corresponding argument where the minimum is obtained as M_{kj}.
For location k, find the predicted values P_k as
if $M_{k1} \neq M_{k2} \neq M_{k3}$ **then**
$P_k = \arg\min_j D_{kj}$
else
$P_k = M_{k1}$

typically a few meters. The three sensors extract the hue-spectrum properties of the nearest LED and its neighbouring LED lights, provided these LED lights are in the sensor's FoV.

4.3 Localization Technique

This section details how HueSense provides spatial awareness, indicating the target's presence area, and elaborates on the technique to determine the exact location.

4.3.1 Light Identification

HueSense utilizes the method in Algorithm 2 for passive positioning, identifying LED lights via detected hue properties. The sensor module, as depicted in Figure 4.6, can be positioned atop a target device, such as a robot, equipped with a stored LED ID database. This database allows the system to estimate the device's location within a room, specifically under which LEDs it is moving. This estimation is done by finding the minimum Euclidean error between the stored LED ID values and newly measured power ratios at dominant wavelengths, denoted as $\tilde{L}$. Once the LED unit is identified, one can pinpoint the target's accurate location by focusing

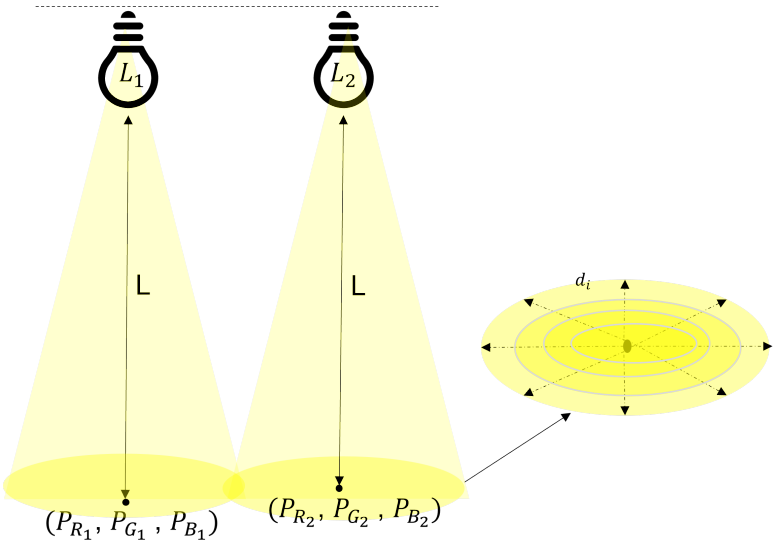

Figure 4.4: The received power at dominant wavelengths varies under different LEDs even at the same link distance (as shown for LED L_1, L_2 at position C). HueSense utilizes a regression learning model to understand these power variations. The model is trained on the relationship between power and distance (d_i), where d_i represents the distance from the central position (directly beneath the LED, where the light received by the receiver has a 90-degree incidence angle) to various training points within the LED's emission pattern.

on the area lit up by that specific LED unit. The steps to accomplish this are explained in the following Section 4.3.2.

4.3.2 Performing Accurate Localization

The light ID remains unique and constant under the LED, irrespective of the link distance or FOV (demonstrated experimentally in the Section 4.4. This feature is used for LED identification, but for localization- the feature should vary either w.r.t distance or angle. In classical RSS methods, the received power values are used to determine either the distance or angle w.r.t LED to determine the receiver location w.r.t the LED, i.e. by utilizing the channel model [138, 131]. However, the use of color sensor modules, which output digital power values for incident light, prevents direct determination of distance from received power. Furthermore, power received at dominant wavelengths varies at a fixed distance under different LEDs, complicating localization with channel models. No direct mathematical relation for power variation with distance and angle can be derived from the IDs, as they differ for each LED (a principle of HueSense). To address this, a combined classical and learning-based approach is proposed for accurate location determination with HueSense. After identifying the light, sensors S2 and

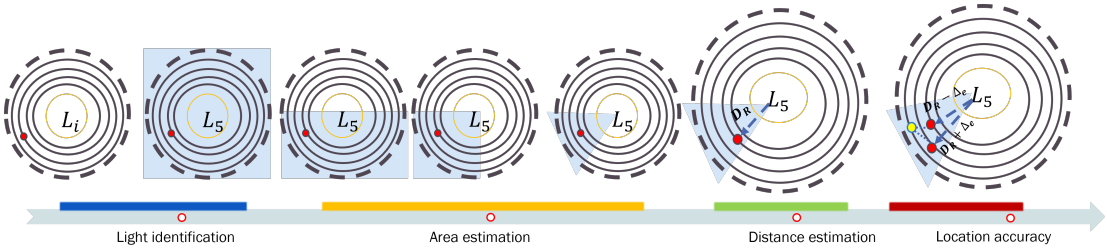

Figure 4.5: Steps in HueSense Localization Process - The circle depicts the emission pattern of light, with the shaded area indicating the potential target location zone.

S3 are used to further halve or quarter the detected area, and then the target's position within this reduced area is determined using a regression-based learning method. Training involves exposing the model to power values at dominant wavelengths from a single LED at varying distances to learn the behavior of power with distance, pictorially shown in Figure. 4.4.

A challenge with learning approaches is the extensive training required for all possible locations, which is time-consuming. HueSense simplifies this by learning the behavior of power changes with distance for a single LED only, since theoretically, the intensity behavior should be similar for each LED at different distances, though the power at dominant wavelengths differs. The complete steps for analyzing the proposed method are outlined below in Procedure and illustrated in Figure 4.5.

Localization Approach. Following successful light identification, the detection/search area is confined to where the light impacts the ground. For simplicity, envision a circular light emission pattern on the ground, with the aim to pinpoint the receiver's position within this circle (refer to Figure 4.5). The following steps outline the process in HueSense for determining the target position.

Step 1: *Determine the forward direction of the mobile target:*

i. Choose the forward sensor (e.g., S2) to identify the forward direction of the mobile target.

ii. Determine the minimum Euclidean error in light fingerprints from neighbouring lights using the procedure described in Algorithm 2. This narrows the search area for the receiver's position to half the detection area, i.e., a semi-circle aligned with the forward direction of the light receiver (third circle from left in Fig. 4.5).

Step 2: *Determine which side/direction of the light source, the target is present:* Repeat Step 1 to determine which side of the light source the receiver is located. This step helps to determine whether the receiver is on the left or right side of the light source within the semi-circle

Algorithm 3 Regression-based Learning Method

Require: Sensor S1, LED L_{train}
Ensure: Trained localization model M
Data Collection:
for each location (x_i, y_i, z_i) under L_{train} **do**
    Measure light features P_{R_i}, P_{G_i}, P_{B_i} using S1.
Model Training:
Let $\mathbf{P}_i = [P_{R_i}, P_{G_i}, P_{B_i}]^T$ be the feature vector for x_i.
Define d_i as the distance or angle from L_{train} to (x_i, y_i, z_i).
Train model $M : \mathbf{P} \mapsto d$ with $\{(\mathbf{P}_i, d_i)\}$.
Model Evaluation:
Calculate test error Δ_e using 80% of data for training and 20% for testing.
Model Storage:
Archive M for runtime use.
Runtime Localization:
On detecting L_{test}, extract $\mathbf{P}^{ID}_{L_{\text{test}}}$.
Compute $\Delta\mathbf{P} = \mathbf{P}^{ID}_{L_C} - \mathbf{P}^{ID}_{L_{\text{test}}}$.
Adjust $P_{\text{adjusted}} = P_{L_{\text{test}}} + \Delta\mathbf{P}$.
Use $M(P_{\text{adjusted}})$ to predict D_{R}.
Final Location Determination:
Find location minimizing Δ_e within $D_R \pm \Delta_e$ range.
Assign coordinates based on minimized Δ_e and known L_{test} position.

search area (fourth circle from left in Fig. 4.5). Please note that in this case, the search for the minimum Euclidean error with the installed lighting unit is limited to only the light units present around the detected light source in Step 1. This focused search approach helps streamline the localization process and increases efficiency by considering only the relevant light units in the vicinity of the detected light source. The detected area in this step can further be reduced to one by eight (fifth circle from left in Fig. 4.5) by repeating *Steps 1-2* provided the neighbour LEDs are present. If a wall is present on the side of the searching area, this step would be omitted. The identified quarter search area would be used for further position estimation.

Step 3: Determine the precise location: To determine the mobile target's precise location relative to the detected LED, `BLoB` employs a regression-based learning model, M, as detailed in Algorithm 3. This model calculates the distance between the target device and the LED and then utilizes the LED's known coordinates to ascertain the target's location coordinates.

4.4 Evaluation & Results

This section outlines the implemented prototype of HueSense, designed to assess its capability in passively identifying LEDs and determining their locations using a robot in both static and

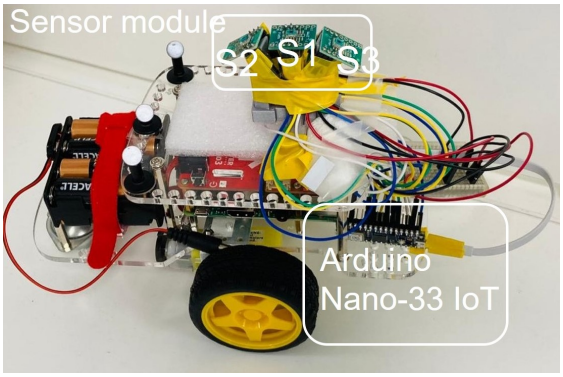

Figure 4.6: HueSense implemented prototype: robot equipped with three hue sensors to collect light features and send them over a WiFi network for localization.

moving scenarios. The evaluation focuses on two aspects: first, the light identification in an uncontrolled lighting environment, specifically the corridor at the premises[4]. The second aspect involves testing the localization performance of HueSense in a specially designed LED dense network at the premises.

4.4.1 Implementation

Prototype: The developed prototype, depicted in Figure 4.6, is utilized to experimentally analyze and test the performance of HueSense. Three HAMAMATSU colour sensors are integrated with an Arduino board to simultaneously collect R, G, and B channel power (P_R, P_G, and P_B) from each sensor. The sensors are power-efficient, operating on a *3.3-volt* (V) battery. Sensor integration with the Arduino uses the repository[5] for `TCS34725`-color-sensors, *modified* for compatibility with the sensors in MATLAB Simulink. The Arduino board, a `33-Nano IoT`[6], features integrated WiFi capability and is both compact and power-efficient, ideal for low-power IoT devices. The developed Simulink model deployed on the Arduino board collects and transmits light information over WiFi to the host machine, which runs the MATLAB-based light identification and localization algorithm. For accurate ground truth location information, a highly precise Optitrack system is employed.

Testbed: Figure 4.7a depicts the initial testing environment, an uncontrolled lighting setting with ambient light sources and sunlight. A dense LED network, consisting of 9 standard white LEDs and covering an area of $10m^2$, is established as illustrated in Figure 4.7b to assess the

[4]The initial experiments were conducted during an internship at TU Delft. Subsequent testing was carried out on a Testbed built at Toshiba premises.

[5]`https://github.com/adafruit/Adafruit_TCS34725`

[6]https://docs.arduino.cc/hardware/nano-33-iot

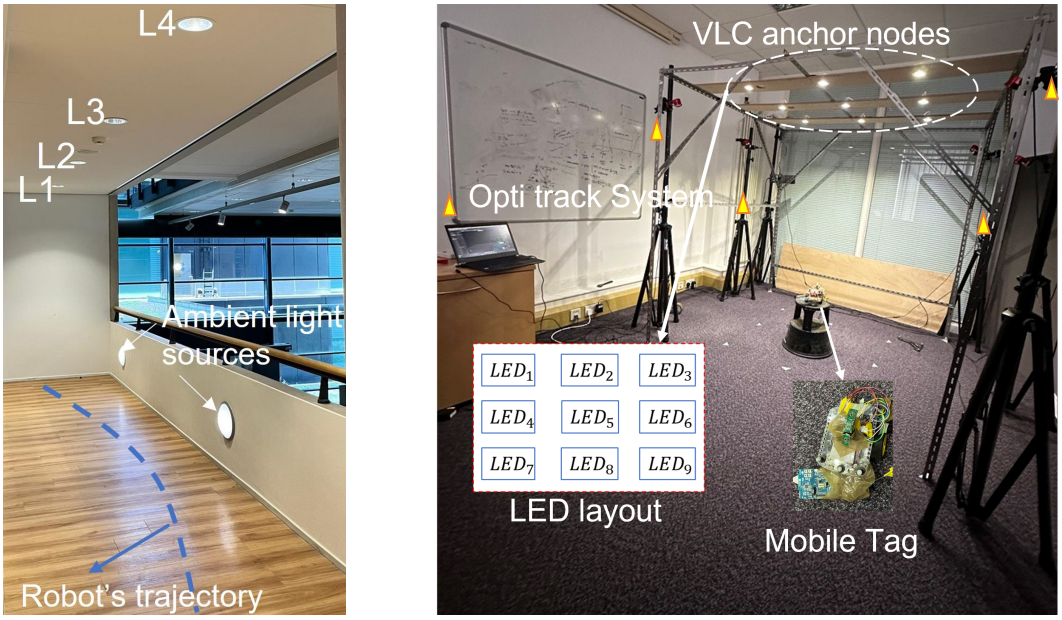

(a) Corridor.

(b) Dense LED network.

Figure 4.7: HueSense experimental setup in a university corridor **(a)** and the developed dense LED testbed.

HueSense localization performance. These LEDs are placed approximately 55cm apart, center to center, creating interference due to their 36° FOV.

4.4.2 Impact of Distance and Incident Angle

The evaluation examines whether spectral power ratio values stay consistent when varying the distance and incident angle relative to the light source. Using a single LED, the spectral power is measured at different incident angles (by shifting the sensor from position A to B, at a 1 m distance) and at various distances (moving the sensor from C to D), as shown in Figure 4.8a. The measurement results, displayed in Figure 4.8b and Figure 4.8c, indicate that the ratio of dominant wavelengths remains roughly constant (± 0.01) across different LED positions and incident angles. This consistency supports using the average ratio value of the spectral power at the dominant wavelength as an LED identifier.

4.4.3 Light Identification

Static scenario: HueSense aims to passively distinguish light sources based on hue characteristics. Its performance under static conditions—when the sensor remains stationary and directly beneath the light source—is evaluated in various environments like labs and corridors.

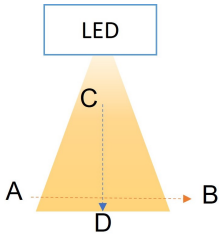

(a) Setup

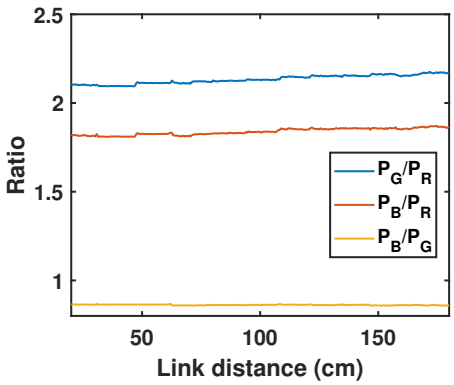

(b) Measured power ratio vs. distance

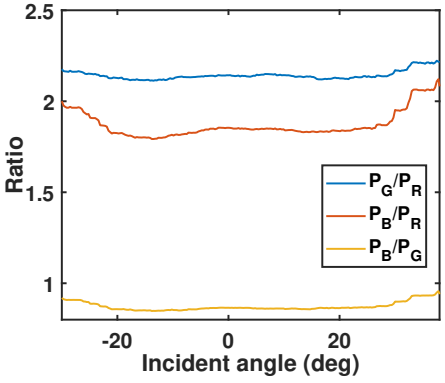

(c) Measured power ratio vs. incident angle

Figure 4.8: Impact of distance and incident angle on the power ratio.

Identification results using four LEDs are shown in Figure 4.9a and Figure 4.9b, identifying the corresponding LED by LEDs with the closest Euclidean distances. Here, HueSense achieves 100% accuracy in light identification.

Moving scenario: To evaluate performance with a moving target, a robot carrying the sensor module is utilized, as depicted in Figure 4.6. The robot's advantage is providing precise ground position while in motion through odometry analysis. The robot moves from LED1 to LED4, following the trajectory shown in Figure 4.7a. The sensor module collects power values and transmits light hue information to the system. MATLAB code for light identification, which contains stored data on light IDs and installation maps, is run on the system. Using the method described in Algorithm 2, the correct LED ID is identified with 80.14% accuracy as the robot moves. These findings are presented in Figure 4.9c. Due to wheel friction errors, the robot follows a curved path, leading to incorrect LED ID predictions under LED L3. Here, proximity to the wall and interference from ambient light sources complicates identification.

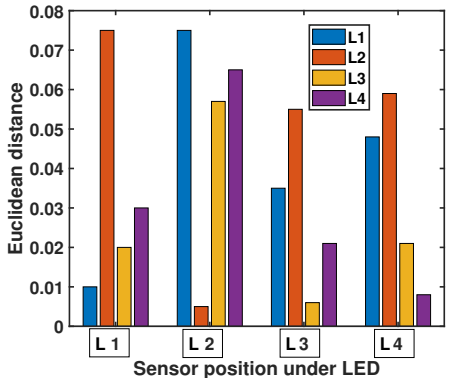

(a) under the LEDs

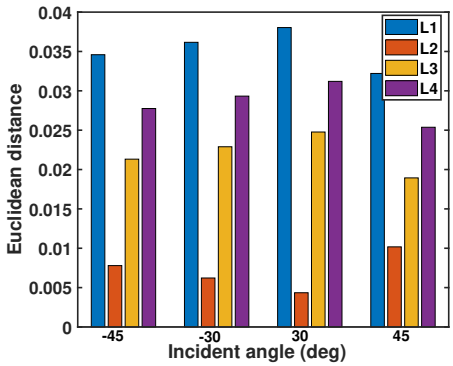

(b) at different incident angles

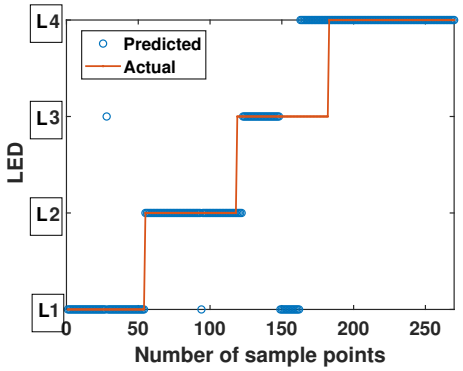

(c) with a moving robot

Figure 4.9: Light identification accuracy in an uncontrolled lighting environment i.e. a corridor (see Figure 4.7a).

4.4.4 Localization Performance

The efficacy of the regression-based learning algorithm is initially showcased by training it with a single LED and testing under both the same and different LEDs. This approach confirms that training with one LED is sufficient to effectively capture power variations at dominant wavelengths for all LEDs. Data collection involves positioning the sensor module at various fixed points within the LED's FOV, amassing over 500 samples in the testbed (see Figure 4.7b). An 80/20 split is utilized for training and testing data, with additional unseen data from a different LED for testing under varied conditions. Results, depicted in Figure 4.10a, reveal 75% accuracy in localization within a decimeter for both scenarios: using test data from the same LED and from a new LED, with a generalization error of 7cm. The consistency in results under different LEDs validates the proposed approach.

Subsequent testing evaluates HueSense's localization performance with a moving target.

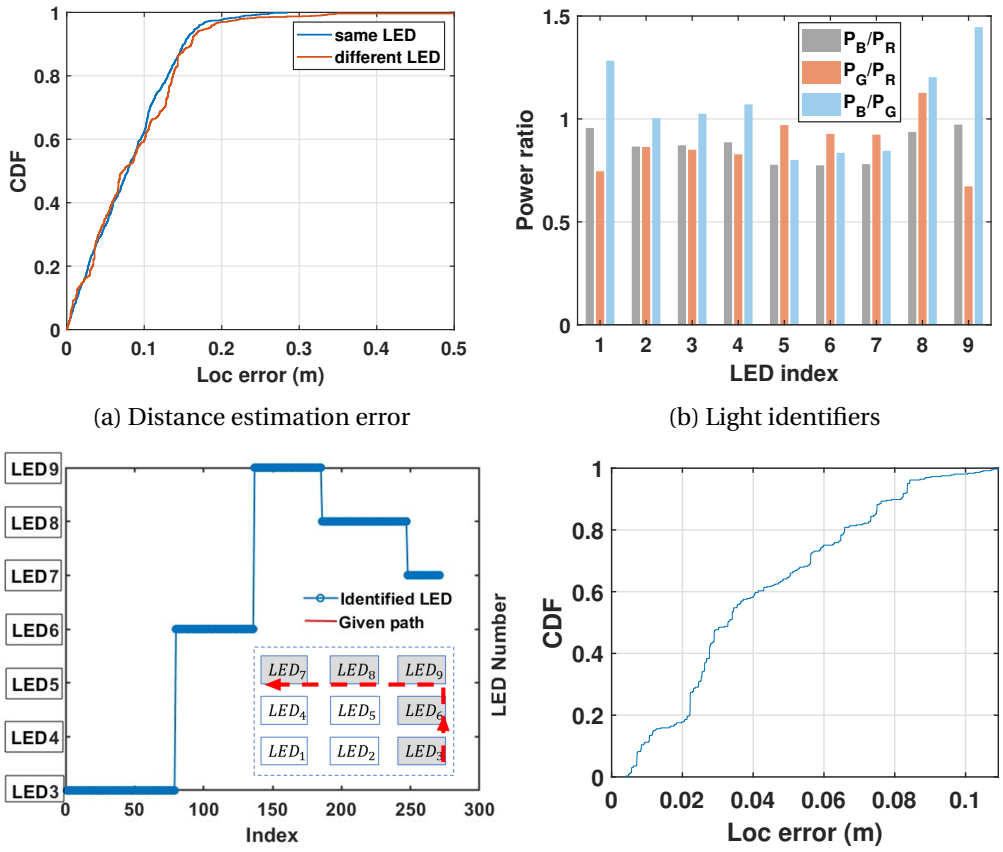

(a) Distance estimation error

(b) Light identifiers

(c) Light identification.

(d) Localization performance.

Figure 4.10: HueSense performance analysis in a dense LED network (see Figure 4.7b).

This involves first identifying the light source the target is moving under, and then determining the location coordinates. Figure 4.10b displays the obtained ID for each LED within the testbed, as shown in Figure 4.7b. A robot moves from 'LED3' to 'LED7' following an 'L'-shaped path to initially identify the correct LED (trajectory shown in Figure 4.10c). The LED numbers are used solely for differentiation. The robot collects power values and transmits the light hue data to the system. MATLAB code for light identification and localization is executed on the system, using data from the ID collection phase and the light installation map. The true LED under which the robot moves is identified and its coordinates are determined using Algorithm 3. Results are presented in the Figure 4.10, show 100% accuracy in light identification using Algorithm 2. Localization coordinates are determined and compared against the ground truth to evaluate errors. These results are statistically shown in Figure 4.10d, with 90% of the errors within decimeter-level, substantiating the proposed technique's validity.

4.5 Related Work

LiTell [137] was the pioneering work in the passive-VLP category, utilizing unmodified FLs as location landmarks and commodity smartphones as light sensors. It achieved an impressive 10cm accuracy 90% of the time when the phone was placed still and level, and a median precision as high as 15cm, with 90% accuracy at 25cm when held by a walking user. However, as the number of lights increases, the probability of collisions of unique IDs among groups of lights also increases. Moreover, LiTell's method is limited to FLs, which restricts its usage in current indoor environments [137, 143]. It also requires high-resolution back cameras with raw output, and it suffers from a high misidentification rate (around 40%). A similar feature is extracted by Pulsar [138] for LEDs, using dual-PDs, but the system demands specially designed detectors with a specific FOVs, a requirement that is relaxed in HueSense, making it a complex VLP system. Pulsar achieved a median localization error of 0.6 m and a heading direction error of 4 degrees while walking; however, its prototype implementation incurs a response latency of 840 ms, which may not be suitable for real-time applications. Auto-LiTell [144] also employs a similar feature as LiTell [137], using a custom deep-learning model for light identification only. However, the localization accuracy was not evaluated. In contrast, HueSense has used more light weight linear regression methods and a complete localization evaluation is performed. In another work, iLAMP [145] extracts the spatial radiance pattern of the lights, i.e., the radiance intensity distribution across a light's surface, from images captured by a smartphone's camera. This approach is power-hungry and achieved close to 100% accuracy in identifying the location but was tested only under one FL, with the target placed at 25 random spots, no mobility involved, achieving 3.5 cm accuracy.

The other passive-VLP works reported in the literature are primarily focused on occupancy determination and gesture monitoring, lacking the capability to provide location/navigation services to mobile targets [133, 130, 128]. On the other hand, most of the active VLP systems are designed for localization and navigation services, but they often require modifying the lighting unit and rely on power-hungry cameras as receiving units, resulting in significant processing latency [79, 135, 146].

While camera-based systems [79] are more readily available compared to photodiode-based alternatives [134, 131, 147], they necessitate additional units on the receiver side. Nevertheless, the cost of adding extra sensing units to the receivers is considerably lower than the expense of changing lighting units. The research presented in HueSense, aligns with the objectives of *p*-VLP systems, aiming to eliminate the need for altering existing lighting units, offering location services. Additionally, HueSense offers the advantage of using cheaper, power-efficient colour sensors and requires no strict arrangement of sensors, making them easily

integratable with low-power IoT devices. The power at different wavelengths is influenced by corresponding wavelengths reflected from different objects. In [148, 149], experiments have done with participants wearing white clothes to avoid any reflections affecting the system performance. In contrast, HueSense experiments are conducted regardless of clothing color, indicating the minimal affect of wavelength refection with the achieved results. Also, by aligning color sensors differently, HueSense can reduce reflection from certain colors or materials. Further detailed studies could be pursued in the future.

4.5.1 Discussion & Concluding Remarks

Training a model to learn power changes at dominant wavelengths with just one LED might affect accuracy due to varying power levels across LEDs. An alternative, as mentioned in [148], uses unique LED features across an area, improving performance but increasing data collection time. While this technique could enhance model performance, it necessitates extended data collection times proportional to the area's size. Nonetheless, HueSense achieves decimeter-level accuracy efficiently without extensive data needs. Furthermore, power variation at different wavelengths is affected by the material's reflection properties at those wavelengths. Unlike the experiments in [148], with participants in white clothing, HueSense's testing was conducted independent of clothing color, showing that adjusting color sensors can mitigate reflections from specific colors or materials. Further detailed studies could be pursued in the future.

To the best of the author's knowledge, HueSense represents the first passive VLP system that utilizes the hue-spectrum of unmodulated LED for light identification and localization with a single-pixel hue sensor. Different unmodulated LED lights have been successfully distinguished by exploiting their intrinsic color properties. The distinctive features of HueSense are expected to enhance the application of VLP in various location-based contexts, such as autonomous robot navigation and indoor localization. However, *p*-VLP systems especially *p*-VLP, like HueSense encounter significant challenges in low light conditions, presenting a technological barrier that HueSense alone cannot surmount. The subsequent chapter introduces a strategy for merging HueSense with BLE-based technology, outlining a method to effectively integrate these technologies. This integration aims to maximize their potential and achieve the goals outlined in this thesis. Despite these hurdles, HueSense remains applicable for various scenarios without RF fusion, especially in situations where continuous tracking is not a critical requirement.

CHAPTER 5

BLELIGHT: HYBRID BLE-VLP LOCALIZATION SYSTEM

The growing demand for intelligent indoor spaces has underscored the importance of developing highly precise indoor positioning systems. Chapter 4 and Chapter 2, introduced two innovative localization systems in this direction, one utilizing BLE and the other using VLC. While both systems have showcased impressive performance when compared to the SOTA localization solutions, they each encounter certain challenges primarily stemming from technological limitations. This chapter will enumerate these challenges and propose solutions to address them.

5.1 Introduction

As previously mentioned in this thesis, VLP is a promising technology for achieving highly precise indoor localization by harnessing the directional properties of light. However, existing VLP systems demonstrate optimal performance only in controlled lighting environments. In real-world scenarios, various factors such as external ambient light sources, obstacles, shadows, and sensor blockage contribute to a decline in performance, ultimately restricting the range of effective localization areas. Additionally, active VLP systems, which use light sources such as LED units modified to transmit location information and a camera as a VLP receiver, are power-hungry, and have high latency, while the requirement for changes in the luminaire design limits wide market adoption [8]. As an alternative to active VLP systems, *p*-VLP, such as our solution, HueSense, offers a viable option. However, it does not completely eliminate some of the aforementioned issues, such as challenges posed by ambient light

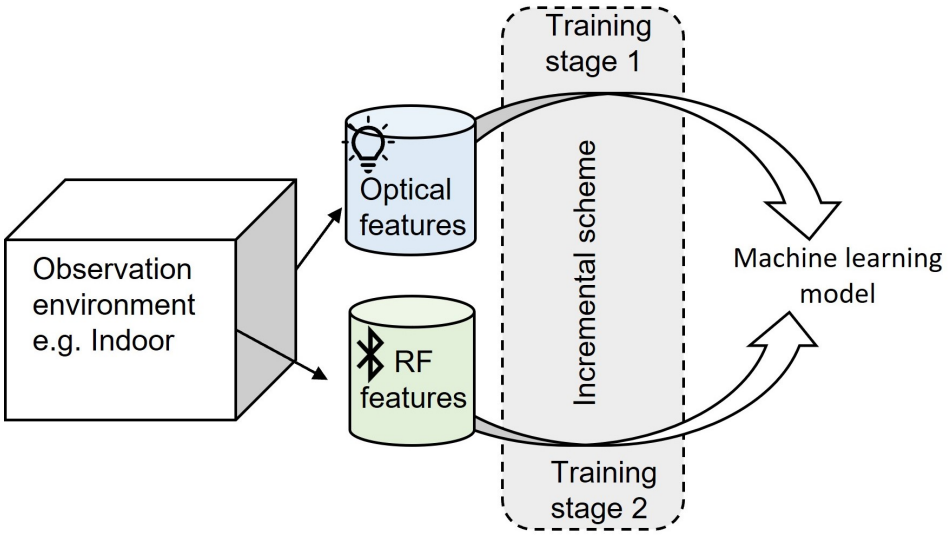

Figure 5.1: BLELight: a multi-modality model.

sources and low-light conditions.

Conversely, RF technologies like BLE have witnessed a surge in popularity for indoor localization systems, primarily owing to their widespread availability and cost-effective hardware. Nonetheless, the inherent narrowband characteristic of BLE makes it vulnerable to multipath fading, which, in turn, restricts the attainable ranging accuracy. While BLoB system, the pioneer in beating-based localization systems for BLE, has showcased sub-meter accuracy, achieving decimeter-level accuracy remains a formidable challenge due to the limitations of narrowband technology. Furthermore, currently available chipsets are unable to provide the precise timing synchronization required for such high levels of accuracy [150, 151].

Hybrid Localization. In order to tackle these challenges and alleviate the constraints inherent in the individual systems presented in Chapter 2 and Chapter 4, these chapters explore the integration of BLE and VLP to create a hybrid localization system that is both reliable and highly accurate. The goal with this approach is to overcome BLE's inherent low accuracy and VLP's restricted usage range by harnessing the strengths of both technologies. To achieve this, NN-based data fusion technique is employed, to effectively combine signal features from both modalities, as illustrated in Figure 5.1. DNNs hold significant promise in modelling the relationship between signal features and target locations, thereby addressing the complexities posed by multipath propagation in indoor environments [11]. This chapter has further proposed an incremental approach to fuse these technologies, details are discussed in the subsequent sections. The main contributions of this chapter are summarized as follows:

i) BLELight, a hybrid accurate localization system for large indoor spaces, is proposed.

BLELight fuses the intrinsic features of unmodulated light (the ratio of power at dominant wavelengths from Chapter4) with the BLE RSS measurements from both the beating and signal spectrum(2).

ii) An incremental learning-based approach for training the DNN model is proposed, in contrast to traditional joint training methods. This approach efficiently leverages the multimodality features from both technologies for localization purposes.

iii) Experimental results show that BLELight achieves a mean localization error of approximately 12cm, enhancing the localization performance of individual *p*-VLP and BLE by about 47% and 64%, respectively.

The core idea of this chapter has been patented (please refer [152]), and the results were published as an extended abstract in the Proceedings of the 29^{th} Annual International Conference on Mobile Computing and Networking (ACM MobiCom 2023). Additionally, this work was qualified for the Student Research Competition at the conference.

5.2 BLELight: Multi-modal Fusion

5.2.1 Framework

BLELight focuses on indoor settings characterized by multi-modality observations, as shown in Figure5.1. It utilizes optical and RF signals as two separate observational modalities for target localization. Employing these modalities concurrently aids in achieving greater localization accuracy. The system specifically combines the modalities *p*-VLP and BLE, applying an Incremental Learning (IL) methodology to train a DNN model. IL represents a learning paradigm that equips models with the ability to continually evolve and update their knowledge base with new data. This method facilitates progressive knowledge refinement in the model, leading to innovative strategies for combined RF signal and VLP-based localization. The core concept of IL in this context is that both RF and optical, or VLP, modalities, despite their differences, convey relevant information about the signal-location dynamics within a particular indoor setting. Moreover, IL effectively minimizes feature interference or imbalances arising from diverse sources. Training the DNN model sequentially with individual signal features reduces interference from multiple sources, enabling a more focused and effective learning process.

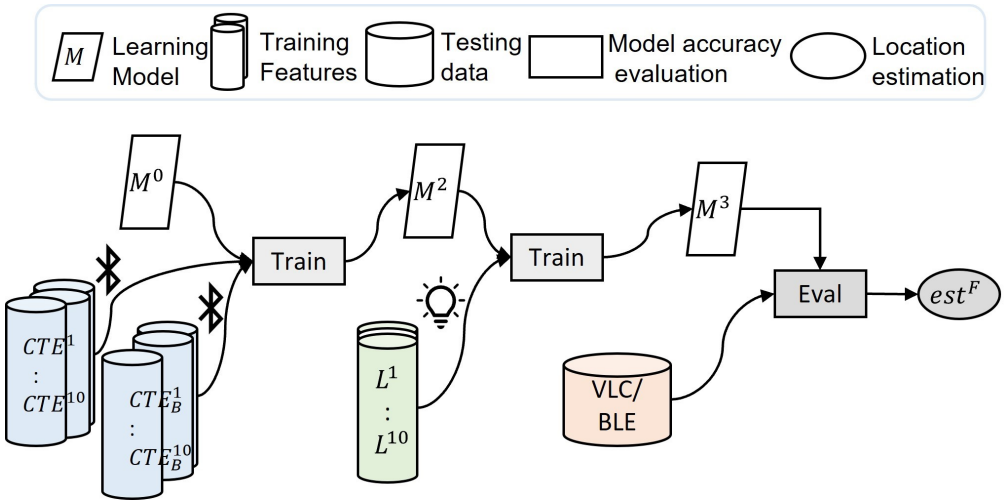

Figure 5.2: The proposed two-stage incremental learning scheme in which BLE and *passive*-VLP features are fed into the DNN model at different training stages to improve the localization performance.

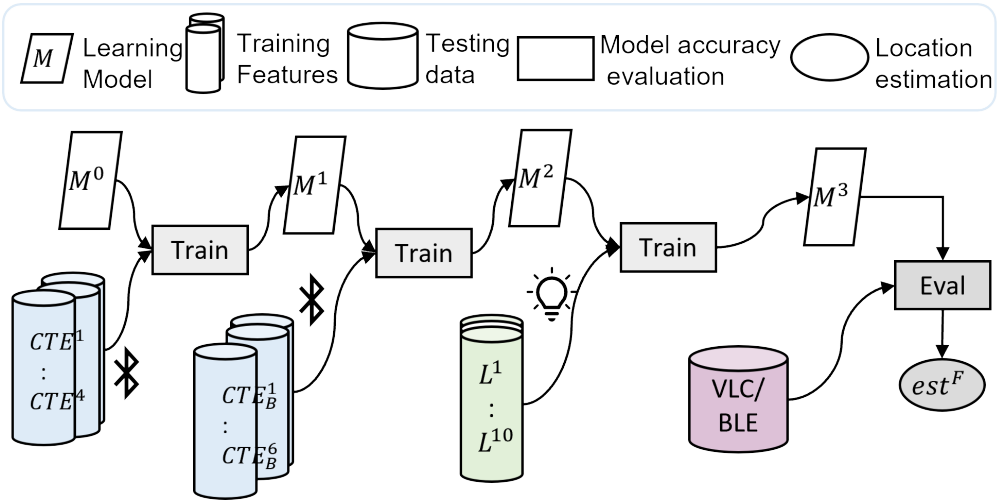

Figure 5.3: The proposed three-stage incremental learning scheme in which BLE features from the signal and beating spectrum features are fed into the DNN model at different training stages to improve the localization performance.

5.2.2 Sytsem Design

Figure5.2 shows the architecture of `BLELight` using an IL-based technique. During training, the initial step incorporates features from BLE, specifically extracted from both signal and beating spectrums[102]. IL enables the DNN model to progressively enhance its understanding of location-related features. In the subsequent stage, the model continues to refine its localiza-

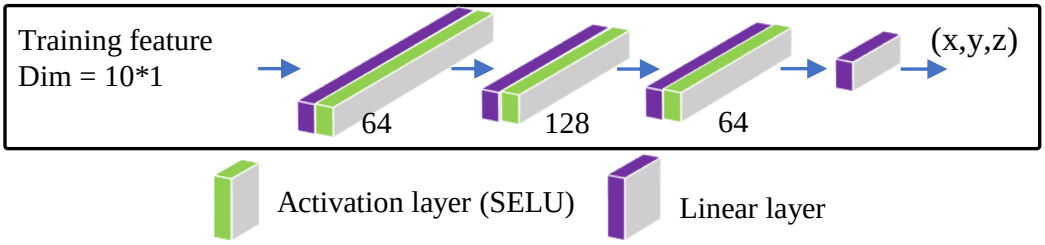

Figure 5.4: The designed DNN architecture in `BLELight`.

tion capabilities by utilizing light signature features. Localization performance evaluation can be conducted at each stage.

In Chapter 2, the utility of the beating spectrum for improved localization accuracy in the BLE localization system is demonstrated. Building upon this insight, an advanced model, `BLELight+`, is developed, extending beyond the architecture in Fig.5.2. The training phase involves integrating BLE-derived features from both the signal and beating spectra in the initial steps. In the third stage, the model continues to augment its localization abilities using light signature features. Despite the finer tuning of optical features, light signal blockages often result in missing locations. Localization performance evaluation is feasible at either the BLE or VLP stage. The DNN model in `BLELight` is a fully connected NN, with its architecture depicted in Figure 5.4. The input is a 10×1 vector, and the output comprises estimated location coordinates (x, y, z). Scaled Exponential Linear Unit (SELU) [153] is the chosen activation function for the intermediate layers.

Please note that incremental learning and joint learning are the two different approaches of machine learning techniques, the performance comparison of these would be data dependent.

5.3 Testbed & Data Collection

Testbed: The LED network testbed, previously used in Chapter 4, is employed again for data collection from LEDs. Additionally, four BLE anchor boards, as utilized in Chapter 2, are arranged in a square within a $25m^2$ area (see Figure 5.5). The prototype from Chapter 4, equipped with hue sensors, is reused with the inclusion of a BLE tag, enabling simultaneous data collection from both technologies. The testbed's proximity to windows facilitates ambient noise interference for VLP, while its metallic components create multipath effects for BLE.

Features selection: Three light hue sensors (S9706 [9]), labeled as $i = 1,2,3$, gather light features such as power at dominant wavelengths, forming light signatures:
$< P_{B_i}/P_{G_i}, P_{G_i}/P_{R_i}, PB_i/PR_i, P_{G_1} - P_{R_1} >$. This yields 10 light features for each target location.

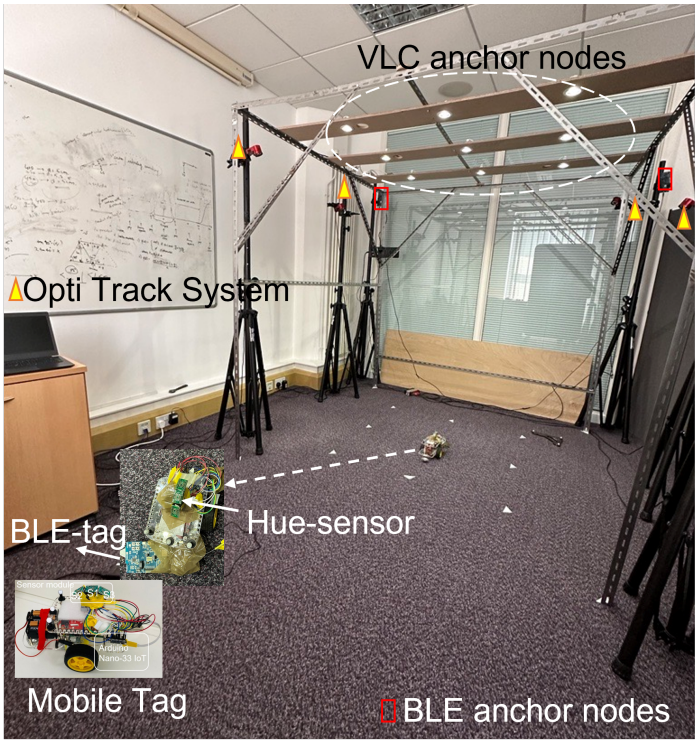

Figure 5.5: Evaluation: `BLELight` experimental setup.

While Chapter 4 utilized the first nine features for localization, the tenth feature is also included here to match the number of features with BLE. A detailed explanation is provided in Section 5.4. For BLE, RSS measurements are taken using `nrf52830` (details in [108]), extracting 10 features from each collected packet. These features comprise received power at signal tones (f_1, f_2, f_3, f_4) and beating frequencies $(f_1 - f_2, f_2 - f_3, f_1 - f_3, f_1 - f_4, f_2 - f_4, f_3 - f_4)$.

Data Collection: In this study, data collection is simultaneously carried out for both technologies using a robot equipped with both BLE and light sensors. This innovative approach allows for the concurrent gathering of data, ensuring that the conditions and environmental factors affecting each technology are identical during each data collection instance. For the *p*-VLP technology, the data is collected throughout the area, focusing on diverse and strategically chosen locations. These include spots directly under the LED lights, areas with low-light conditions typically found near walls, and places where the sensors may encounter obstructions due to human movement or metallic elements present in the testbed. This varied selection of locations is critical for evaluating the *p*-VLP technology's performance in a range of different environmental scenarios. Furthermore, the data collection spans across different days to encapsulate the variations in ambient light conditions caused by weather changes. In

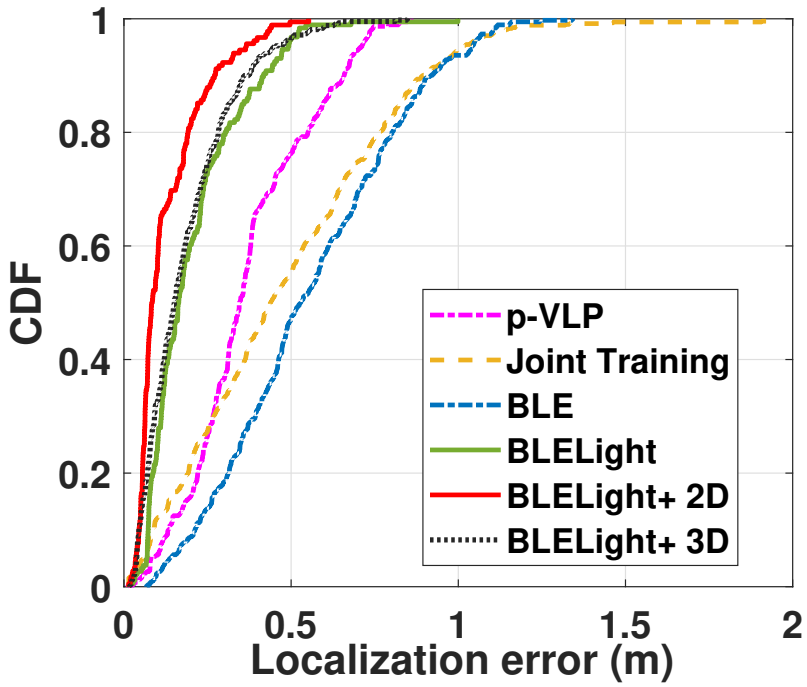

Figure 5.6: Comparative Analysis of CDF for localization error across various systems i.e. Passive-VLP and BLE vs. `BLELight`.

addition, the experiment is designed to emulate realistic conditions by having participants, present during the data collection, wear clothing of various colors on different days. This aspect is vital in testing the system's capability to handle reflections from diverse materials, specifically for wavelength VLP systems a common occurrence in real-world environments. In total, the robot collects 8813 samples for BLE and 4776 samples for *p*-VLP. This data is then divided using an 80%-20% split between training and testing sets, a distribution that balances the need for extensive training data with adequate testing samples to validate the system's performance. This methodical approach in data collection and segmentation is fundamental for an exhaustive evaluation of the technologies and their potential applications in practical scenarios.

5.4 Results & Discussion

`BLELight` is statistically evaluated using the CDF of localization error (Figure5.6). The effectiveness of `BLELight` is compared with joint training, a common data fusion technique where all features are inputted into a model simultaneously. Figure 5.6 presents the obtained results, where it can be found that joint training shows limitations in feature learning and

Table 5.1: 3D Localization error (unit: meter).

	***p*-VLP**	**BLE**	**Joint Learning**	BLELight	BLELight +
Mean localization error	0.369	0.556	0.48	0.20	0.12
Median error	0.34	0.52	0.43	0.16	0.08
80th-percentile error	0.54	0.80	0.75	0.29	0.19

performance enhancement, while BLELight & BLELight+ exhibit clear advantages with the usage of the incremental learning approach. As IL enables continual learning adaptation, it significantly enhances accuracy. Incorporating new information and incrementally fine-tuning the model leads to a reduced MLE, with $0.12m$ in BLELight+ & $0.20m$ in BLELight, surpassing joint training by up to 75% & 58%, respectively. Moreover, BLELight+ exceeds both BLELight and joint training by 40%, due to the separation of signal and beating spectrum features. While the beating spectrum aids in localization improvement, the learning algorithms for signal and beating features may be data-dependent. Moreover, Figure 5.6 showcases the 3D localization capabilities of BLELight+, revealing that 90% of errors fall below $0.35m$, along with a mean localization error of $0.15m$, marking a significant accomplishment. The performance of both systems surpasses the current SOTA in VLC and BLE localization such as [40, 154, 149, 142, 145, 155, 156]. This superior performance takes into account the variety of environmental conditions addressed in this thesis, the cost-effectiveness of the sensing units used, and the innovative methods of data extraction employed.

IL significantly transforms the approach to data fusion in hybrid systems by eliminating the conventional necessity to maintain an equal number of samples or features, a standard in joint fusion-based methods[1]. This change addresses a significant challenge: the complex requirement of synchronizing time across different receivers, each equipped with their unique crystal oscillators, and reconciling the disparate sampling rates inherent in various technologies. To facilitate a straightforward comparison in the study, a balanced number of features are incorporated within the joint training framework.

The study extends its analysis to underscore the efficacy of the hybrid model compared to solutions reliant on single technologies. This is achieved by developing and assessing the performance of distinct DNN models for both BLE and *p*-VLP. The performance evaluation, as detailed in Figure 5.6, reveals that the hybrid model BLELight+ notably outperforms the capabilities of both individual BLE and *p*-VLP technologies. The improvements are substantial,

[1]Please be aware that incremental learning and joint learning represent distinct training methods within the realm of machine learning, while their performance being heavily influenced by the specific nature of the training data involved. Therefore, the comparative effectiveness of these approaches is contingent upon the unique characteristics of the datasets (features) they are applied to.

with BLELight+ exhibiting a 79% and 67% enhancement over BLE and *p*-VLP respectively, while BLELight shows a 64% and 47% improvement in the same comparative parameters.

It is particularly noteworthy that the MLE for BLE is recorded at $0.556m$, representing a marked advancement from traditional BLE methodologies [40, 150, 151]. However, it falls short of achieving the high-performance levels of *p*-VLP. This thesis previously introduced a novel classical BLE localization method named BLoB, which achieved sub-meter accuracy and is comparable to the BLE system discussed in this chapter. Given the diverse performance parameters, a direct comparison between these two BLE-based approaches presents a complex challenge. This comparison becomes even more nuanced when considering the varied indoor environments that have yet to be tested with the BLELight+ system. Such an analysis, which could significantly contribute to the evolution and refinement of these systems, is earmarked for future research endeavors.

Compared to the current SOTA, such as [155, 156, 157, 158, 159], the integration in BLELight+ stands out not only in achieving decimeter-level localization performance but also in the uniqueness of the data types being integrated. A key aspect is the extraction of data from VLC technology within the pre-existing lighting infrastructure, which is then combined with BLE features, presenting a novel solution. This approach sets it apart from most SOTA implementations, where integration tests are typically confined to a limited number of LEDs and controlled environmental conditions.

5.5 Concluding Remarks

BLELight+ significantly enhances indoor localization by addressing the individual limitations of BLE and *p*-VLP technologies through its hybrid system. Moreover, it introduces an incremental learning-based method for training the DNN model, effectively harnessing the advantages of multimodal features from both technologies. Experimental evaluations validate the effectiveness of this method, successfully achieving a decimeter-level indoor localization system, thereby meeting the primary objective of this thesis.

CHAPTER 6

BMMW: JOINT BLE AND MMWAVE RADAR SYSTEM FOR ACCURATE TRACKING

This chapter marks a shift from the autonomous localization systems discussed in previous chapters to advanced tracking solutions, such as tracking an asset in a warehouse, specifically utilizing BLE 5.1 direction-finding standards. It explores how these solutions are enhanced through integration with mmWave radar systems, aiming to achieve a decimeter-level accurate 3D tracking system.

6.1 Introduction

This chapter delves into enhancing the tracking performance of BLE devices, with a specific focus on the advanced capabilities introduced in the BLE 5.1 standard. Notably, this standard brings new direction-finding techniques like AoA and AoD, promising sub-meter level tracking accuracy. Previous chapters, particularly Chapter 2, have discussed how these techniques, typically requiring multiple antennas, can be adapted for single antenna BLE devices to achieve autonomous localization with sub-meter accuracy.

The exploration in this chapter takes a two-fold approach to BLE localization. First, it examines the BLE 5.1 standard's AoA capabilities using multiple antennas, aiming to achieve the claimed sub-meter accuracy. Then, aligning with the thesis' objective of designing cost-effective solutions, the chapter proposes a single antenna BLE tracking method that offers comparable sub-meter accuracy. However, the challenge of BLE's narrowband nature persists,

particularly its limitation in achieving decimeter-level precision in indoor environments due to significant multipath interference. This calls for innovative solutions and the integration of other technologies.

In contrast, mmWave radar sensors, with their few gigahertz bandwidth, are capable of sensing objects with a few centimeters resolution. These sensors, surprisingly affordable (≈$10), can be employed in the passive localization of objects by harnessing Multiple Input Multiple Output (MIMO) techniques [84]. When paired with BLE devices, mmWave sensors have the potential to significantly refine location estimations, all without necessitating any extra infrastructure. However, it's important to note the limitations of mmWave radar sensors, such as their susceptibility to rapid signal attenuation and their diminished efficacy in scenarios involving stationary targets or multiple objects [5].

Therefore, this chapter proposes and examines a synergistic approach that aims to harness the strengths of both BLE and mmWave radar measurements while mitigating their respective limitations. This approach is centered around the adoption of a DNN for the fusion of signal features collecting from both BLE and mmWave sources. This methodology draws inspiration from the recent advancements made in Machine Learning (ML), particularly in addressing the complexities of multipath propagation and in developing accurate mappings between radio signal features and the precise locations of targets [160, 161, 162]. DNNs, with their robust capabilities in function approximation and their flexibility in design, have already proven their success in a wide array of applications, ranging from image processing [163] to gaming [164], and even in advanced language models [165].

Balancing computational complexity. Furthermore, considering the low-power consumption features of the BLE devices, their computational capabilities and memory are usually low. Therefore, in this chapter, an alternative option to *offload the localization-related computations from the edge device to the cloud* is proposed. The benefits gained from this option are twofold: (i) the cloud can host more advanced ML algorithms for more accurate localization [166], and (ii) one can minimize energy consumption at the edge IoT devices while decreasing their computational load. However, uploading the raw localization features to the cloud becomes challenging when the volume and types of data are considerable and the network bandwidth is limited (or when RF interference may affect the dependability of communications [167]). The concept of *goal-oriented communication*[1], which primarily focuses on conveying the main information contained in the radio features from end-devices to the cloud addresses this challenge. This approach minimizes the data sent by using an NN-based information encoder and decoder at both ends of the transceiver, thereby conserving bandwidth for

[1] In some literature, the term "goal-oriented" is also referred to as "semantic communications" or "goal-oriented semantic communications" [168].

such transmissions [169]. The encoder model deployed on the edge device generates new data samples that resemble the input data distribution and encodes I/Q data into a lower-dimensional space while capturing the input data's underlying distribution. The data reduction saves network bandwidth and energy consumption, however, typically at the expense of a (slight) reduction in localization accuracy.

Contributions. This chapter introduces BmmW, an innovative indoor tracking system that effectively harnesses the capabilities of BLE and mmWave radar technology for accurate 3D tracking of mobile tags with decimeter-level accuracy. It builds upon the advanced AoA feature from the BLE 5.1 standard, which uses a multi-antenna array to measure the phase difference of the received signal at multiple antennas and translate it into angular information. A key contribution of this chapter is the development of BmmW's unique approach, which integrates this angular data with mmWave radar measurements for training a robust DNN model. Further enhancing this system, a novel signal processing method for mmWave radar is presented, along with a signal heatmap generation method. This approach effectively converts irregular radar point clouds into regular probability distributions, aiding in accurate target localization.

Additionally, the chapter presents BmmW-LITE, a streamlined variant of BmmW. It utilizes raw IQ samples from a single-antenna BLE device in conjunction with mmWave radar measurements. This technique streamlines the computational demands associated with angle measurements in BmmW and further cuts down the expense of BLE anchor devices since it is compatible with single-antenna devices. Both BmmW and BmmW-LITE are designed to run on edge devices, but as their computational capabilities and memory are sometimes limited, it may be desirable to off-load the localization task to the cloud. When doing so, vast amounts of sensor data needs to be transmitted to the cloud, which takes a significant portions of the network bandwidth, increases latency, and slows down the update rate – all factors that are detrimental to tracking applications in B5G networks. To tackle these challenges while keeping both cost and computational overhead low, the chapter introduces BmmW-LITE+, an extension of BmmW-LITE which shares the computational complexity of the localization between the edge device and the cloud, enabling the preliminary deployment of the learning model directly on the edge device. This approach allows to capture the semantics of the raw I/Q data, enabling efficient feature extraction and noise mitigation at the edge device. The experimental results show that the BLE features can be compressed to 12% of their initial size without a substantial loss in the final localization accuracy.

The practical effectiveness of BmmW, BmmW-LITE, and BmmW-LITE+ is demonstrated through real-world environment testing. The results showcase that mobile tags can be tracked with mean 3D localization accuracy of 10 cm, 36 cm and 39 cm, respectively. Such accuracy is

superior to that of classical BLE localization methods by up to 80% [40] – albeit at a price of an increased computational complexity – and is especially remarkable for BmmW-LITE and BmmW-LITE+, as the latter does not require the use of bulky and costly multi-antenna arrays.

This chapter's findings were presented at the 19^{th} International Conference on Distributed Computing in Smart Systems and the Internet of Things (DCOSS-IoT), 2023, where they received the prestigious '**Best Paper Award**'. Furthermore, an extended version of this research has been invited for submission to the Special Issue of the 'Pervasive and Mobile Computing' Journal, and the submission has been completed.

Chapter outline. The remainder of this chapter is structured as follows: Section 6.2 provides an overview of the employed technologies and related work. In Section 6.3, the inner details and implementation of BmmW are provided. The experimental extraction of DNN model features is presented in Section 6.4, and the corresponding localization evaluation and results obtained with a mobile target are discussed in Section 6.5. Finally, the paper concludes with a discussion about the main benefits and limitations in Section 6.6, and with a summary of the main findings in Section 6.7.

6.2 Background and Related Work

This section provides a detailed overview of mmWave technologies and data fusion methods based on NNs, building upon the BLE 5.1. It then delves into the most relevant works related to BmmW, encompassing studies that leverage multiple technologies for indoor localization, implement multi-sensor fusion to enhance accuracy and apply goal-oriented communications for efficient feature data compression.

6.2.1 Bluetooth Low Energy

Building on the SOTA BLE 5.1 AoA localization technique covered in previous chapters, this chapter introduces BmmW. BmmW trains an NN using both BLE and mmWave radar measurements to create a localization system capable of decimeter-level accuracy for mobile targets, effectively handling dense multipath effects. Additionally, BmmW-LITE is presented, which eliminates the need for multi-antenna designs, as explored in prior research. Furthermore, this chapter introduces BmmW-LITE+, enhancing semantic capabilities at the end-device level. This reduces the volume of data transmitted to the cloud, thereby easing the localization processing load on edge devices, which often have limited memory.

6.2.2 mmWave Radar

mmWave technology commonly refers to the use of RF signals above 60 GHz. The use of sensors operating at these frequencies in contrast to narrowband technologies, has shown great promise for high-precision indoor tracking applications. These sensors typically have a wide bandwidth of a few gigahertz and the Frequency Modulated Continuous Wave (FMCW) Radar approach, enabling them to sense objects with a high distance resolution of a few centimeters. The principle of mmWave radars and the underlying FMCW[2] approach have been documented in detail in the literature, like in [5]. When combined with MIMO antennas, whose size is typically very small (e.g., 2x2 mm [170]), mmWave radars can operate as 3D imaging sensors. With accurately detecting the 3D coordinates of objects and generating point clouds that encode their spatial shape [5].

Many researchers have used commercial mmWave radars as a low-cost and easy-to-deploy solution, and have shown that they can locate a target (e.g. human) within a 20 cm error provided the target is within the effective detection range of the radar. For example, authors in [171] and [172] use radars from Texas Instrument (TI) that have integrated transmitters and receivers on a single chip. Zhao et al. [171] use NNs to process mmWave radar data and propose a human identification and tracking system with a 16 cm median error, but that can only detect one person at a time. Cui et al. [172] have shown that a single radar can have a high false alarm rate: while this can be significantly improved by fusing information from multiple radars, a minimum distance (15 cm) between people is necessary to correctly discern multiple individuals. Wu et al. [173] have used separate mmWave transmitters and receivers, and designed a novel system that can locate multiple people simultaneously with a 10 cm error. However, they have also shown that the accuracy would decrease significantly to more than 30 cm when the person is more than 1.5 m away, as well as when there are more than two people present. Hence, while mmWave radars offer several advantages over other tracking technologies (such as not requiring tags or smart devices to be carried by subjects), *the problem of failing to distinguish between multiple targets and being prone to clutters in the environment and occlusion on the line of sight are intrinsic weaknesses of this technology. Additionally, mmWave signals attenuate quickly through the air and rely on Doppler detection, which can reduce their range of view and limit their effectiveness in monitoring stationary targets [5].*

Figure 6.1 gives an illustration of the theoretical RSS of a typical mmWave radar operating in an indoor environment. The RSS calculation is based on the antenna radiation pattern of the TI `IWR1843`[3] mmWave radar model. The radiation pattern defines the relative strength of

[2] FMCW radar works by continuously transmitting a signal with a frequency that linearly changes over time, and it measures the frequency shift of the reflected signal to determine target range and velocity.

[3] `https://www.ti.com/product/IWR1843`

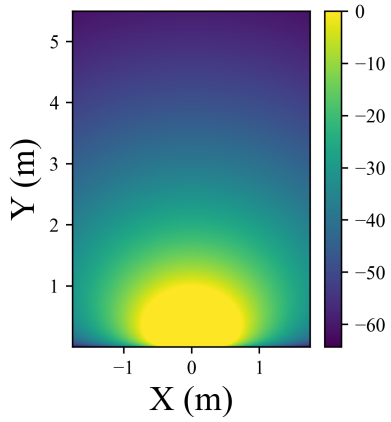

Figure 6.1: Simulated RSS (in dBm) of a typical mmWave radar placed at position (0,0).

the radio signal transmitted and received at different directions. In the case of the `IWR1843` model, its signal strength is attenuated to approximately −3 dB at an azimuth angle of 45° and to −6 dB at 60°. Considering together the fact that RF signals attenuate proportionally to the square of propagation distance, the mmWave signal reflections are often strong only at close distances, with a substantial decrease of over 30 dB within a few metres, as shown in Figure 6.1. Therefore, it is often found that a mmWave radar can effectively sense the position and posture of a person within a close distance, but the accuracy drops dramatically as the person moves away from the radar due to the rapid decrease in signal strength. To address these challenges and enhance localization performance, BmmW proposes a joint tracking system that combines information from BLE and mmWave technologies: by leveraging the strengths of both technologies, BmmW improves the accuracy and reliability of indoor tracking in challenging environments. Moreover, this chapter adopts the concatenation-based NN for radio feature fusion, wherein a two-head input NN is designed for BLE and mmWave feature processes, and then the processed features are concatenated together for the following joint training.

6.2.3 Multi-Sensor Data Fusion

Several research works have proposed the combination of multiple communication technologies to improve the accuracy of indoor localization. For instance, Liu et al. [67] fuse Wireless Fidelity (Wi-Fi), inertial sensors, and BLE beacons for indoor localization. However, this method requires users to carry a smartphone with extra sensors, which may not be practical in some situations. Bala et al. [174] combine UWB and BLE signals to provide real-time location updates, but require installation of UWB and BLE devices throughout the indoor environment, which

can be expensive and time-consuming. Jeong et al. [68] propose a machine learning-based fusion that requires a large amount of training data to predict the user's location accurately. Istomin et al. [175] propose a dual-radio protocol to enable energy-efficient and accurate social contact detection, leveraging a narrowband radio (BLE) and an UWB radio. Zhang et al. [69] propose a system that fuses Wi-Fi and Bluetooth fingerprints in edge computing. Several other works [70] have also used multi-sensor fusion to increase the accuracy of indoor localization (e.g., inertial measurements unit (IMU) data, etc.). However, these approaches are highly dependent on the quality of the radio signal, which can be affected by factors such as signal interference and the number of access points in the environment. The main limitations of these approaches are related to the complexity and cost of the technology, the need for user participation, and environmental factors that affect the accuracy of the localization system. In contrast to these approaches, BmmW does not require additional hardware on the target device and leverages angular information, which is less affected by multipath.

6.2.4 Goal-oriented Semantic Information Extraction

The deployment of advanced ML localization models faces significant challenges due to computational limitations and power constraints within the local IoT environment. BmmW traditionally runs on the edge device but allows to address the aforementioned issue in its BmmW-LITE+ variant by shifting the transfer of computationally intense tasks to the cloud using goal-oriented communication. In this scenario, the objective is to efficiently transmit essential information from the raw radio signal features to the cloud, minimizing the use of network bandwidth. This information will then be reconstructed in the cloud without compromising its fidelity, with the ultimate goal of enabling accurate localization.

A key challenge in this process is the extraction and recovery of vital information: currently, the concept of goal-oriented communication relies heavily on Semantic Communications (SemCom) to achieve this goal. A substantial body of research has been dedicated to developing robust and comprehensive methods for semantic extraction, transmission, and recovery [176, 177, 178, 179]. Under the paradigm of goal-oriented semantic communication, the autoencoder is arguably the most prevalent SemCom framework [180]. With an autoencoder, the raw feature can be compressed to a latent space via an encoder for transmission, and a corresponding decoder on the receiver can reconstruct the features embedded in the latent space. In the context of location estimation within BmmW, by leveraging goal-oriented SemCom, it becomes possible to transmit the compressed sensor data to a central unit or location engine in the cloud. In this setup, the pre-trained encoder model can be deployed on the edge device, while the decoder is situated in the cloud.

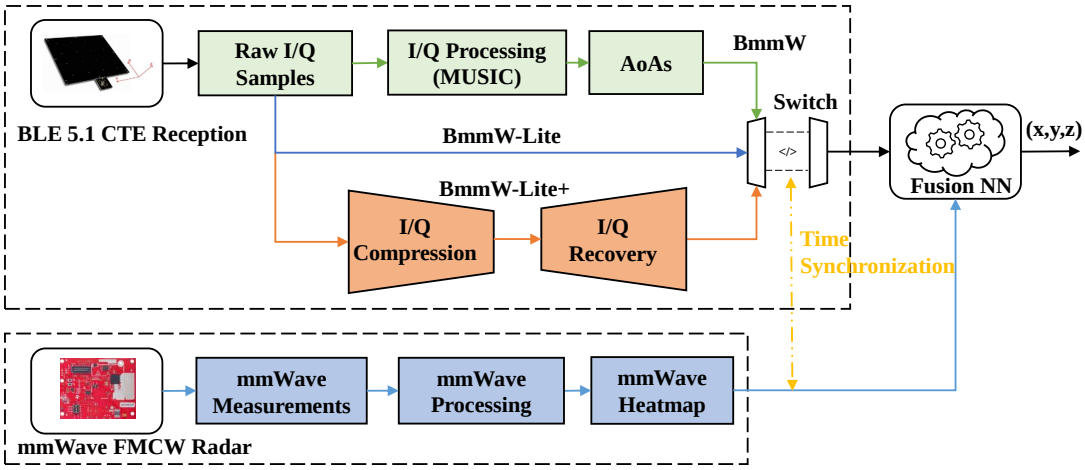

Figure 6.2: Overview of BmmW, an indoor localization system leveraging BLE 5.1 and mmWave measurements to jointly train a DNN and predict the 3D coordinates of a mobile tag. The BmmW-LITE variant uses raw I/Q measurements and can be run on single-antenna devices. The BmmW-LITE+ variant extends BmmW-LITE with the ability to efficiently off-load the localization task to the cloud by means of an effective compression of the raw features.

6.3 BmmW: Design and Implementation

This section describes the design and implementation of BmmW, further providing the technical details of its components, including the BLE and mmWave subsystems, as well as the fusion DNN model.

6.3.1 Overview of BmmW

The structure of the proposed joint localization framework is shown in Figure 6.2. BmmW's foundation lies in the reception of BLE 5.1's CTE and mmWave FMCW radar measurements. The *reception* and *processing* of the BLE CTE packets are selective. Two variants of BmmW are proposed in parallel with BmmW, i.e., BmmW-LITE and BmmW-LITE+, to accommodate different application scenarios, as further elaborated below:

- BmmW: The raw I/Q samples are collected from BLE anchors with *multiple* antennas, and are processed by the MUltiple SIgnal Classification (MUSIC) algorithm for AoA estimation, which serves as the default BLE feature for the proposed fusion model.
- BmmW-LITE: Only raw I/Q samples from a *single* antenna constitute the BLE feature, in order to reduce the feature processing time and decrease the system's cost as well as complexity.

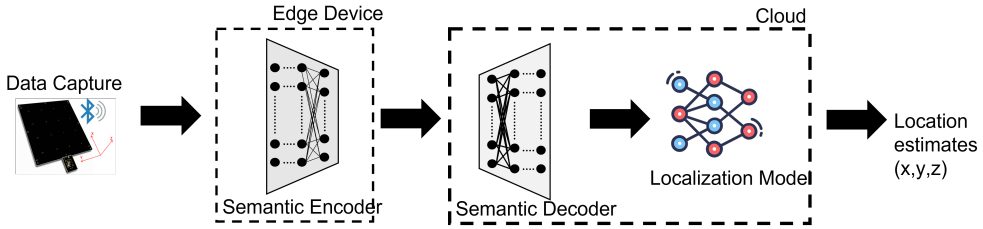

Figure 6.3: Framework of BmmW-LITE+: balancing the computational complexity by sharing the computational complexity of the localization between the edge device and the cloud, by enabling the preliminary deployment of the learning model directly on the edge device.

- BmmW-LITE+: It compresses the raw I/Q samples from a *single* antenna by extracting the latent information under the framework of goal-oriented semantic communication. This way, it reduces the amount of BLE feature data that needs to be transmitted when the localization task is off-loaded to the cloud. Hence, in BmmW-LITE+, the functions of the BLE feature reconstruction, mmWave heatmap generation, and final fusion moded are located in the cloud server to alleviate the computational stress on the local devices[4]. A simplified framework is shown in Figure 6.3.

The switch in Figure 6.2 represents the BLE feature selection process. The techniques used to extract the relevant *features* from BLE will be detailed in Section 6.3.2. For the mmWave measurement, the critical step is the generation of the heatmap, which aims to overcome the irregularity of the radar point cloud: details about this component will be discussed in Section 6.3.3. Please note that, for accurate location prediction, the BLE features stream should be synchronized with the mmWave heatmap stream according to the recorded timestamps. Ultimately, the synchronized BLE & mmWave features are fed into the fusion DNN model for 3D location estimation. The architecture of such a DNN model is detailed in Section 6.3.4. Lastly, the BLE feature compression and the corresponding Variational Autoencoder (VAE) architecture is elaborated in Section 6.3.5.

6.3.2 BLE Direction Finding

AoA and AoD are the direction-finding enhancements introduced in the BLE 5.1 standard [42]. The key concept behind these techniques involves measuring the phase difference of the received waveform across multiple antennas and determining the direction of the signal from the computed phase difference. Given the known separation between the antennas, the AoA

[4]The compression of mmWave features are not taken to account, as the mmWave data has been processed into a $n \times 3$ point cloud matrix. Transmitting this vector directly is acceptable when comparing its size to that of the raw BLE I/Q data.

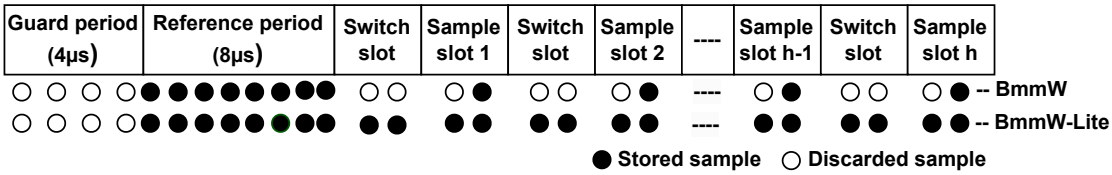

Figure 6.4: CTE packet & sampling structure for '*multiple-antenna*' (BmmW) & '*single-antenna*' (BmmW-LITE) system.

and AoD can be calculated using Eq. 6.1:

$$\theta_A = arccos((\phi\lambda)/(2\pi D)) \qquad \theta_D = arcsin((\phi\lambda)/(2\pi D)) \tag{6.1}$$

where λ is the wavelength ($0.125m$ mm in BmmW), ϕ is the phase difference, and D is the distance between adjacent antennas (11.8 mm in BmmW) in an antenna array. However, to determine the true AoA, MUSIC is run on the obtained angles, a detailed process outlined in [181, 113].

To perform these techniques, the Bluetooth SIG added a new field called *Constant Tone Extension (CTE)* at the end of a Bluetooth packet, details of which have already been discussed in the previous chapter.

CTE Sampling. The sampling band of 148 μs in the CTE field does not necessarily equate to collecting the maximum possible number of samples due to the duration of the switching slots, making it difficult for classical AoA/AoD techniques to utilize the entire band. While the BLE 5.1 standard defines the sampling period, manufacturers have the flexibility to develop their own methods for efficient utilization. One such method, proposed by Silabs [113] and adopted by BmmW with added I/Q samples collection, allows to collect a maximum of 74 samples with a 1 μs switching slot, as illustrated in Figure 6.4. In the ideal scenario, simultaneous sampling of all antennas would be required, implying the use of multiple radio switches, which is impractical. As an alternative, antennas can be sampled sequentially in a time-division manner. However, this approach introduces a phase shift. To accurately calculate angles, phase compensation must be applied. The initial eight samples of the CTE packet (refer to Figure6.4) are obtained from a single antenna and serve as reference points for assessing phase variation. This procedure is replicated for each packet. Subsequently, employing Equation6.1, the angle θ_A is calculated. The utilization of the MUSIC [181] algorithm then assists in determining the true AoA.

The technique described above for BmmW discards the remaining 74 samples during antenna switching slots, and the samples are reduced to half when the switching slot is 2 μs. To optimally utilize the CTE sampling band, this thesis proposes BmmW-LITE: a *single-antenna*

system, illustrated in Figure 6.4, that eliminates the need for multiple antenna switching, hence allowing a single antenna to collect all I/Q samples within the 148 μs CTE band. The collected raw I/Q samples are utilized as a 'feature' to train the NN model. As the CTE is a constant frequency tone, the model can learn channel impairments. Additionally, these samples are jointly trained with the information from the mmWave radar, as described in Section 6.3.4.

6.3.3 mmWave Radar Heatmap Construction

The principle of mmWave radars and the underlying FMCW approach have been documented in detail in the literature, e.g., in [5]. The radar sends mmWave signals to detect objects in the scene, receives the reflections, and uses a set of signal processing techniques to produce a point cloud that encodes the 3D location and shape of the objects. As an FMCW radar, it uses chirp signals to sense objects, where the frequency of the signal is modulated to linearly increase over the transmission. The radar sends out a series of chirp signals and tracks the phase changes across them to measure the velocity of objects. It also compares the phase differences between antennas to measure the angle of the objects. This procedure is illustrated in Figure 6.5 and to demonstrate let N_c denote the number of chirps per frame, N_s denote the number of samples per chirp, and N_{rx} denote the number of transceiving antenna pairs, then the input of the Digital Processing Chain (DPC) is a 3D matrix I of size $N_{rx} \times N_c \times N_s$. A range-FFT is performed along the N_s axis. It gives an output matrix $R^{(N_{rx} \times N_c \times N_s^*)}$ that encodes the object location in the range domain, where N_s^* is the size of the range-FFT. Then, a Doppler-FFT is performed along the N_c axis of R and gives an output matrix $D^{(N_{rx} \times N_c^* \times N_s^*)}$ that measures the velocity distribution of the objects, where N_c^* is the size of the Doppler-FFT. The average of D along the N_{rx} axis is calculated as $\bar{D}^{(N_c^* \times N_s^*)}$. A peak detection algorithm, such as the Constant False Alarm Rate (CFAR), is then applied over $\bar{D}$, which gives a list of the k detected objects, with their indices in the Doppler and range domain $\{(c_1, s_1), (c_2, s_2), ..., (c_k, s_k) | c \in N_c^*, s \in N_s^*\}$. For each object in the detection list, the corresponding value in the Doppler-FFT output matrix D is taken using c and s as indices, resulting in a 1-D array $O^{(N_{rx})}$ which corresponds to the signal at each receiving antenna. An AoA calculation algorithm, such as an angle-FFT or a beamforming-based algorithm, is performed on O. Together with the object's range index s, the calculation gives the object's x-y-z coordinates with respect to the radar, which becomes a point cloud.

However, *the density and the accuracy of the point cloud are prone to noise and can have arbitrary population, making them unsuitable to be processed by an NN directly*. Additionally, commercial off-the-shelf mmWave radars are commonly designed for automotive driving applications and suffer from a *lack of elevation resolution*. For instance, the TI AWR series

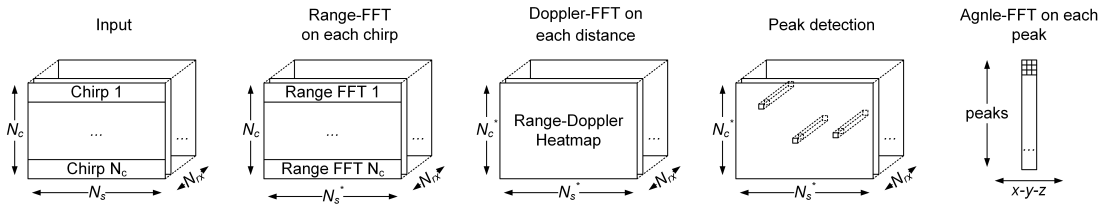

Figure 6.5: Point cloud generation procedure of a typical mmWave radar [5].

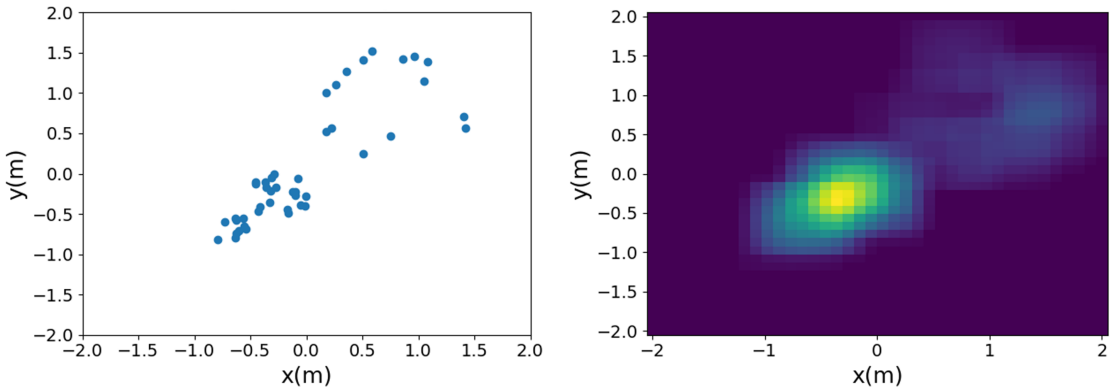

Figure 6.6: Heatmap construction e.g., with 3D point cloud from the radar (top view) (left), and constructed 2D heatmap (right).

features 'eight' virtual antennas along the azimuth direction, but only two along the elevation direction [182], rendering it unsuitable for numerous geometry-based solutions due to its unbalanced resolution. As a result, since the elevation information may prove less dependable, BmmW relies solely on 2D information (i.e., azimuth and depth) from the radar, and converting it into heatmaps. These heatmaps encode the probability distribution of the person's position in the scene, offering a feasible alternative. The heatmap approaches deliver low computational complexity and facilitate the NN's ability to extract features by compressing the feature space.

Heatmap Generation The complete mmWave data processing chain involves three parts. The first part follows the standard FMCW approach as shown in Figure 6.5 and is completed by the radar on-chip processors. It processes the raw mmWave RF signal and generates a 3D point cloud that accurately represents the scene. Then, a clutter removal stage is introduced. In indoor environments, there are often plenty of clutters that typically remain stationary and produce constant reflections to the radar. By eliminating clutters, the radar can focus on detecting and tracking the actual target(s) of interest. This provides the radar with increased sensitivity in detecting weaker target signals, as well as reduced false alarm rate when dif-

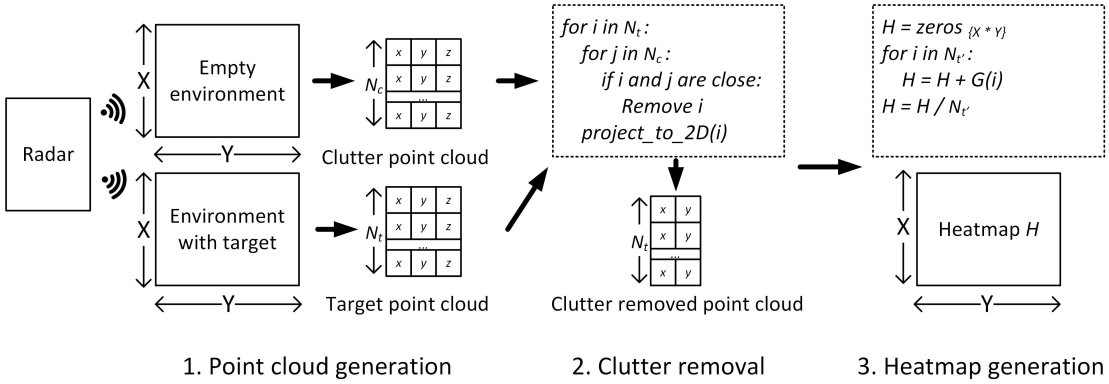

Figure 6.7: The full data processing chain of the mmWave radar.

ferentiating between real targets' signals and irrelevant signals. A traditional way of clutter removal is by simply filtering out all zero-Doppler signals during the Doppler-FFT stage described earlier. However, as the experiments also involve the detection of stationary targets, eliminating zero-Doppler signals would reduce the sensitivity of the system. Therefore, in this work, clutter removal by recording the detected point cloud from the empty environment and subtracting them from the actual detection using geometrical distance-based filtering is performed. Targets within several centimeters of a recorded clutter will be discarded from the point cloud, effectively removing the unwanted reflections. This is especially beneficial when the detection of stationary people is required. In the third stage, a heatmap representing a probability distribution on the target's location in the area is generated, where the probabilities are calculated based on the strength of the mmWave signal (i.e., the population of the point cloud in each unit region):

$$H(P) = \begin{cases} \sum_{(x,y)\in P} \frac{G(x,y)}{|P|}, & \text{if } |P| > 0 \\ 0, & \text{otherwise} \end{cases} \tag{6.2}$$

where P is a set representing a 2D point cloud with a population of $|P|$ and coordinates $\{(x_1, y_1), ..., (x_{|P|}, y_{|P|})\}$. $G(x, y)$ creates a 2D Gaussian kernel at point (x, y). $H(P)$ is the resulting 2D heatmap that represents the point cloud distribution in the environment. The heatmap, illustrated in Figure 6.6, indicates a higher probability for points with a larger population, such as the person cluster in the middle, compared to the clutter on the left. The entire procedure is displayed in Figure 6.7.

6.3.4 Fusion Neural Network Design

Figure 6.8 shows the architecture of the designed fusion NN, which contains two branches for different inputs. The top branch is designed as Fully Connected Network (FCN) for the processing of the BLE feature, while the bottom branch is a Convolutional Neural Network (CNN), taking the mmWave heatmap as the input feature. After the convolution, this feature is flattened to a linear layer and eventually coated with the output of the top NN branch. The output of this NN is the (x, y, z) coordinate of the estimated location. The neuron numbers of each linear layer and the involved activation functions are annotated in Figure 6.8. Please note that, for BmmW and BmmW-LITE, the neuron number of each layer in FCN is different due to the diverse dimensions of the training features. Specifically, in BmmW, the estimated azimuth angle θ, elevation angle ϕ, and corresponding estimated distance to the objective of all anchors consist of the ultimate training feature, which is a $3 * 4$ dimensional vector. Hence, the number of neurons of each linear layer is 100, 100, 50, 50, and 50. Instead, in BmmW-LITE, the training features are I/Q samples with dimensions of $164 * 4$. Hence, the number of neurons of each linear layer is set to 1000, 500, 100, 100, and 50. Adam [183] is selected as the optimizer of the entire NN. The initial learning rate lr is the default value, while it decays according to

$$lr = lr * 0.3^{epoch//20} \tag{6.3}$$

where, $epoch$ indicates the index of current training epoch, and // represents the discard remainder operation. The Mean Absolute Error (MAE) is the selected loss function for NN training, which is defined as $loss = mean(|(\hat{x}, \hat{y}, \hat{z}) - (x, y, z)|)$, with (x, y, z) being the ground truth coordinate and $(\hat{x}, \hat{y}, \hat{z})$ the estimated coordinate.

6.3.5 Variational Autoencoder-based BLE Data Compression and Recovery

Figure 6.9 illustrates an NN architecture based on VAE designed for compressing and recovering BLE features. The VAE framework provides a powerful method for training deep latent-variable models and learning posterior inference models through the use of stochastic gradient descent, as detailed in [184]. As depicted in Figure 6.9, the VAE architecture comprises two main components: an encoder and a decoder. The encoder, often referred to as the inference model, is responsible for learning the posterior distribution in the low-dimensional latent space based on the input data samples. On the other hand, the decoder functions as a generative model, learning the joint distribution of the latent variables and the input data. The loss function of the VAE is formally defined in Eq. 6.4.

$$\mathscr{L}_{VAE} = -\sum_{i} \Big[\mathbb{E}_{z\sim q_\theta(z|x_i)} \big[\log p_\phi(x_i|z) \big] + \mathbb{D}_{KL}\big(q_\theta(z|x_i)||p(z)\big) \Big] \tag{6.4}$$

where θ and ϕ represent the learnable parameters of the encoder NN and the decoder NN, respectively. $q_\theta(z|x_i)$ is used to denote the posterior inference for input sample i and $p_\phi(x_i|z)$, to represent the generative model given the latent distribution, as described in [185]. The initial term in Eq. 6.4 corresponds to the expected log-likelihood of the data, assuming a Gaussian probability density function. Maximizing this term is equivalent to minimizing the mean squared error in the reconstruction. The second term in the equation represents the Kullback–Leibler divergence between $q_\theta(z|x_i)$ and the prior distribution $p(z)$. This divergence term serves as a regularization mechanism for the latent space [186].

In BmmW-LITE+, this VAE framework is built upon BLE I/Q samples. The BLE local anchors are assumed to be able to conduct semantic compression using the associated encoder. Each BLE sample comprises 164 features, out of which 82 represents amplitude information and the remaining 82 represents phase information extracted from each I/Q sample. To ensure symmetrical semantic processing capability, the NN consisting of the encoder and decoder is structurally symmetrical along the bottleneck, which adheres to the paradigm of FCNs. The VAE model, once trained, will be divided into an encoder and a decoder for *practical* deployment in the real world. The encoder will be deployed on BLE local devices, while the decoder will operate on the cloud server. The objective of this process is to compress the raw I/Q dataset using the embedded encoder on BLE devices, and then transmit the compressed data to the cloud server through a wireless channel for subsequent reconstruction and utilization. Notably, the dimension of the VAE bottleneck layer (C value in Figure 6.9) has a significant impact on both data compression quality and the final localization outcome. Therefore, careful consideration must be given to the signal compression ratio. Since the VAE is a lossy compression, higher compression ratios result in greater information loss. In this work, the relationship between the VAE's bottleneck dimension and the mean localization error will be discussed in Section 6.5.2.

6.3.6 Implementation of Neural Network Models

Next, this section provides a detailed description of the implementation of three main components described in Figure 6.2.

6.3.6.1 BLE Data Branch

The collection of BLE features is performed using Silabs EFR32xG22 boards [58], which serve as anchor nodes, and the implementation is performed by employing the direction-finding solution provided by Silabs' AoA implementation [187, 113]. The I/Q sampling capability is added to this stack to collect the raw measurements, as detailed in [113]. Please refer to

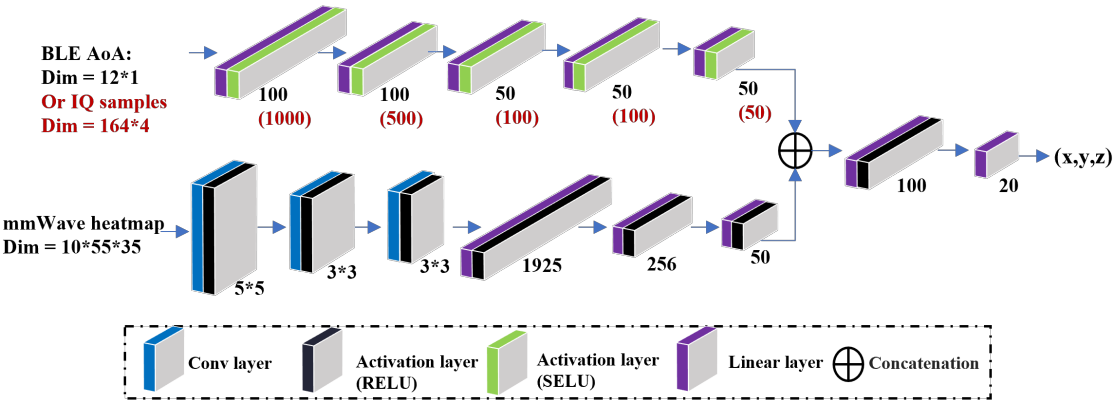

Figure 6.8: The concatenated two-branch NN architecture employed for feature fusion, where the top branch is the FCN aiming to process the BLE features, and the bottom branch is designed as the CNN to handle the mmWave heatmaps.

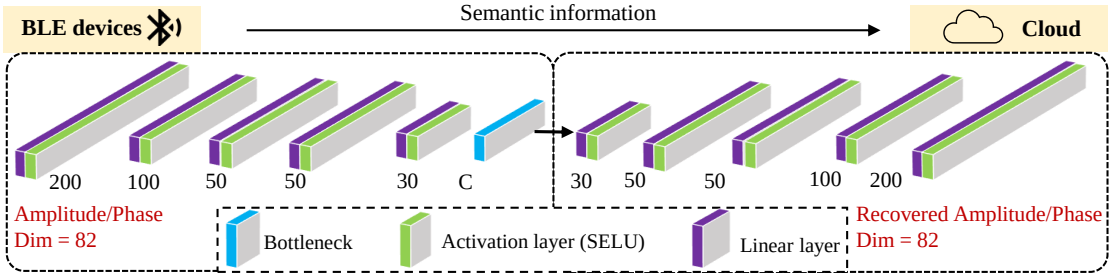

Figure 6.9: The VAE architecture for BLE feature compression and reconstruction based on goal-oriented semantic communications.

Silabs[188] for a comprehensive overview of the BLE software architecture. The ID of anchor nodes/locators, their positions relative to local-coordinate systems, and antenna orientation are all input into the host locator system using .json format files. The `EFR32xG22` boards are equipped with a 4×4 antenna array, but as in BmmW-LITE & BmmW-LITE+, there is no need to switch between antennas, only a single antenna is utilized for I/Q collection. The `EFR32BG22` Thunderboard, detailed in [189], is used as a target device that operates in the *connectionless-mode* sending the CTE packets in periodic advertisements [113]. For the BmmW, the BLE stack implementation is the same, but all the antennas on the array board are utilized to determine the phase difference of the incoming signal, as antenna switching is necessary to analyze the AoA technique [42].

6.3.6.2 mmWave Radar Data Branch

An `IWR1843` radar from TI is used to perform experiments, operating within the 77 GHz to 81 GHz frequency range. The heatmap is set to a size of 55×35 pixels, covering a 5.5 m $\times$ 3.5 m

area (refer to Section 6.4.1), resulting in a resolution of 0.1 m per pixel. To transform a point cloud into a heatmap, the point cloud is projected to 2D. A Gaussian kernel with a radius of 4 is defined for each point, and these kernels are cumulatively added to the heatmap according to their 2D coordinates.

The resultant heatmap is normalized to range between 0 and 1, indicating the radar's confidence in pinpointing the target's location. In the data recording phase, the radar is first directed towards an empty scene to capture the background reflection from clutters, creating a clutter heatmap. This clutter heatmap is then subtracted from the actual data recordings. The radar operates at 25 frames/sec, and 10 consecutive frames are combined into a single data instance to diminish the impact of outliers. Each data instance is transformed into a heatmap of the predefined size and these heatmaps are input into one branch of the NN, where they are fused with the BLE data branch.

6.3.6.3 VAE for BLE Data

The primary function within BmmW-LITE+ is the goal-driven VAE framework designed for compressing and reconstructing BLE data. The distributions of BLE amplitude and phase exhibit significant deviations. During the training experiments with the VAE, a noticeable drop in reconstruction accuracy occurred when combining amplitude and phase information as joint input features for the VAE. Consequently, this work presents the training of two distinct VAE models: one dedicated to amplitude and the other to phase. Considering the computational and resource limitations on edge devices, both VAEs adopt the simplest FCN architecture, depicted in Figure 6.9. The SELU activation function, chosen for its proven stability in training scenarios, is used in these models.

6.4 Real-time Data Collection

This section describes the scenario employed to collect real-time data for training and testing the BmmW's NN model.

6.4.1 Experimental Setup

A real-time indoor testbed for joint data collection from BLE and mmWave is built, employing four BLE anchors at the corner of a 5.5 m × 3.5 m area and placing the mmWave transceiver in the middle between two BLE anchor nodes, as presented in Figure 6.10. The BLE anchors nodes are placed at a height of 2 m from the ground, while the mmWave transceiver is placed at 0.8 m. A highly accurate Optitrack system consisting of eight cameras is erected around the edge of

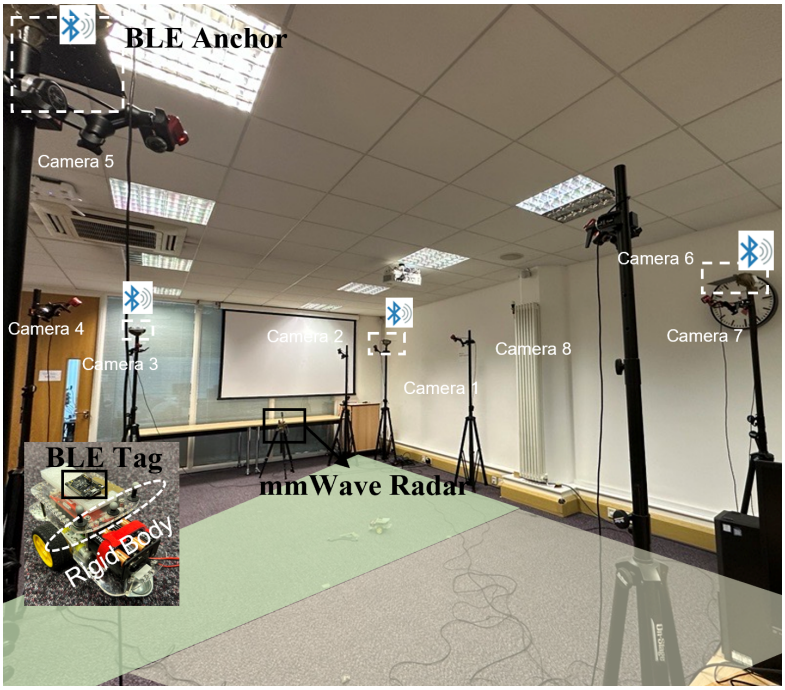

Figure 6.10: Experimental testbed used to simultaneously collect the real-time data from both BLE & mmWave sources with a moving target. The target, held by a human subject, follows a random trajectory within the testbed arena.

the site to gather ground truth coordinates of the mobile target. The Optitrack system is initially calibrated to achieve a localization accuracy of 0.44 mm. A total of 12 trials are conducted for data collection, involving a person holding a BLE tag. In each trial, the individual traverses a random path within the experimental area. The trials are further diversified by involving three different individuals of varying heights to enhance the robustness of the data collection process. Throughout these trials, the BLE anchors continuously receive I/Q packets from the asset tag (i.e., the target beacon), while the mmWave radar simultaneously collects the reflected signals from the moving person. This experimental setup leads to the collection of 12 sessions, each session capturing two minutes of data from BLE, mmWave radar, and the Optitrack system. The total volume of data collected and synchronized amounts to approximately 66000 entries.

6.4.2 Dataset Collection

The methodology for dataset collection is illustrated in Figure 6.10. Three data streams (from BLE, mmWave, and OptiTrack) are synchronized according to the *UTC time stamping* for training the NN. For one sample, the BLE I/Q features form a $164 * 4$ vector consisting of

amplitude and phase information extracted from the recorded I/Q samples. The BLE AoA features for one sample consist of a $3 * 4$ vector with estimated azimuth angles, elevation angles, and corresponding distances. As discussed in Section 6.3.6.2, one mmWave sample contains a $55 * 25 * 10$ array as the feature. To evaluate the effects of the mmWave signal in different regions, the entire experimental area is divided into two parts: the *mmWave strong* area, which is the square area in front of the mmWave board (with a size of 3 m × 3 m, marked in light green); and the *mmWave weak* area, which is far from the mmWave board (marked in light yellow). This division is necessary because ≈ 48% of the 66000 data instances of the mmWave radars fail to detect the target person at all, confirming the argument that the mmWave radar alone has a limited range/angle of view, thus emphasizing the importance of combining multiple technologies in BmmW.

6.5 Experimental Evaluation

This section describes the performance of BmmW and shows the achieved 3D localization accuracy for a mobile target, as well as a detailed characterization of the performance of BmmW's variants BmmW-LITE and BmmW-LITE+.

6.5.1 Evaluation Metric

The model evaluation is conducted on a server with Intel 2 E5-2640v4 CPU and 2 RTX 2080Ti GPU. The splitting of the training and test dataset follows the 80%-20% principle. For the model training and testing, the batch size is set to 100, and early stopping is adopted, with the stopping patience equal to 10. This implies that if the 'test loss' fails to decrease for the next 10 epochs, the training will be terminated. The MLE is used as the model performance evaluation criteria, defined as the averaged Euclidean distance between the predicted location and the ground truth location among all test samples, as shown in Eq. 6.5:

$$MLE = \sum_{i=1}^{N_t} \sqrt{(\hat{x}_i - x_i)^2 + (\hat{y}_i - y_i)^2 + (\hat{z}_i - z_i)^2} / N_t \tag{6.5}$$

where N_t represents the number of test data. It is worth mentioning that the NN predictions $(\hat{x}, \hat{y}, \hat{z})$ are raw predictions *without* any further processing like smoothing or filtering.

6.5.2 Results: BmmW and BmmW-LITE

A comprehensive evaluation of both BmmW and BmmW-LITE is conducted, examining their performance across a range of BLE anchor configurations, denoted as BLE*k, where k rep-

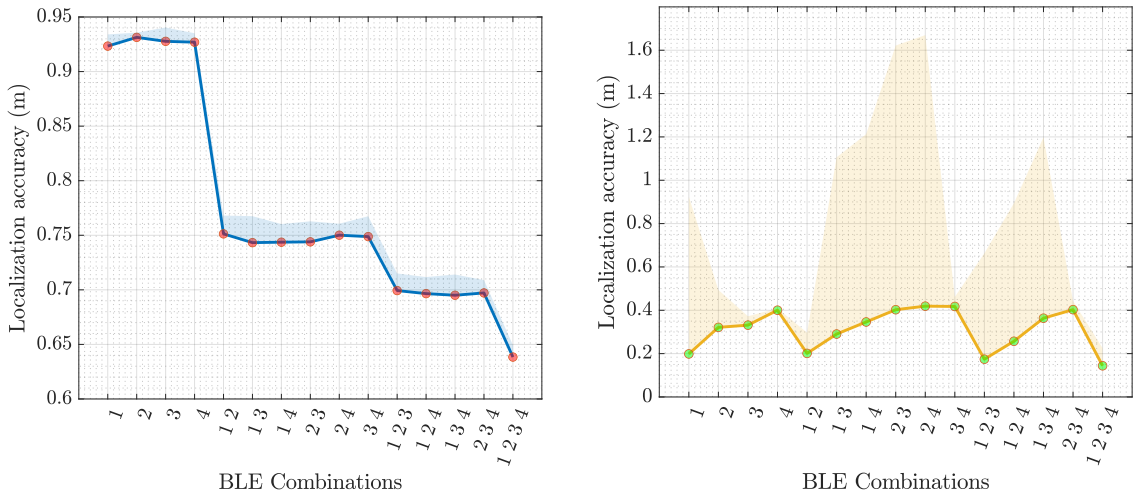

Figure 6.11: Localization accuracy (in meters) w.r.t. the combination of BLE anchors, wherein (a) depicts the results of using BLE I/Q samples for localization alone, while (b) illustrates that results of fusing BLE I/Q samples and mmWave, i.e.,BmmW-LITE.

resents the number of BLE devices used. The choice of BLE anchor configuration, when combined with mmWave radar, plays a crucial role in determining localization accuracy.

In this experiment, a total of four BLE anchors are employed, each labeled as anchor 1 through anchor 4. The physical locations of these anchors within the experimental area are illustrated in Figure 6.10. The first objective is to analyze how the localization accuracy of both BmmW and BmmW-LITE is influenced by the selection of BLE anchors. Various combinations of BLE anchor selections are illustrated on the x-axis of Figure 6.11, ranging from the exclusive selection of anchor 1 to the inclusion of anchors 1-4. The cross-validation scheme is adopted in this evaluation, which splits the dataset, trains the model on some subsets, evaluates on others, and repeats the process with different subsets for each iteration. In Figure 6.11, the outcomes of this objective are illustrated. The y-axis displays the corresponding localization accuracy for each selection. These two sub-figures show both the mean accuracy value and the upper/lower bounds.

The presented findings indicate that when utilizing solely BLE I/Q samples for localization (see Figure 6.11a), there is an improvement in accuracy with an increase in the number of BLE anchors. This observation aligns with the general trend in BLE localization. Having a greater number of anchors results in a larger pool of RSS data available at the receiver, which, in turn, facilitates more precised localization. Interestingly, this improvement appears to be relatively independent of the specific anchors selected; for example, choosing anchors 1 or 2

does not result in a notable difference. This observation is thought to be dependent on the environmental conditions.

However, the scenario becomes more intricate when integrating BLE and mmWave features for joint localization as depicted in Figure 6.11b. The upper bound for localization exhibits fluctuations across all combinations of BLE anchors, with higher values observed when anchors 3 and 4 are included. This pattern can be attributed to the potentially unstable nature of model training. The training process encompasses regions where mmWave signals experience strong propagation decay with distance (example see Figure 6.1), notably further from anchors 1 and 2 and in proximity to anchors 3 and 4. Because of the inherent randomness in the train/test set allocation during cross-validation, there exists a certain probability of inducing training failures for the model. This randomness contributes significantly to the observed substantial variations in the results.

To evaluate the effect of data selection under ideal model training conditions, the focus is placed on the lower boundary of this distribution. This is represented by the yellow line with green dots in Figure 6.11b. It can be analyzed from this line that overall, the fusion process enhances accuracy compared to solely using BLE. Moreover, as the number of BLE anchors increases, there is an evident enhancement in the overall accuracy of the fusion model. Nevertheless, the specific selection of anchors significantly impacts the fusion model's accuracy. For example, the yellow line highlights a notable disparity in the effect of choosing anchor 1 (0.2 m) versus anchor 4 (0.4 m) in the fusion process. This discrepancy arises because anchors 1 and 2 share the same side as the mmWave radar placement, whereas anchors 3 and 4 are on the opposite side. Additionally, compared to anchors 1 and 3, anchors 2 and 4 face a wall, introducing more multipath components in the I/Q samples. Consequently, anchor 1 contains more valuable/direct BLE response information for training the fusion models compared to anchors 2, 3, and 4. Therefore, the selection of BLE anchors 1, anchors 1-2, anchors 1-3, and anchors 1-4 achieves the highest accuracy compared to their individual counterparts. Under these optimal BLE selections, the results of the evaluation are presented in Table 6.1, which shows the comparison of BmmW and BmmW-LITE against results obtained without fusion with mmWave radar.

Feature *fusion* provides clear benefits for both methods across all scenarios, with the highest accuracy gain of 53.91% achieved in the case of three BLE anchors. The highest accuracy achieved is 0.09 m and 0.341 m for BmmW and BmmW-LITE, respectively, which is 80% and 60% higher than that of classical BLE localization methods [40]. BmmW provides significantly higher localization accuracy, especially with an increase in BLE anchors. Moreover, by comparing different rows in Table 6.1, it is evident that the performance improvement of the fusion NN model in the mmWave strong region is greater than that in the mmWave weak

Table 6.1: The MLE (in meters) in the test set under different scenarios using BmmW model and BmmW-LITE model with optimal BLE anchor selection.

Area	Method	BLE*1		BLE*2		BLE*3		BLE*4	
		BmmW	BmmW-LITE	BmmW	BmmW-LITE	BmmW	BmmW-LITE	BmmW	BmmW-LITE
Entire	BLE alone	0.663	0.914	0.398	0.727	0.291	0.664	0.222	0.582
	Fusion BLE & mmWave	0.643	0.731	0.320	0.578	0.134	0.428	0.107	0.369
	Gains of Fusion over BLE	3.05%	19.94%	19.58%	20.57%	53.91%	35.55%	51.62%	36.53%
mmWave Strong		BmmW	BmmW-LITE	BmmW	BmmW-LITE	BmmW	BmmW-LITE	BmmW	BmmW-LITE
	BLE alone	0.420	0.642	0.233	0.501	0.213	0.517	0.181	0.473
	Fusion BLE & mmWave	0.331	0.385	0.227	0.341	0.191	0.398	0.090	0.362
	Gains of Fusion over BLE	21.20%	40.07%	2.48%	31.95%	10.27%	22.97%	50.26%	23.40%
mmWave Weak		BmmW	BmmW-LITE	BmmW	BmmW-LITE	BmmW	BmmW-LITE	BmmW	BmmW-LITE
	BLE alone	0.646	0.704	0.427	0.658	0.253	0.547	0.191	0.478
	Fusion BLE & mmWave	0.524	0.656	0.426	0.502	0.242	0.464	0.148	0.402
	Gains of Fusion over BLE	18.95%	6.87%	0.28%	23.67%	4.37%	15.28%	22.40%	15.90%

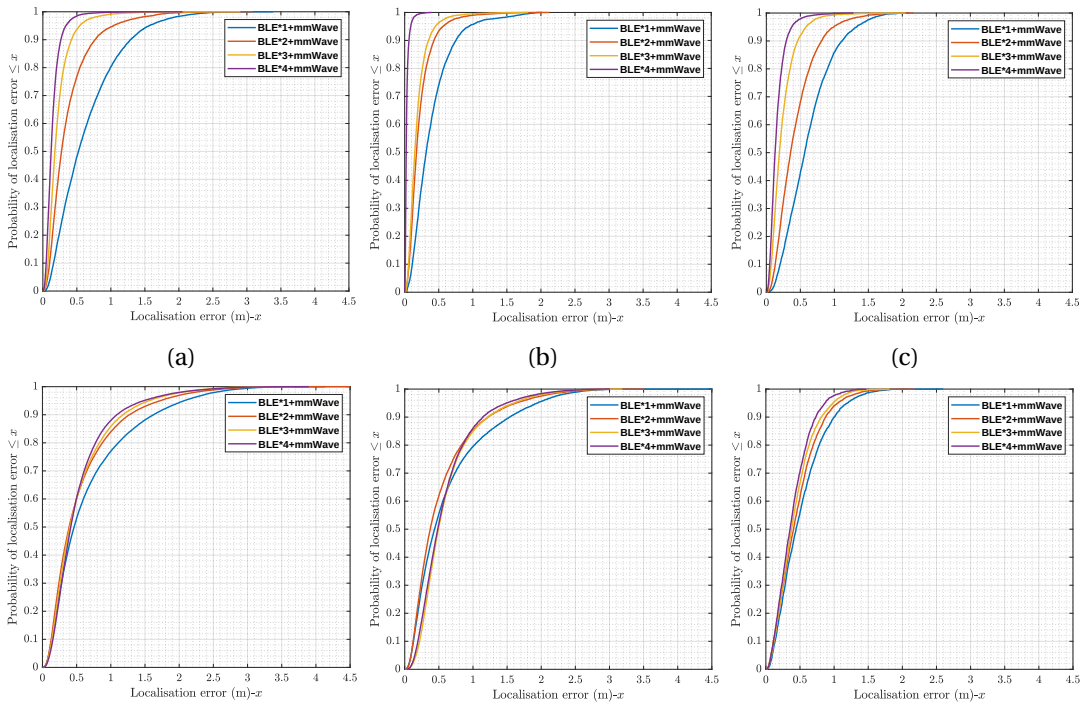

Figure 6.12: The MLE CDF of the BmmW and BmmW-LITE models in an entire area (a,e); in the mmWave strong area (b, f); and in the mmWave weak area (c, g). Comparison of the ground truth locations and NN-predicted locations in a part of the test set for BmmW (d) and BmmW-LITE (h).

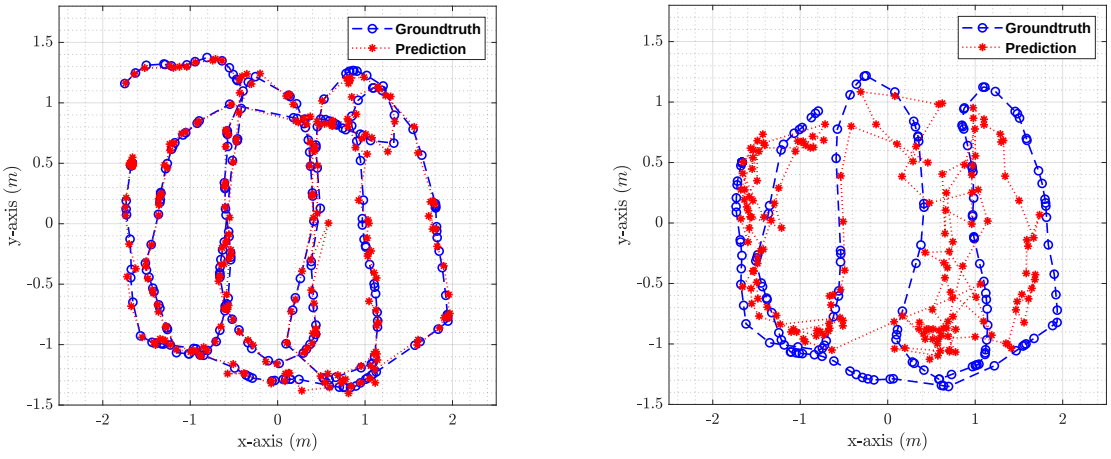

Figure 6.13: The MLE CDF of the BmmW and BmmW-LITE models in an entire area (a,e); in the mmWave strong area (b, f); and in the mmWave weak area (c, g). Comparison of the ground truth locations and NN-predicted locations in a part of the test set for BmmW (d) and BmmW-LITE (h).

Table 6.2: % increment in MLE for BmmW w.r.t. BmmW-LITE.

Areas	BLE*1	BLE*2	BLE*3	BLE*4
Entire Room	12.12%	44.65%	68.65%	70.92%
mmWave Strong	14.01%	33.27%	51.94%	75.12%
mmWave Weak	20.10%	15.12%	47.74%	63.15%

region. This is due to the decay of mmWave signals with increasing detect distance. Although the mmWave radar may fail to detect the person around half of the time, that information can still be helpful as it indicates that the person may not be in the mmWave strong area. The highest improvement in BmmW-LITE is observed with 1 BLE anchor fused with mmWave heatmap, which reduces error by 40.07%. Notably, even when using a single BLE anchor, the fusion model achieves sub-metre accuracy in all testing areas, with a maximum error of 0.73 m.

In addition, CDF is used to statistically evaluate the localization performance of BmmW and BmmW-LITE in different scenarios, as shown in Fig 6.12. The CDF results show that BmmW achieves almost 90% localization accuracy within 0.5 m in all scenarios. Especially with the 'BLE*4+mmWave' scenario shown in Figure 6.12b (which corresponds to the fusion of BLE and mmWave measurements when using 4 BLE anchors), the CDF curve is extremely steep, demonstrating highly-accurate predictions. BmmW-LITE achieves 60% localization accuracy under 50 cm across all scenarios, and up to 90% when using four BLE anchors. Furthermore, to visualize the 2D tracked trajectory, random predicted locations are selected from the test set and compared with the ground truth locations. This comparison is shown in Figure 6.13a and 6.13b for the "Entire room with BLE*4" scenario with BmmW and BmmW-LITE, respectively. BmmW's estimated trajectory closely matches the ground truth trajectory. BmmW-LITE's estimated trajectory also matches the ground truth, but there are some out-of-the-box predictions at certain locations hindering its performance. These outliers can be removed in a post-processing step, if necessary.

Table 6.3: The MLE (in meters) in the test set under different scenarios using BmmW-LITE+ model with optimal BLE anchor selection.

Areas	BLE*1	BLE*2	BLE*3	BLE*4
Entire Room	0.747	0.668	0.583	0.494
mmWave Strong	0.732	0.628	0.419	0.392
mmWave Weak	0.720	0.591	0.554	0.522

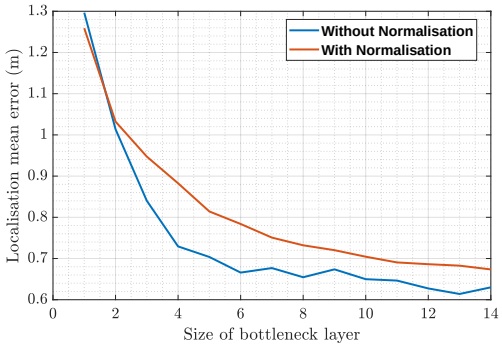

Figure 6.14: Localization accuracy (MLE in meters) w.r.t. the size of the VAE bottleneck.

6.5.3 Results: BmmW-LITE+

Before delving into the localization accuracy achieved by BmmW-LITE+, the performance of the VAE in reconstructing BLE features for localization is evaluated. In particular, attention is given to how the size of the VAE bottleneck layer influences localization accuracy when using VAE-reconstructed BLE features.

Figure 6.14 depicts the relationship between the VAE bottleneck layer size and localization accuracy. The experiment covers bottleneck layer sizes from 1 to 14, corresponding to BLE amplitude/phase compression ratios of 1.2% to 17%. The accuracy is compared in two scenarios: normalizing input BLE amplitude/phase features or not. Interestingly, normalization does not significantly aid the process. As the bottleneck layer size increases to $10-14$, the localization accuracy using the reconstructed BLE approach remains close to that of raw BLE features, around 60 cm. This suggests that using goal-oriented communication, raw BLE features can be compressed to 12% of their initial size without a substantial loss in localization accuracy.

In a manner similar to Section 6.5.2, the effect of using reconstructed BLE features on the accuracy of both the BLE localization model and the BLE-mmWave fusion model (with a compression ratio of 12%) is also evaluated. To reduce variability in accuracy due to a typical model training and to prevent confusion for readers, Figure 6.15 presents only the minimum values achieved after multiple training iterations, omitting the full distribution display[5].

Figure 6.15a compares the accuracy of selectively using raw and reconstructed BLE features for localization. Overall, raw BLE and reconstructed BLE features exhibit similar properties in contributing to localization accuracy – whereby an improved accuracy is obtained with an

[5]It is important to highlight that, in this context, the indicated values represent the highest attainable accuracy for various BLE combinations under ideal training conditions. However, achieving these values may not always be possible due to the variation of mmWave features and randomness of training/validation splitting. Therefore, the accuracy depicted on the y-axis should be regarded merely as a reference, facilitating quantitative analysis of BLE anchor selection and fusion.

increase in the number of BLE anchors. However, the adoption of reconstructed BLE features sacrifices accuracy compared to the use of raw BLE features. This discrepancy arises because VAE compression is essentially a lossy compression method, leading to the loss of some intrinsic information during compression. Nevertheless, the figure indicates that the accuracy gap diminishes with an increase in BLE anchors, and – when utilizing all reconstructed BLE features from 4 anchors – the localization difference becomes negligible (less than 3 cm). Figure 6.15b compares the fusion model using raw BLE and reconstructed BLE features. Generally, the reconstructed BLE features perform similarly in terms of localization accuracy compared to the raw BLE features for fusion. After reconstruction, anchor 1 retains the most valuable information for localization, followed by anchors 2, 3, and 4. The increase in the number of BLE anchors contributes to the enhancement of localization accuracy. Similar to the observations in Figure 6.15a, there is a performance decay when using reconstructed BLE features in the fusion model, but the increase in BLE anchors helps mitigating this loss in accuracy.

Assuming an optimal selection of BLE anchors, Table 6.3 quantifies the localization accuracy achieved by BmmW-LITE+. Different areas are considered, including the entire, the mmWave strong, and the mmWave weak areas, and the average accuracy from the 5-fold cross-validation is reported. The results, when compared to those in Table 6.1, indicate that the accuracy of BmmW-LITE+ is marginally lower than that of BmmW-LITE. This is particularly obvious when less number of anchors are adopted as localization beacons. In the scenarios using 4 BLE anchors, the accuracy of the entire room is down to 0.494 m from 0.369 m (a decrease of roughly 34%). However, in the mmWave strong area, the accuracy is 0.392 m, only 3 cm worse than when utilizing the raw BLE feature (0.362 m). Additionally, the CDF is employed to statistically assess the localization performance of BmmW-LITE+ across various scenarios, as illustrated in Figure 6.16. When compared to Figure 6.12d, 6.12e, and 6.12f, the overall CDF in the entire room or in the mmWave strong area does not exhibit a significant difference. However, in the mmWave weak area, the inclusion of BLE anchors shows a more pronounced impact on enhancing accuracy.

6.6 Discussion and Future Work

The following discussion addresses additional aspects of BmmW, including its advantages and main limitations, as well as areas worthy of further investigation in future studies.

Models' parameter and computational complexity. In BmmW and BmmW-LITE, a mobile tag is designed to transmit CTE packets consistently. These packets are then relayed to a centralized server, often situated in the cloud, where they serve as foundational data for the

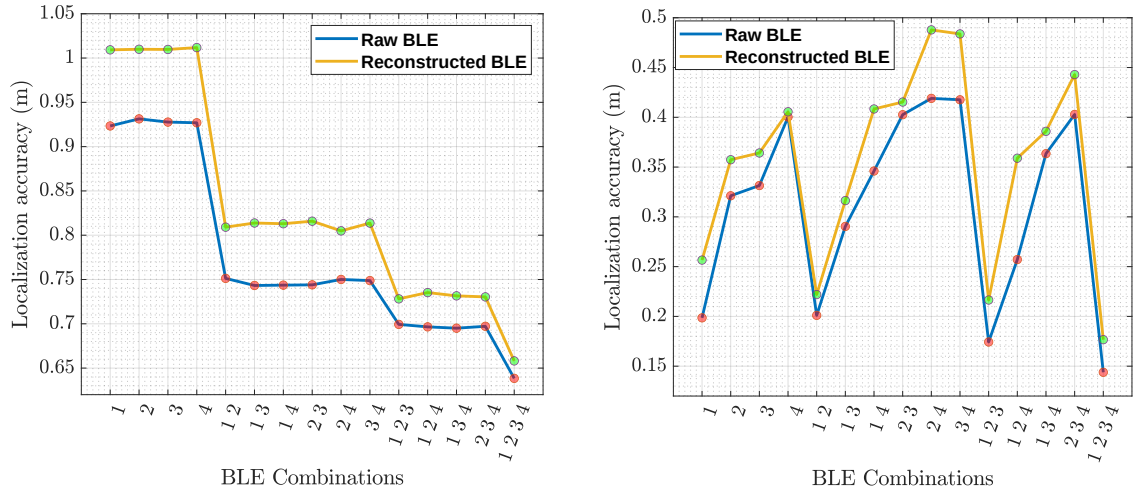

(a) (b)

Figure 6.15: Comparison of the best possible localization performance based on the combination of anchors for raw BLE features and reconstructed BLE features, wherein (a) shows the results of BLE-alone localization and (b) demonstrates the accuracy of the fusion model.

training and validation of NN models. Conversely, within the framework of BmmW-LITE+, the NN encoder model is deployed directly on edge devices. This allows all BLE anchors in the network to collaboratively employ the model for the purpose of compressing features efficiently. Furthermore, to quantitatively assess the system's complexity, the parameters and Floating Point Operations per Second (FLOPs) for each model (BmmW, BmmW-LITE, and BmmW-LITE+) have been carefully documented, as detailed in Table 6.4. The parameter count, which encompasses all weights and biases, serves as an indicator of the NN's size, reflecting its structural complexity and learning capacity. FLOPs, on the other hand, measure the computational complexity by quantifying the number of floating-point operations executed per second, offering insight into the model's operational demands.

The maximum number of parameters across the models is 2.02 million, and the peak FLOPs recorded is 72.16 million. This configuration underscores a design focused on balancing computational efficiency with sufficient model complexity to address the task at hand. For context, the well-known Resnet-34 model, often deployed in image processing applications, boasts approximately 3.6 billion parameters [163], highlighting a significantly higher computational complexity.

In terms of hardware complexity, the obtained numbers of parameters and FLOPs effectively position BmmW models within the operational capacities of very low-power systems (less than 1 W) and embedded systems (1 W to 10 W), which are capable of performing Giga-

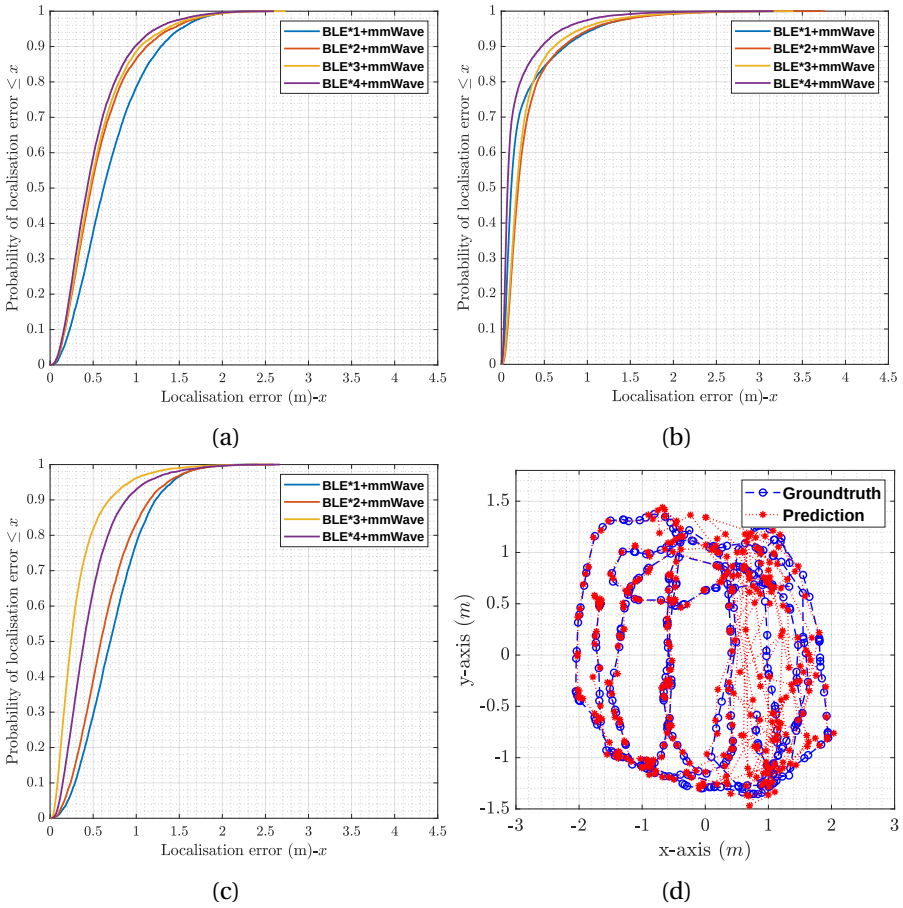

Figure 6.16: The MLE CDF of the BmmW-LITE+ models in an entire area (a); in the mmWave strong area (b); and in the mmWave Weak area (c). Comparison of the ground truth locations and NN-predicted locations in a part of the test set for BmmW-LITE+ (d).

level operations per second, as stated in the survey by Reuther *et al.*[190]. This alignment indicates that the BmmW, BmmW-LITE, and BmmW-LITE+ systems are ideally suited for deployment on common edge devices, such as those in the Jetson series [191, 192]. Their design ensures that inference operations are nearly real-time, benefiting from both the compact model size and the minimized computational complexity.

Performance comparison. The effectiveness of indoor localization systems can greatly differ based on indoor environmental conditions. To ensure a fair comparison, this work benchmarks against two systems, as referenced in previous studies [160] and BLoB [193](Chapter 2). Both systems are tested under similar conditions and settings in the same indoor environment, providing a relevant and meaningful basis for comparison.

In the study by Li *et al.* [160], Wi-Fi indoor localization is explored using a DNN and

Table 6.4: The number of parameters and FLOPs for BmmW, BmmW-LITE, and BmmW-LITE+ models with different BLE anchor selections.

	Parameters				FLOPs			
	BLE1	BLE2	BLE3	BLE4	BLE1	BLE2	BLE3	BLE4
BLoB	527.27 k	531.03 k	536.72 k	544.56 k	69.16 M	69.16 M	69.18 M	69.20 M
BmmW-LITE	621.53 k	903.36 k	1.37 M	2.02 M	69.36 M	69.92 M	70.84 M	72.16 M
BmmW-LITE+	46.45 k				92.90 k			

commercial Wi-Fi anchors. The localization accuracy of the implemented CNN model, utilizing Channel State Information (CSI) from three Wi-Fi anchors, is reported at 0.57 m. The model comprises 6 million parameters and approximately 100 million FLOPs. Each localization sample has a shape of $75 \times 30 \times 6$, leading to higher communication overhead compared to our BmmW series scheme. Consequently, it is evident that the BmmW series outperforms the [160] scheme in terms of accuracy, complexity, and communication overhead.

Another study, BLoB [193], unlike BmmW and the work by Li *et al.* [160], does not rely on NN models but rather adopts a traditional approach to localization and offers sub-meter accuracy. The hardware expenses and communication demands of BmmW work align closely with those of BLoB, even though the computational complexity of BmmW is marginally increased due to the incorporation of NNs. Despite this, the BmmW series excels in localization precision and enhances adaptability for deployment, offering various versions tailored to mobile targets and ensuring broader applicability across different use cases.

Blending technologies. The incorporation of BLE with mmWave technology in BmmW is also driven by the concept of JSAC. JSAC is widely recognized as a cornerstone for the upcoming generation of Radio Access Networks (RAN), where communication and radar sensing capabilities are seamlessly integrated into a unified system. Among the potential JSAC solutions, mmWave and MIMO techniques have garnered the most attention. For example, Nokia has presented a blueprint for mmWave indoor localization systems leveraging JSAC [194]. In this context, this study explores fusion methods for mmWave radar signals and *ubiquitous* BLE signals, aiming to unleash the potential of multi-modal signals for indoor localization. Thanks to its ubiquity, widespread availability, power efficiency, cost-effectiveness, and ease of deployment [2], BLE is indeed considered to be the primary low-power communication technology to develop indoor IoT localization solutions [28], especially after the introduction of the direction-finding features in BLE 5.1 [42]. It is worth noting that other low-power wireless communication technologies enabling the creation of location-aware IoT applications have recently emerged – above all, UWB technology. The latter is increasingly popular following

the integration of UWB radios into high-end smartphones and modern vehicles, as it allows highly accurate ranging and centimeter-level localization. However, UWB radios are not yet ubiquitous and are often paired to a BLE radio aiding device discovery and low-power data communication. The BmmW work hence also provides an alternative solution to existing UWB-based systems that combine the future JSAC feature with legacy BLE devices.

Accuracy vs costs. Tab. 6.2. 6.3 quantitatively demonstrates the performance of BmmW and its variants. Even though the use of raw IQ measurements in BmmW-LITE, BmmW-LITE+ causes a loss in accuracy, they require less computational effort. In fact, BmmW involves the use of AoA measurements obtained by running the MUSIC algorithm, which has a complexity of $O(N^3)$, where N is the number of antennas [51]. Moreover, BmmW requires multiple bulky antenna arrays, whereas BmmW-LITE, BmmW-LITE+ offers a less complex, cost-efficient solution. Still, both methods offer superior performance than the SOTA [40, 26, 195].

Scalability. The addition of more BLE anchors increases the coverage area, but also incurs extra costs. The experimental evaluation has shown that the use of 4 BLE anchors is sufficient to achieve a high localization accuracy. Please note that BmmW has been tested only within one office room, and performed both training and testing in the same environment: this leaves open questions with respect to the generality of the proposed NN. Such an evaluation can be conducted in the future with collection of data across diverse dynamic & large indoor environments.

Clock-drift. Multi-modality sensing models may experience clock drift caused by differences in sampling rates between the modalities. BLE boards, on the other hand, have a predictable curve of clock drift which can be used to mitigate this issue [98]. Additionally, addressing the discrepancy in sensing frequency between diverse sensors can be investigated in future studies.

Enhancing the NN through hyper-parameter tuning. The NN model architecture in BmmW, BmmW-LITE, and BmmW-LITE+ has been developed based on the author's expertise. However, this may not fully exploit the potential of the input data (i.e., there is room for performance enhancement). Future work includes conducting hyper-parameter tuning [196] to determine an optimal model structure.

Optimal compression ratio. In BmmW-LITE+, the determination of the VAE bottleneck size serves as a proof of concept for remote sensing, but cannot be guaranteed to be optimal. Real-world trade-offs between compression ratio, localization accuracy, and bandwidth consumption exist, and should be carefully considered in real-world deployments.

6.7 Concluding Remarks

This chapter has introduced BmmW, a novel localization/tracking system that combines the strengths of BLE 5.1 direction-finding and mmWave radar technology through a DNN-based fused model, achieving decimetre-level accuracy. Three methods for incorporating BLE data into the NN model are presented: BmmW utilizes AoA ranging data, BmmW-LITE uses raw I/Q measurements, while BmmW-LITE+ extends BmmW-LITE by off-loading the localization task to the cloud. Specifically, BmmW-LITE+ addresses the need for data compression before sending data to the cloud by adopting goal-oriented communications. Experimental results show that BmmW, BmmW-LITE, and BmmW-LITE+ can sustain decimetre-level accuracy, with a mean localization error of only 10 cm, 36 cm, and 39 cm respectively, an improvement of up to 80% compared to classical BLE localization methods. Furthermore, over 90% of the errors are within 50 cm across all three approaches, which makes them appropriate for mobile IoT applications: users can simply choose the most suitable approach based on the specific application and deployment requirements. BmmW outperforms BmmW-LITE due to its additional processing and data filtering, but BmmW-LITE offers a computationally and cost-efficient system that eliminates the need for bulky multi-antenna arrays. On the other hand, BmmW-LITE+ stands out as a flexible solution for balancing the computational complexity via centralized localization on the cloud. In summary, BmmW, through the integration of BLE and mmWave radar technology, surpasses the constraints of traditional methods, presenting a viable approach for achieving high-precision localization in 'Beyond 5G' wireless communication systems. Additionally, this study is, to the best of the author's knowledge, the first to investigate the capabilities of the BLE 5.1 standard, specifically the AoA technique, in providing decimeter-level accuracy in complex indoor settings.

CHAPTER 7

CONCLUSION AND FUTURE RESEARCH DIRECTIONS

This thesis, targeting the enhancement of indoor localization accuracy, makes significant contributions in two key areas. The first is the development of cutting-edge autonomous indoor localization systems. In this realm, three innovative systems, `BLoB`, HueSense, and `BLELight`, are introduced, utilizing visible light communication (VLC), BLE, and a hybrid of VLC & BLE, respectively. These developed solutions hold great promise for aiding AGVs/AMRs in various indoor environments like industry and homes, improving their location detection and enabling autonomous navigation in intelligent indoor spaces. The second focal point is the creation of BmmW, a tracking solution that merges BLE and mmWave technologies. This solution is most suited to application in the healthcare sector and for asset tracking in industrial settings, though its use is not limited to these areas, aligning well with the advancements of Industry 4.0.

In the development of these systems, the research successfully addressed challenges CH3, CH4, and CH5, as detailed in Chapter 1. The following section will provide a concise discussion of each system, highlighting how these specific challenges are tackled and the research objectives met.

7.1 Final Synopsis

`BLoB` The first primary challenge addressed is enhancing the accuracy of BLE-based localization systems. Although phase or angle techniques and sophisticated algorithms can be used for this purpose, they often require multi-antenna arrays,

leading to costly solutions. To tackle these issues while keeping costs in check, this research introduces a novel RSS, beating-based BLE localization system, named BLoB. This is considered the first narrowband BLE-beating-based localization system to the best of the author's knowledge. The research advocates for the use of a constant tone extension (CTE) in RSS-based methods, aligning with the BLE 5.1 standard initially devised for Angle of Arrival (AoA)/Angle of Departure (AoD) techniques. The system employs CTE to create a 'beating effect'—a sinusoidal pattern of constructive and destructive interference in the received signal, caused by synchronous transmissions—and uses this effect for localization. The research details the signal processing techniques necessary to identify peaks in the beating spectrum of the superimposed signal from multiple synchronous transmitters. These peaks provide key information about the locations of anchors and, combined with received signal strength data, enable BLoB to determine a tag's position with sub-metre accuracy. A unique aspect of BLoB is its use of single-antenna configurations for both anchors and tags, differentiating it from contemporary localization methods that rely on AoA/AoD information and typically need expensive, bulky antenna arrays for similar accuracy. The thesis findings show that BLoB achieves sub-metre localization precision in complex indoor environments and large spaces, comparable with angle-based techniques. This confirms hypothesis H1, H2 and meets objective 1, demonstrating the system's effectiveness and innovation in Bluetooth indoor localization.

HueSense To overcome the challenge of adding an extra control unit to light sources or modifying existing lighting infrastructure, which incurs additional costs, this research has been directed towards developing passive Visible Light Positioning (VLP) system. In this realm, an innovative passive-VLP system named HueSense has been devised. The fundamental insight of this research is the realization that LEDs emit slightly varied colour spectra which, while indistinguishable to the human eye, can be detected by colour sensors. This finding implies that light sources can be uniquely identified by their spectrum without the need for modulation or alteration. More specifically, HueSense operates by extracting power at dominant wavelengths of white LEDs to create unique signatures for light identification. This process facilitates location awareness and enhances accurate localization. Moreover, the system employs off-the-shelf, low-power colour sensors that can be easily integrated into low-power IoT devices. Additionally, HueSense relies on computationally lightweight linear algorithms. The system's

effectiveness has been proven in real-world settings, including an uncontrolled lighting environment like a university corridor, as well as in a densely configured VLP lab testbed. In these settings, HueSense has demonstrated 100% accuracy in location-mapping (i.e., identifying lights based on the proposed feature) with a moving robot and has achieved localization accuracy within decimetre levels. This validates hypothesis H3 and fulfils objective 2, proving the system's efficacy and innovation in the field of VLC-based indoor localization.

BLELight While Systems 1 and 2 introduced innovative localization solutions utilizing VLC and BLE technologies, they faced inherent technological limitations. To address these challenges, this research introduced a novel hybrid solution named `BLELight`. To effectively merge the two technologies, the research employed DNN. Additionally, to capitalize on the multimodal features of both VLP and BLE, an incremental learning-based approach utilized for training the DNN. This approach uses incremental learning to integrate data from visible light (*extracted passively*) and BLE, thus mitigating their individual constraints and achieving localization accuracy at the decimetre level. Incremental learning is particularly effective in reducing feature interference from different sources, allowing the model to learn predominantly from one signal feature at a time. The core premise of this approach is that, despite their distinct characteristics, both BLE and optical (or VLP) modalities provide valuable insights into the signal-location relationship within a specific indoor environment. The research achieved decimetre-level localization accuracy and a remarkable improvement in localization accuracy, showing an approximate average 1.5-fold enhancement over individual VLP and BLE technologies. Particularly notable is the more than 1.75-fold improvement over the BLE localization systems, attributed to the finer localization data derived from VLP measurements. This substantial enhancement confirms that the unique features identified in HueSense can significantly augment BLE or RF localization, validating hypotheses H4, H5 and fulfilling objective 3. Importantly, this system passively fuses light features from light sources, requiring no modifications to the light source. These features can be integrated with other indoor technologies besides BLE, offering the potential for further advancements in their localization performance.

Although the `BLELight` system attains superior accuracy compared to the HueSense and `BLoB` systems, the process of gathering features from both technologies and training the DNN model is somewhat arduous. However, more

advanced training methods could potentially alleviate this issue. Meanwhile, HueSense and BLoB stand as two innovative localization systems that are well-suited for applications where reliable decimetre-level accuracy is not a critical requirement.

BmmW This thesis further developed an innovative tracking system, BmmW, designed for effective asset tracking in factory settings or similar indoor environments. Despite the introduction of new direction-finding techniques in the BLE 5.1 standard in 2019, promising sub-metre accuracy, their experimental validation in field tests remains incomplete and underdeveloped. A primary challenge faced by companies has been the design of the required multiple-antenna arrays for these techniques. This research delves into maximizing the potential of BLE 5.1 direction-finding techniques, particularly AoA.

The BmmW system enhances AoA estimations provided by BLE 5.1's constant tone extension feature with mmWave radar measurements, achieving real-time 3D localization of mobile tags with decimetre-level precision. It incorporates a DNN trained on both BLE and mmWave data, effectively harnessing the strengths of each technology. This system addresses the inherent limitations of mmWave radar, such as difficulties in monitoring stationary targets and multiple objects, and its limited range due to rapid signal attenuation. Additionally, it compensates for the lower accuracy typically associated with BLE. It is important to note that this research primarily focuses on BLE technology, with mmWave radar being incorporated for research purposes as part of a collaborative effort. Addressing the issue of bulky and expensive multiple antenna systems, this thesis explores the use of single-antenna BLE devices and has developed a variant of BmmW, named BmmW-LITE. Both systems adhere to 802.15.4 BLE standard and do not employ synchronous transmission. The experimental testing of BmmW's performance demonstrates that its joint DNN training approach enables real-time tracking of mobile tags with decimetre-level accuracy when combining BLE angle-of-arrival measurements with mmWave radar data. Moreover, BmmW-LITE offers sub-metre accuracy thus providing accurate tracking of objects in indoor environments, even with the use of cost-effective, single-antenna BLE devices. Furthermore, a variant of BmmW-LITE, called BmmW-LITE+ is introduced to further facilitate data transfer from the edge to the cloud, optimizing bandwidth, power, and memory usage by incorporating *semantic* capabilities at the edge device.

This thesis has made substantial contributions towards advancing indoor localization systems, particularly in enhancing existing RF-based localization methods through introduction of novel approaches and integration with optical technologies. The systems developed herein represent significant strides in the quest for more accurate and efficient indoor localization, a crucial component in the evolving landscape of smart indoor environments.

The insights and innovations presented in this work hold the potential to greatly benefit society. By aligning with the growing trend of smart, artificially intelligent robots in diverse indoor settings—from homes and industries to the healthcare sector—these advancements promise to elevate the quality of life, facilitate assisted living, and optimize resource utilization. As the future increasingly leans towards smart indoor environments, the research encapsulated in this thesis is poised to play a pivotal role. It not only addresses the immediate needs of these evolving spaces but also lays the groundwork for future developments.

Despite the considerable progress made, it's important to acknowledge that the systems developed in this thesis are still in their early stages. As highlighted in the first chapter, the ecosystem of bringing an indoor localization system from a conceptual stage to a commercially viable reality involves numerous steps. There remain several areas ripe for further development, and the advancements presented in this work can serve as a catalyst for advancing more intelligent indoor environments.

7.2 Future Research Directions

In this section, an exploration of potential future research directions is presented, aimed at accelerating the creation of more intelligent indoor spaces. This discussion is not just a reflection on what has been achieved, but a forward-looking perspective, contemplating the future of indoor localization. The aim is to identify and navigate pathways that could lead to the realization of fully integrated, smart indoor environments, thereby contributing to a more technologically advanced and efficient society.

7.2.1 Joint Sensing And Communication

This research has explored localization solutions that pave the way for pioneering advancements in JSAC applications. This involves harnessing a diverse array of technologies to develop systems that excel in delivering not only high-precision localization but also seamless communication capabilities. Such innovative systems have the potential to significantly transform JSAC, achieving both sensing and communication objectives in a unified framework. The BLoB system, grounded in BLE technology, holds potential for such applications. The flexibility

offered by the initially empty payload in the BLoB (BLE) packets provides an opportunity to integrate information bits for concurrent communication and ranging in future applications. The incorporation of the CTE, an optional bit sequence used for direction-finding at the end of the BLE packet, while still maintaining the capability for communication in the payload, presents an innovative and adaptable approach for future explorations in this field.

Furthermore, this thesis lays a solid foundation for future research, wherein the joint localization solutions developed can be adeptly applied to JSAC applications. A notable instance of this advancement is BmmW, which combines BLE with mmWave radar technology. BLE's renowned energy efficiency renders it ideal for long-lasting applications. In contrast, the mmWave component is integral for its high localization accuracy and its bandwidth capacity, essential for rapid data transmission in scenarios with intensive communication demands. The synergy between mmWave radar's precise localization and its fast communication capabilities is poised to revolutionize sectors such as autonomous vehicles, smart city infrastructure, and IoT ecosystems, exemplifying the core principles of JSAC applications. Looking forward, the possibility of incorporating mmWave multi-antenna radar into RAN base stations presents a fascinating direction for enhancing JSAC solutions.

7.2.2 Seamless Integration with Smart Building Management

In the dynamic sphere of smart building management, the deployment of various environmental monitoring sensors, such as those for temperature and humidity, etc, are crucial for efficient operation and control. While these sensors adeptly capture environmental data, the true utility of this information is significantly enhanced when correlated with accurate location data. In modern smart buildings, LEDs are a ubiquitous presence, and herein lies an opportunity for the advancement integration of the HueSense system. By aligning with existing LED infrastructure, HueSense can provide essential location information, bridging a critical gap in the smart building management process. The integration of HueSense stands out due to several key advantages: its cost-effectiveness, power efficiency, and the ease with which it can be incorporated into low-power IoT devices. These attributes make HueSense an ideal solution for smart buildings, where the optimization of energy use and the minimization of additional infrastructure costs are paramount. This integration not only streamlines the management process by providing precise location context to environmental data but also propels the building's infrastructure toward a more interconnected and intelligent system.

7.2.3 Advanced Sensor Fusion

The potential to elevate the capabilities of the developed systems is substantial, particularly through the integration of data from a variety of onboard sensors commonly equipped in automated vehicles, such as IMU, among others. This refined approach of sensor fusion seeks to amalgamate the unique strengths of various sensing technologies, alongside the application of machine learning models, to forge a system with unparalleled accuracy and dependability. Specifically, the incorporation of data from IMUs offers critical insights into the dynamics of a vehicle, capturing essential metrics like acceleration and rotational movements. These details are vital in navigating complex scenarios and environments. By blending these additional sensor data streams with the established framework of technology fusion, one can markedly amplify the system's proficiency in accurately pinpointing locations.

7.2.4 Enhanced Annotation Strategies for Data

This thesis emphasizes the importance of labelled data in developing integrated systems, particularly when jointly training models using datasets from different technologies. The current method utilizes an intricate camera (OptiTrack) system for recording ground truth locations, which, while accurate, is both expensive and labour-intensive. To address these challenges, the development of a high-accuracy, yet cost-effective, data annotation approach is imperative. Potential alternatives could include the use of a dual-camera system or various wireless sensing technologies for labelling. Approaches such as semi-supervised learning or contrastive learning, a deep learning technique for unsupervised representation learning , could be key in extracting and utilizing the rich information embedded within these unlabeled datasets, thereby optimizing the data annotation process and enhancing the overall efficacy of the system.

7.2.5 Optimization and Refinement of Neural Network Model architectures

The NN model architectures developed in this thesis, while informed by the author's experience, may not yet fully exploit the potential of the data. To enhance performance, future work could focus on hyper-parameter tuning to fine-tune the model for optimal efficiency. Through systematic adjustments and evaluations of various parameters like learning rate, batch size, and layer configurations, the model can be fine-tuned to process and learn from the data more effectively. Additionally, exploring model pruning techniques—aimed at reducing model complexity by eliminating redundant layers or neurons—could streamline the models. This

approach not only makes the models leaner and more efficient but may also improve their effectiveness by focusing computational resources on the most impactful elements.

7.2.6 Generalization Ability of Neural Network Models

The effectiveness and reliability of NN models are intrinsically tied to the characteristics of the datasets on which they are trained. A notable challenge arises when there is a shift in data distribution, which can result in a notable decline in model accuracy. This issue is particularly pronounced in complex environments, such as densely populated areas or smart industrial settings. In these scenarios, the variability in room configurations, although not always significant, can still contribute to shifts in data distribution. Moreover, the interference in the 2.4 GHz frequency band, which is the operational band for BLE technology explored in this thesis, adds another layer of complexity. Such environmental factors can lead to changes in the data landscape, potentially impacting the performance and generalization ability of the NN models.

Addressing these challenges requires a focus on improving the models' ability to generalize across varied and dynamically changing environments. This involves developing strategies that enable the models to maintain high accuracy and robustness, even when confronted with data that differ from the conditions they were initially trained on. Techniques such as data augmentation, domain adaptation, and the incorporation of environmental variability into the training process can be instrumental in achieving this.

Additionally, to ensure the effective real-world deployment of these models, it's crucial to establish a continuous performance monitoring system. This system should not only evaluate the models' effectiveness but also offer insights and avenues for necessary updates. Adopting a comprehensive approach is essential for the successful implementation of the developed systems in real-world scenarios. This approach should encompass all aspects of the model's lifecycle, including its design, deployment, ongoing monitoring, and periodic updating.

Drawing a parallel with the emerging concept of digital twins, there's a need for a seamless flow of information from the real world to the digital realm. This continuous feedback loop is vital for ensuring that the system operates effectively and adapts to changing conditions over time. By integrating these practices, the models can remain relevant and robust, accurately reflecting and responding to the dynamic nature of real-world indoor environments.

CHAPTER 8

APPENDIX A

To extract the frequency power spectrum of the squared envelope of the received analytic signal, assume the received signal is represented as:

$$r(t) = \sum_k \cos(\omega_k t) \tag{8.1}$$

The analytic signal of the received signal can be written as [197]:

$$r_a(t) = r(t) + j\widetilde{r}(t) = r(t) + j\left(\frac{1}{\pi t} * r(t)\right) = r(t)\left(\delta(t) + j\frac{1}{\pi t}\right) \tag{8.2}$$

The Hilbert transform of $\cos(\omega t) = \sin(\omega t)$ (8.3)

$$r_a(t) = \sum_k \cos(\omega t) + j\sin(\omega t) = \sum_k e^{j\omega_k t} \tag{8.4}$$

$$= |r_a(t)|e^{j\angle r_a(t)} \tag{8.5}$$

Fourier transform of $r_a(t)$ can be expressed as:

$$R_a(\omega) = 2\pi \sum_k \delta(\omega - \omega_k) \tag{8.6}$$

Envelope extraction of the $r_a(t)$ signal:

$$|r_a(t)|^2 = \left(\sum_k \cos(\omega_k t)\right)^2 + \left(\sum_k \sin(\omega_k t)\right)^2 \tag{8.7}$$

$$= \sum_{k,l} \cos(\omega_k t)\cos(\omega_l t) + \sum_{k,l} \sin(\omega_k t)\sin(\omega_l t) \tag{8.8}$$

$$= \sum_{k,l} \cos(\omega_k - \omega_l)\, t \tag{8.9}$$

$$= N\,(\text{dc component}) + 2\sum_{k,l} \cos(\omega_k - \omega_l)\, t \tag{8.10}$$

Fourier transform of the squared envelope:

$$S_a(w) = 2\pi N\delta(w) + 2\pi \sum_{k>l} [\delta(\omega - \omega_k + \omega_l) + \delta(\omega - \omega_k - \omega_l)] \tag{8.11}$$

If the received signal is composed of signals of different amplitudes:

$$r(t) = \sum_k a_k \cos(\omega_k t) \tag{8.12}$$

then,

$$S_a(w) = 2\pi \left(\sum_k (a_k)^2\right)\delta(w) + 2\pi \sum_{k>l} a_k a_l [\delta(\omega - \omega_k + \omega_l) + \delta(\omega - \omega_k - \omega_l)] \tag{8.13}$$

BIBLIOGRAPHY

[1] MarketsandMarkets, "Indoor Location Market Report." https://www.marketsandmarkets.com/Market-Reports/indoor-location-market-989.html, 2023. [Last accessed 10.03.2024].

[2] ABI Research, 2023, "2023 Market Update." https://www.bluetooth.com/2023-market-update/, 2023. [Last accessed on 10.03.2024].

[3] M. Baddeley, C. A. Boano, A. Escobar-Molero, Y. Liu, X. Ma, U. Raza, K. Römer, M. Schuß, and A. Stanoev, "The impact of the physical layer on the performance of concurrent transmissions," in *2020 IEEE 28th International Conference on Network Protocols (ICNP)*, pp. 1–12, IEEE, 2020.

[4] Silicon Labs, "AN1297: Custom direction-finding solutions using the Silicon Labs Bluetooth stack." https://www.silabs.com/documents/public/application-notes/an1297-custom-direction-finding-solutions-silicon-labs-bluetooth.pdf. [Last accessed on 10.03.2024].

[5] H. Cui, J. Wu, and N. Dahnoun, "Millimetre-wave Radar for Low-Cost 3D Imaging: A Performance Study," *arXiv preprint 2301.13553*, 2023.

[6] F. Song, Z. Ai, Y. Zhou, I. You, K.-K. R. Choo, and H. Zhang, "Smart Collaborative Automation for Receive Buffer Control in Multipath Industrial Networks," *IEEE Transactions on Industrial Informatics*, vol. 16, no. 2, pp. 1385–1394, 2019.

[7] F. Liu, Y. Cui, C. Masouros, J. Xu, T. X. Han, Y. C. Eldar, and S. Buzzi, "Integrated Sensing and Communications: Towards Dual-functional Wireless Networks for 6G and Beyond," *IEEE Journal on Selected Areas in Communications*, vol. 40, no. 6, pp. 1728–1767, 2022.

[8] J. Singh and U. Raza, "Passive visible light positioning systems: An overview," in *Proceedings of the Workshop on Light Up the IoT*, pp. 48–53, 2020.

[9] J. Singh, Q. Wang, M. Zuniga, and T. Farnham, "Huesense: Featuring LED Lights Through Hue Sensing," in *Proceedings of the 1st ACM Workshop on AI Empowered Mobile and Wireless Sensing*, pp. 19–24, 2022.

[10] R. S. Pol, V. N. Aher, S. V. Gaikwad, D. G. Bhalke, A. Y. Borkar, and M. T. Kolte, "Autonomous Differential Drive Mobile Robot Navigation with SLAM, AMCL using ROS," *International Journal of Intelligent Systems and Applications in Engineering*, vol. 12, no. 5s, pp. 46–53, 2024.

[11] P. Li, J. Singh, H. Cui, and C. A. Boano, "BmmW: A DNN-Based Joint BLE and mmWave Radar System for Accurate 3D Localization," in *19th International Conference on Distributed Computing in Smart Systems and the Internet of Things (DCOSS-IoT)*, pp. 47–54, IEEE, 2023.

[12] F. Ahmed, M. Phillips, S. Phillips, and K.-Y. Kim, "Comparative study of seamless asset location and tracking technologies," *Procedia Manufacturing*, vol. 51, pp. 1138–1145, 2020.

[13] F. Bernardini, A. Buffi, D. Fontanelli, D. Macii, V. Magnago, M. Marracci, A. Motroni, P. Nepa, and B. Tellini, "Robot-based indoor positioning of UHF-RFID tags: The SAR method with multiple trajectories," *IEEE Transactions on Instrumentation and Measurement*, vol. 70, pp. 1–15, 2020.

[14] A. Nayak, I. Satpathy, B. Patnaik, R. Gujrati, and H. Uygun, "Simplified Hospital Management System: Robotic Process Automation (RPA) to Rescue," in *Data-Centric AI Solutions and Emerging Technologies in the Healthcare Ecosystem*, pp. 281–302, CRC Press, 2024.

[15] M. V. Martínez-López, G. Díaz-Cobacho, A. M. Astobiza, and B. Rodríguez López, "Exploring the Ethics of Interaction with Care Robots," in *Ethics of Artificial Intelligence*, pp. 149–167, Springer, 2024.

[16] Wang, Huiwen and Yi, Wen and Zhen, Lu, "Optimal policy for scheduling automated guided vehicles in large-scale intelligent transportation systems," *Transportation Research Part A: Policy and Practice*, vol. 179, p. 103910, 2024.

[17] Thomas, Peter R and Sarhadi, Pouria, "Geofencing Motion Planning for Unmanned Aerial Vehicles Using an Anticipatory Range Control Algorithm," *Machines*, vol. 12, no. 1, p. 36, 2024.

[18] J.-H. Youn and Y. Cho, "Performance Study of an Ultra-Wideband Indoor Localization and Asset Tracking System," *IntechOpen*, 2010.
[Last accessed on 10.03.2024].

[19] J. Zhao, S. Liu, and J. Li, "Research and Implementation of Autonomous Navigation for Mobile Robots Based on SLAM Algorithm under ROS," *Sensors*, p. 4172, 2022.

[20] Y. D. Yasuda, L. E. G. Martins, and F. A. Cappabianco, "Autonomous Visual Navigation for Mobile Robots: A Systematic Literature Review," *ACM Computing Surveys (CSUR)*, vol. 53, no. 1, pp. 1–34, 2020.

[21] A. Archangelskaya, I. Gerasimov, M. Al Sardar, and A. Abramova, "City AR: Augmented reality navigation in the smart cities infrastructure," in *2022 IEEE International Smart Cities Conference (ISC2)*, pp. 1–7, IEEE, 2022.

[22] Z. Zheng, Z. Liao, Y. Xue, and Y. Li, "Rapid Establishment of Indoor Wifi Positioning Database in Shopping Malls Based on Wearable Navigation Device (weartrack)," *The International Archives of the Photogrammetry, Remote Sensing and Spatial Information Sciences*, vol. 46, pp. 293–299, 2022.

[23] P. Li, J. Singh, H. Cui, and C. A. Boano, "BmmW+: A DNN-based Joint BLE and mmWave Radar System for Accurate 3D Localization with Goal-oriented Communication." Under review (Invited paper) for publication in Pervasive and Mobile Computing, 2024.

[24] X. Chen, H. Li, C. Zhou, X. Liu, D. Wu, and G. Dudek, "Fidora: Robust WiFi-based indoor localization via unsupervised domain adaptation," *IEEE Internet of Things Journal*, vol. 9, no. 12, pp. 9872–9888, 2022.

[25] P. Spachos and K. Plataniotis, "BLE beacons in the smart city: Applications, challenges, and research opportunities," *IEEE Internet of Things Magazine*, vol. 3, no. 1, pp. 14–18, 2020.

[26] L. Mo, Y. Zhu, and D. Zhang, "UHF RFID Indoor Localization Algorithm Based on BP-SVR," *IEEE Journal of Radio Frequency Identification*, vol. 6, pp. 385–393, 2022.

[27] Spherical Insights, "Indoor Location Market Report." `https://www.sphericalinsights.com/reports/indoor-location-market`, 2023.
[Last accessed on 10.03.2024].

[28] ABI Research, 2021, "2021 Market Update." `https://www.bluetooth.com/wp-content/uploads/2021/01/2021-Bluetooth_Market_Update.pdf`, 2021.
[Last accessed on 10.03.2024].

[29] X. Li, X. Zhang, X. Ren, M. Fritsche, J. Wickert, and H. Schuh, "Precise positioning with current multi-constellation global navigation satellite systems: GPS, GLONASS, Galileo and BeiDou," *Scientific reports*, vol. 5, no. 1, p. 8328, 2015.

[30] X. Li, M. Ge, X. Dai, X. Ren, M. Fritsche, J. Wickert, and H. Schuh, "Accuracy and reliability of multi-GNSS real-time precise positioning: GPS, GLONASS, BeiDou, and Galileo," *Journal of geodesy*, vol. 89, no. 6, pp. 607–635, 2015.

[31] G. A. Zhbankov, N. P. Danilkin, and O. A. Maltseva, "Influence of the ionosphere on the accuracy of the satellite navigation system," *Acta Astronautica*, vol. 190, pp. 194–201, 2022.

[32] E. D. Kaplan and C. Hegarty, *Understanding GPS/GNSS: Principles and Applications, Third Edition*.
Artech house, 2017.

[33] M. Kotaru, K. Joshi, D. Bharadia, and S. Katti, "SpotFi: Decimeter Level Localization using WiFi," in *Proceedings of the 2015 ACM conference on special interest group on data communication*, pp. 269–282, 2015.

[34] X. Liu, B. Zhou, Z. Wu, A. Liang, and Q. Li, "An Indoor 3D Quadrotor Localization Algorithm Based on WiFi RTT and MEMS Sensors," *IEEE Internet of Things Journal*, vol. 9, no. 21, pp. 20879–20888, 2022.

[35] T. Savić, X. Vilajosana, and T. Watteyne, "Constrained Localization: A Survey," *IEEE Access*, vol. 10, pp. 49297–49321, 2022.

[36] D. Lymberopoulos and J. Liu, "The microsoft indoor localization competition: Experiences and lessons learned," *IEEE Signal Processing Magazine*, vol. 34, no. 5, pp. 125–140, 2017.

[37] S.-H. Fang, C.-H. Wang, T.-Y. Huang, C.-H. Yang, and Y.-S. Chen, "An enhanced ZigBee indoor positioning system with an ensemble approach," *IEEE Communications Letters*, vol. 16, no. 4, pp. 564–567, 2012.

[38] A. R. J. Ruiz, F. S. Granja, J. C. P. Honorato, and J. I. G. Rosas, "Accurate pedestrian indoor navigation by tightly coupling foot-mounted IMU and RFID measurements," *IEEE Transactions on Instrumentation and measurement*, vol. 61, no. 1, pp. 178–189, 2011.

[39] F. Höflinger, R. Zhang, J. Hoppe, A. Bannoura, L. M. Reindl, J. Wendeberg, M. Bührer, and C. Schindelhauer, "Acoustic Self-calibrating System for Indoor Smartphone Tracking (ASSIST)," in *2012 international conference on indoor positioning and indoor navigation (IPIN)*, pp. 1–9, IEEE, 2012.

[40] M. Cominelli, P. Patras, and F. Gringoli, "Dead on arrival: An empirical study of the Bluetooth 5.1 positioning system," in *Proceedings of the 13th international workshop on wireless network testbeds, experimental evaluation & characterization*, pp. 13–20, 2019.

[41] G. De Blasio, A. Quesada-Arencibia, C. R. Garcia, J. C. Rodriguez-Rodriguez, and R. Moreno-Díaz, "A protocol-channel-based indoor positioning performance study for bluetooth low energy," *IEEE Access*, vol. 6, pp. 33440–33450, 2018.

[42] Bluetooth SIG, "Bluetooth Core Specification v5.1." `https://www.bluetooth.com/bluetooth-resources/bluetooth-core-specification-v5-1-feature-overview/`, 2019.
[Last accessed on 10.03.2024].

[43] Y. Wang, Q. Ye, J. Cheng, and L. Wang, "RSSI-Based Bluetooth Indoor Localization," in *2015 11th international conference on mobile ad-hoc and sensor networks (MSN)*, pp. 165–171, IEEE, 2015.

[44] X.-Y. Lin, T.-W. Ho, C.-C. Fang, Z.-S. Yen, B.-J. Yang, and F. Lai, "A Mobile Indoor Positioning System based on iBeacon Technology," in *2015 37th Annual International Conference of the IEEE Engineering in Medicine and Biology Society (EMBC)*, pp. 4970–4973, IEEE, 2015.

[45] M. Ji, J. Kim, J. Jeon, and Y. Cho, "Analysis of Positioning Accuracy Corresponding to the Number of BLE Beacons in Indoor Positioning System," in *2015 17th International Conference on Advanced Communication Technology (ICACT)*, pp. 92–95, IEEE, 2015.

[46] T. Pizer, "White Paper: iBeacon: Matrix Realized." `https://www.gpstrategies.com/wp-content/uploads/2016/04/wpBeaconMatrix.pdf`, 2015.
[Last accessed on 10.03.2024].

[47] A. Dasgupta, R. Nagaraj, and K. Nagamani, "An internet of things platform with Google eddystone beacons," *Journal of Software Engineering and Applications*, vol. 9, no. 6, pp. 291–295, 2016.

[48] Y. Hu, F. Qian, Z. Yin, Z. Li, Z. Ji, Y. Han, Q. Xu, and W. Jiang, "Experience: Practical Indoor Localization for Malls," in *Proceedings of the 28th Annual International Conference on Mobile Computing and Networking*, pp. 82–93, 2022.

[49] J. Powar, C. Gao, and R. Harle, "Assessing the Impact of Multi-Channel BLE Beacons on Fingerprint-based Positioning," in *2017 International Conference on Indoor Positioning and Indoor Navigation (IPIN)*, pp. 1–8, IEEE, 2017.

[50] L. Yao, "Bluetooth Direction Finding." `https://repository.tudelft.nl/islandora/object/uuid:c07eb3a2-a303-4690-ac3e-e96f0064afcd`, 2018.
[Last accessed on 10.03.2024].

[51] J. Kim, D. Oh, S. Park, S. Lee, and Y. Jung, "Design of MUSIC-based DoA Estimator for Bluetooth Applications," *Journal of IKEEE*, vol. 24, no. 1, pp. 339–346, 2020.

[52] Z. Zhu *et al.*, "A Computationally Efficient Method for Direction Finding with Known Transmit Sequence," in *Proc. of IPIN*, 2018.

[53] R. Schmidt, "Multiple Emitter Location and Signal Parameter Estimation," *IEEE transactions on antennas and propagation*, vol. 34, no. 3, pp. 276–280, 1986.

[54] Nordic Semiconductor, "Direction Finding nWP-036." `https://infocenter.nordicsemi.com/pdf/nwp_036.pdf`, 2021.
[Last accessed on 10.03.2024].

[55] M. Woolley, "Bluetooth Direction Finding: A Technical Overview, Version 1.0.3." `https://www.bluetooth.com/wp-content/uploads/Files/developer/RDF_Technical_Overview.pdf`, 2021.
[Last accessed on 10.03.2024].

[56] G. Pau, F. Arena, Y. E. Gebremariam, and I. You, "Bluetooth 5.1: An Analysis of Direction Finding Capability for High-Precision Location Services," *Sensors*, vol. 21, no. 11, p. 3589, 2021.

[57] M. Qian, K. Zhao, A. Seneviratne, and B. Li, "Performance Analysis of BLE 5.1 New Feature Angle of Arrival for Relative Positioning," *The International Archives of the Photogrammetry, Remote Sensing and Spatial Information Sciences*, vol. 46, pp. 155–161, 2022.

[58] Silicon Labs, "BG22 Bluetooth Dual Polarized Antenna Array Radio Board." `https://www.silabs.com/development-tools/wireless/bluetooth/bg22-rb4191a-bg22-bluetooth-dual-polarized-antenna-array-radio-board?tab=overview`.
[Last accessed on 10.03.2024].

[59] CoreHW, "Antenna Array PCB." `https://www.corehw.com/products/antenna-array-ant1/`.
[Last accessed on 10.03.2024].

[60] Bluetooth SIG, "Bluetooth Channel Sounding: A Step Towards 10 cm Ranging Accuracy for Secure Access, Digital Key, and Proximity Services." `https://www.bluetooth.com/blog/bluetooth-channel-sounding-a-step-towards-10-cm-ranging-accuracy-for-secure-access-digital-key-and-proximity-services/`.
[Last accessed on 10.03.2024].

[61] Bluetooth SIG, "Bluetooth® Core Specification Version 5.4 - Technical Overview." `https://www.bluetooth.com/specifications/specs/core-specification-5-4/`.
[Last accessed on 10.03.2024].

[62] Texas Instruments, "TOF Initiator Example in SimpleLink CC2640R2 SDK." https://software-dl.ti.com/simplelink/esd/simplelink_cc2640r2_sdk/2.30.00.28_new/exports/examples/rtos/CC2640R2_LAUNCHXL/blestack/tof_initiator/README.html.
[Last accessed on 10.03.2024].

[63] BeaconZone, "New TOF Distance Measurement Bluetooth Sensor." https://www.beaconzone.co.uk/blog/new-tof-distance-measurement-bluetooth-sensor/.
[Last accessed on 10.03.2024].

[64] B. Großwindhager, M. Stocker, M. Rath, C. A. Boano, and K. Römer, "SnapLoc: An ultra-fast UWB-based indoor localization system for an unlimited number of tags," in *Proceedings of the 18th International Conference on Information Processing in Sensor Networks*, pp. 61–72, IEEE, 2019.

[65] H. Chen and A. Dhekne, "Pnploc: Uwb based plug & play indoor localization," in *2022 IEEE 12th International Conference on Indoor Positioning and Indoor Navigation (IPIN)*, pp. 1–8, IEEE, 2022.

[66] Y. Zhuang, L. Hua, L. Qi, J. Yang, P. Cao, Y. Cao, Y. Wu, J. Thompson, and H. Haas, "A Survey of Positioning Systems Using Visible LED Lights," *IEEE Communications Surveys & Tutorials*, vol. 20, no. 3, pp. 1963–1988, 2018.

[67] J. Liu, Y. Li, X. Li, Y. Li, and J. Zhang, "Fusing WiFi, Inertial Sensors and Bluetooth Beacons for Accurate Indoor Positioning," *Sensors*, vol. 21, no. 1, p. 227, 2021.

[68] S. Jeong, H. Kim, Y.-S. Kim, and K.-A. Yi, "Robust Indoor Positioning System with UWB, Bluetooth, and Machine Learning," *Journal of Ambient Intelligence and Humanized Computing*, vol. 12, no. 7, pp. 7445–7460, 2021.

[69] K. Ma, X. Dai, Y. Zhao, and W. Meng, "A Differentially Private Indoor Localization Scheme with Fusion of WiFi and Bluetooth Fingerprints in Edge Computing," *IEEE Access*, vol. 9, pp. 41107–41116, 2021.

[70] S. Deb and S. Bhowmick, "Indoor Localization using Magnetometer and Wi-Fi Fingerprinting Techniques," *Journal of Ambient Intelligence and Humanized Computing*, vol. 11, no. 3, pp. 1169–1181, 2020.

[71] P. Xie, L. Li, J. Wang, and Y. Liu, "Passive Visible Light Tag system for Localization and Posture Estimation," *IEEE Transactions on Mobile Computing*, 2024.

[72] M. Xu, Y. Wang, B. Xu, J. Zhang, J. Ren, Z. Huang, S. Poslad, and P. Xu, "A critical analysis of image-based camera pose estimation techniques," *Neurocomputing*, p. 127125, 2023.

[73] M. S. Alam, F. B. Mohamed, A. Selamat, and A. B. Hossain, "A review of recurrent neural network based camera localization for indoor environments," *IEEE Access*, 2023.

[74] Z. Li, C. Jiang, X. Gu, Y. Xu, J. Cui, *et al.*, "Collaborative positioning for swarms: A brief survey of vision, LiDAR and wireless sensors based methods," *Defence Technology*, 2023.

[75] X. Xia, N. P. Bhatt, A. Khajepour, and E. Hashemi, "Integrated inertial-LiDAR-based map matching localization for varying environments," *IEEE Transactions on Intelligent Vehicles*, 2023.

[76] C.-F. J. Kuo, S.-H. Chen, and C.-Y. Huang, "Automatic detection, classification and localization of defects in large photovoltaic plants using unmanned aerial vehicles (UAV) based infrared (IR) and RGB imaging," *Energy Conversion and Management*, vol. 276, p. 116495, 2023.

[77] M. Schenkluhn, C. Peukert, and C. Weinhardt, "Augmented Reality-based Indoor Positioning for Smart Home Automations," in *Extended Abstracts of the 2023 CHI Conference on Human Factors in Computing Systems*, pp. 1–6, 2023.

[78] Z. Yang, Z. Wang, J. Zhang, C. Huang, and Q. Zhang, "Wearables can afford: Light-weight indoor positioning with visible light," in *Proceedings of the 13th Annual International Conference on Mobile Systems, Applications, and Services*, pp. 317–330, 2015.

[79] Y.-S. Kuo, P. Pannuto, K.-J. Hsiao, and P. Dutta, "Luxapose: Indoor positioning with mobile phones and visible light," in *Proceedings of the 20th annual international conference on Mobile computing and networking*, pp. 447–458, 2014.

[80] Q. Wang and M. Zuniga, "Passive sensing and communication using visible light: Taxonomy, challenges and opportunities," *arXiv preprint arXiv:1704.01331*, 2017.

[81] Philips, "Carrefour in France Installs Philips LED-Based Indoor Positioning System." `http://www.lighting.philips.com/main/cases/cases/food-and-large-retailers/carrefour-lille.html`, 2015.
[Last accessed on 10.03.2024].

[82] A. Jovicic, "Qualcomm® Lumicast™: A High Accuracy Indoor Positioning System Based on Visible Light Communication," tech. rep., Qualcomm, San Diego, CA, USA, Apr. 2016.

[83] P. Chen, M. Pang, D. Che, Y. Yin, D. Hu, and S. Gao, "A survey on visible light positioning from software algorithms to hardware," *Wireless Communications and Mobile Computing*, vol. 2021, pp. 1–20, 2021.

[84] Z. Gao, Z. Wan, D. Zheng, S. Tan, C. Masouros, D. W. K. Ng, and S. Chen, "Integrated Sensing and Communication with mmWave massive MIMO: A Compressed Sampling Perspective," *IEEE Transactions on Wireless Communications*, 2022.

[85] Traini, Stefano and Sciullo, Luca and Trotta, Angelo and Di Felice, Marco, "Practical Indoor Localization via Smartphone Sensor Data Fusion Techniques: A Performance Study," in *2019 16th IEEE Annual Consumer Communications & Networking Conference (CCNC)*, pp. 1–7, 2019.

[86] S. Kumar and R. M. Hegde, "Multi-sensor data fusion methods for indoor localization under collinear ambiguity," *Pervasive and mobile computing*, vol. 30, pp. 18–31, 2016.

[87] J. Prieto, S. Mazuelas, A. Bahillo, P. Fernandez, R. M. Lorenzo, and E. J. Abril, "Adaptive data fusion for wireless localization in harsh environments," *IEEE Transactions on Signal Processing*, vol. 60, no. 4, pp. 1585–1596, 2012.

[88] X. Liu, B. Zhou, P. Huang, W. Xue, Q. Li, J. Zhu, and L. Qiu, "Kalman filter-based data fusion of Wi-Fi RTT and PDR for indoor localization," *IEEE Sensors Journal*, vol. 21, no. 6, pp. 8479–8490, 2021.

[89] Chen, Jianfan and Zhou, Baoding and Bao, Shaoqian and Liu, Xu and Gu, Zhining and Li, Linchao and Zhao, Yangping and Zhu, Jiasong and Li, Qingquan, "A Data-Driven Inertial Navigation/Bluetooth Fusion Algorithm for Indoor Localization," *IEEE Sensors Journal*, vol. 22, no. 6, pp. 5288–5301, 2022.

[90] J. Vitola, F. Pozo, D. A. Tibaduiza, and M. Anaya, "A Sensor Data Fusion System Based on k-nearest Neighbor Pattern Classification for Structural Health Monitoring Applications," *Sensors*, vol. 17, no. 2, p. 417, 2017.

[91] R. Gu, S.-X. Zhang, Y. Xu, L. Chen, Y. Zou, and D. Yu, "Multi-modal Multi-channel Target Speech Separation," *IEEE Journal of Selected Topics in Signal Processing*, vol. 14, no. 3, pp. 530–541, 2020.

[92] R. Klus, J. Talvitie, and M. Valkama, "Neural network fingerprinting and GNSS data fusion for improved localization in 5G," in *2021 International Conference on Localization and GNSS (ICL-GNSS)*, pp. 1–6, IEEE, 2021.

[93] J. Chen, B. Zhou, S. Bao, X. Liu, Z. Gu, L. Li, Y. Zhao, J. Zhu, and Q. Li, "A data-driven inertial navigation/Bluetooth fusion algorithm for indoor localization," *IEEE Sensors Journal*, vol. 22, no. 6, pp. 5288–5301, 2021.

[94] A. J. Barreto-Cubero, A. Gómez-Espinosa, J. A. Escobedo Cabello, E. Cuan-Urquizo, and S. R. Cruz-Ramírez, "Sensor data fusion for a mobile robot using neural networks," *Sensors*, vol. 22, no. 1, p. 305, 2021.

[95] R. C. King, E. Villeneuve, R. J. White, R. S. Sherratt, W. Holderbaum, and W. S. Harwin, "Application of Data Fusion Techniques and Technologies for Wearable Health Monitoring," *Medical Engineering & Physics*, vol. 42, pp. 1–12, 2017.

[96] D. Michelsanti, Z.-H. Tan, S.-X. Zhang, Y. Xu, M. Yu, D. Yu, and J. Jensen, "An Overview of Deep-Learning-based Audio-Visual Speech Enhancement and Separation," *IEEE/ACM Transactions on Audio, Speech, and Language Processing*, vol. 29, pp. 1368–1396, 2021.

[97] D. Yu, C. Li, and J. Xiao, "Neural Networks-Based Wi-Fi/PDR Indoor Navigation Fusion Methods," *IEEE Transactions on Instrumentation and Measurement*, vol. 72, pp. 1–14, 2022.

[98] M. Baddeley *et al.*, "Understanding Concurrent Transmissions: The Impact of Carrier Frequency Offset and RF Interference on Physical Layer Performance," *Cornell University – arXiv:2304.00371*, 2023.

[99] M. Zimmerling, L. Mottola, and S. Santini, "Synchronous transmissions in low-power wireless: A survey of communication protocols and network services," *ACM Computing Surveys (CSUR)*, vol. 53, no. 6, pp. 1–39, 2020.

[100] A. Escobar-Molero, "Improving reliability and latency of wireless sensor networks using concurrent transmissions," *at-Automatisierungstechnik*, vol. 67, no. 1, pp. 42–50, 2019.

[101] R. Jacob, A.-B. Schaper, A. Biri, R. Da Forno, and L. Thiele, "Synchronous Transmissions on Bluetooth 5 and IEEE 802.15.4: A Replication Study," in *3rd Workshop on Benchmarking Cyber-Physical Systems and Internet of Things (CPS-IoTBench 2020)*, ETH Zurich, Computer Engineering and Networks Laboratory (TIK), 2020.

[102] U. Raza, J. Singh, A. Stanoev, and V. Marot, "Method and system for wireless localisation." `https://patents.google.com/patent/US20230133978A1/en`, May 2022.
Filed US Patent Application, Application Number: 17/453,386. [Last accessed on 10.03.2024].

[103] M. Johansson, "The Hilbert Transform," *Mathematics Master's Thesis. Växjö University, Suecia. Disponible en internet: http://w3. msi. vxu. se/exarb/mj_ex. pdf, consultado el*, vol. 19, 1999.
[Last accessed on 10.03.2024].

[104] D. E. Grzechca, P. Pelczar, and L. Chruszczyk, "Analysis of Object Location Accuracy for iBeacon Technology based on the RSSI Path Loss Model and Fingerprint Map," *International Journal of Electronics and Telecommunications*, 2016.

[105] D. Ordónez-Camacho and E. Cabrera-Goyes, "An Adaptive-bounds Band-Pass Moving-Average Filter to Increase Precision on Distance Estimation from Bluetooth RSSI," in *Proceedings of the International Conference on Information Technology & Systems (ICITS 2018)*, pp. 823–832, Springer, 2018.

[106] MathWorks, "Bluetooth LE Positioning by Using Direction Finding." `https://uk.mathworks.com/help/bluetooth/ug/bluetooth-le-based-positioning-using-direction-finding.html`.
[Last accessed on 10.03.2024].

[107] Z. Hajiakhondi-Meybodi, M. Salimibeni, A. Mohammadi, and K. N. Plataniotis, "Bluetooth Low Energy-based Angle of Arrival Estimation in Presence of Rayleigh Fading," in *2020 IEEE International Conference on Systems, Man, and Cybernetics (SMC)*, pp. 3395–3400, IEEE, 2020.

[108] Nordic Semiconductor, "nRF52833 Product Specification v5.1." `https://infocenter.nordicsemi.com/index.jsp?topic=%2Fps_nrf52833%2Fkeyfeatures_html5.html`, 2021.
[Last accessed on 10.03.2024].

[109] J. Xie, Q. Wang, Y. Wang, and X. Yang, "Efficient Two-Dimensional Direction Finding Algorithm for Rectilinear Sources Under Unknown Mutual Coupling," *Sensors*, vol. 20, no. 7, p. 1914, 2020.

[110] M. Baddeley, U. Raza, A. Stanoev, G. Oikonomou, R. Nejabati, M. Sooriyabandara, and D. Simeonidou, "Atomic-SDN: Is synchronous flooding the solution to software-defined networking in IoT?," *IEEE Access*, vol. 7, pp. 96019–96034, 2019.

[111] OptiTrack, "OptiTrack - Flex13." `https://optitrack.com/products/flex-13/`.
[Last accessed on 10.03.2024].

[112] Silicon Labs, "UG514: Using the Bluetooth Direction Finding Tool Suite." `https://www.silabs.com/documents/public/user-guides/ug514-using-bluetooth-direction-finding-tool-suite.pdf`.
[Last accessed on 10.03.2024].

[113] Silicon Labs, "QSG175: Silicon Labs Direction Finding Solution Quick-Start Guide." `https://www.silabs.com/documents/public/quick-start-guides/qsg175-direction-finding-solution-quick-start-guide.pdf`.

[Last accessed on 10.03.2024].

[114] T. Farnham, "Indoor localisation of iot devices by dynamic radio environment mapping," in *2019 IEEE 5th World Forum on Internet of Things (WF-IoT)*, pp. 340–345, IEEE, 2019.

[115] S. Rinaldi, P. Ferrari, E. Sisinni, A. Depari, and A. Flammini, "An Evaluation of Low-Cost Self-Localization Service Exploiting Angle of Arrival for Industrial Cyber-Physical Systems," in *2021 IEEE AFRICON*, pp. 1–6, IEEE, 2021.

[116] S. He, H. Long, and W. Zhang, "Multi-antenna Array-based AoA Estimation Using Bluetooth Low Energy for Indoor Positioning," in *2021 7th International Conference on Computer and Communications (ICCC)*, pp. 2160–2164, IEEE, 2021.

[117] H. Ye, B. Yang, Z. Long, and C. Dai, "A Method of Indoor Positioning by Signal Fitting and PDDA Algorithm using BLE AoA Device," *IEEE Sensors Journal*, vol. 22, no. 8, pp. 7877–7887, 2022.

[118] B. Großwindhager, M. Rath, J. Kulmer, M. S. Bakr, C. A. Boano, K. Witrisal, and K. Römer, "SALMA: UWB-based Single-Anchor Localization System using Multipath Assistance," in *Proceedings of the 16th ACM Conference on Embedded Networked Sensor Systems*, pp. 132–144, 2018.

[119] V. Navrátil, J. Krška, and F. Vejražka, "Concurrent Bi-directional TDoA Positioning in UWB Network with Free-running Clocks," *IEEE Transactions on Aerospace and Electronic Systems*, vol. 58, no. 5, pp. 4434–4450, 2022.

[120] P. Corbalán and G. P. Picco, "Ultra-wideband concurrent ranging," *ACM Transactions on Sensor Networks (TOSN)*, vol. 16, no. 4, pp. 1–41, 2020.

[121] S. Tan, Y. Ren, J. Yang, and Y. Chen, "Commodity WiFi Sensing in 10 Years: Status, Challenges, and Opportunities," *IEEE Internet of Things Journal*, vol. 9, no. 18, pp. 17832–17843, 2022.

[122] P. Kanakaraja, S. K. Kotamraju, S. Nagulmeera, Y. D. Reddy, and A. Divya, "LoRA based Indoor Localization using LPWAN Gateway and BLE Beacons," in *2022 International Conference on Electronics and Renewable Systems (ICEARS)*, pp. 683–687, IEEE, 2022.

[123] K. Hu, C. Gu, and J. Chen, "LTrack: A LoRa-Based Indoor Tracking System for Mobile Robots," *IEEE Transactions on Vehicular Technology*, vol. 71, no. 4, pp. 4264–4276, 2022.

[124] M. Simka and L. Polak, "On the RSSI-based Indoor Localization employing LoRa in the 2. 4 GHz ISM Band," *Radioengineering*, vol. 31, no. 1, pp. 135–143, 2022.

[125] F. U. Khan, A. N. Mian, and M. T. Mushtaq, "Experimental Testbed Evaluation of Cell Level Indoor Localization Algorithm using Wi-Fi and LoRa Protocols," *Ad Hoc Networks*, vol. 125, p. 102732, 2022.

[126] I. S. B. M. Isa and A. Hanani, "Development of real-time indoor human tracking system using LoRa technology," *International Journal of Electrical and Computer Engineering (IJECE)*, vol. 12, no. 1, pp. 845–852, 2022.

[127] E. Di Lascio, A. Varshney, T. Voigt, and C. Pérez-Penichet, "LocaLight-A Battery-free Passive Localization System Using Visible Light," in *2016 15th ACM/IEEE International Conference on Information Processing in Sensor Networks (IPSN)*, pp. 1–2, IEEE, 2016.

[128] N. Faulkner, F. Alam, M. Legg, and S. Demidenko, "Smart wall: Passive visible light positioning with ambient light only," in *2019 IEEE International Instrumentation and Measurement Technology Conference (I2MTC)*, pp. 1–6, IEEE, 2019.

[129] N. Faulkner, F. Alam, M. Legg, and S. Demidenko, "Watchers on the Wall: Passive Visible Light-Based Positioning and Tracking with Embedded Light-Sensors on the Wall," *IEEE Transactions on Instrumentation and Measurement*, vol. 69, no. 5, pp. 2522–2532, 2019.

[130] D. Konings, N. Faulkner, F. Alam, E. M.-K. Lai, and S. Demidenko, "FieldLight: Device-Free Indoor Human Localization Using Passive Visible Light Positioning and Artificial Potential Fields," *IEEE Sensors Journal*, vol. 20, no. 2, pp. 1054–1066, 2019.

[131] Y. Yang, J. Hao, J. Luo, and S. J. Pan, "CeilingSee: Device-free occupancy inference through lighting infrastructure based LED sensing," in *2017 IEEE International Conference on Pervasive Computing and Communications (PerCom)*, pp. 247–256, IEEE, 2017.

[132] M. Ibrahim, V. Nguyen, S. Rupavatharam, M. Jawahar, M. Gruteser, and R. Howard, "Visible light based activity sensing using ceiling photosensors," in *Proceedings of the 3rd Workshop on Visible Light Communication Systems*, pp. 43–48, 2016.

[133] V. Nguyen, M. Ibrahim, S. Rupavatharam, M. Jawahar, M. Gruteser, and R. Howard, "Eyelight: Light-and-shadow-based occupancy estimation and room activity recognition," in *IEEE INFOCOM 2018-IEEE Conference on Computer Communications*, pp. 351–359, IEEE, 2018.

[134] T. Li, Q. Liu, and X. Zhou, "Practical human sensing in the light," in *Proceedings of the 14th Annual International Conference on Mobile Systems, Applications, and Services*, pp. 71–84, 2016.

[135] L. Li, P. Xie, and J. Wang, "Rainbowlight: Towards low cost ambient light positioning with mobile phones," in *Proceedings of the 24th Annual International Conference on Mobile Computing and Networking*, pp. 445–457, 2018.

[136] Y.-L. Wei, C.-J. Huang, H.-M. Tsai, and K. C.-J. Lin, "Celli: Indoor positioning using polarized sweeping light beams," in *Proceedings of the 15th Annual International Conference on Mobile Systems, Applications, and Services*, pp. 136–147, 2017.

[137] C. Zhang and X. Zhang, "LiTell: robust indoor localization using unmodified light fixtures," in *Proceedings of the 22nd Annual International Conference on Mobile Computing and Networking*, pp. 230–242, 2016.

[138] C. Zhang and X. Zhang, "Pulsar: Towards ubiquitous visible light localization," in *Proceedings of the 23rd Annual International Conference on Mobile Computing and Networking*, pp. 208–221, 2017.

[139] C. Zhang, J. Tabor, J. Zhang, and X. Zhang, "Extending mobile interaction through near-field visible light sensing," in *Proceedings of the 21st Annual International Conference on Mobile Computing and Networking*, pp. 345–357, 2015.

[140] W. Wang, Q. Wang, J. Zhang, and M. Zuniga, "PassiveVLP: Leveraging Smart Lights for Passive Positioning," *ACM Trans. Internet Things*, vol. 1, no. 1, 2020.

[141] K. Majeed and S. Hranilovic, "Performance Bounds on Passive Indoor Positioning Using Visible Light," *Journal of Lightwave Technology*, vol. 38, no. 8, pp. 2190–2200, 2020.

[142] T. Li, C. An, Z. Tian, A. T. Campbell, and X. Zhou, "Human sensing using visible light communication," in *Proceedings of the 21st Annual International Conference on Mobile Computing and Networking*, pp. 331–344, 2015.

[143] C. Zhang and X. Zhang, "Visible Light Localization Using Conventional Light Fixtures and Smartphones," *IEEE Transactions on Mobile Computing*, vol. 18, no. 12, pp. 2968–2983, 2019.

[144] H. Zhang, A. Zhou, D. Xu, S. Xu, X. Zhang, and H. Ma, "Learning to recognize unmodified lights with invisible features," *Proceedings of the ACM on Interactive, Mobile, Wearable and Ubiquitous Technologies*, vol. 3, no. 2, pp. 1–23, 2019.

[145] S. Zhu and X. Zhang, "Enabling high-precision visible light localization in today's buildings," in *Proceedings of the 15th Annual International Conference on Mobile Systems, Applications, and Services*, pp. 96–108, 2017.

[146] S. Shao, A. Salustri, A. Khreishah, C. Xu, and S. Ma, "R-VLCP: Channel modeling and simulation in retroreflective visible light communication and positioning systems," *IEEE Internet of Things Journal*, 2023.

[147] S. Ma, Q. Liu, and P. C.-Y. Sheu, "Foglight: Visible light-enabled indoor localization system for low-power IoT devices," *IEEE Internet of Things Journal*, vol. 5, no. 1, pp. 175–185, 2017.

[148] J. Hu, Y. Wang, H. Jia, W. Hu, M. Hassan, A. Uddin, B. Kusy, and M. Youssef, "Passive light spectral indoor localization," in *Proceedings of the 28th Annual International Conference on Mobile Computing And Networking*, pp. 832–834, 2022.

[149] J. Hu, Y. Wang, H. Jia, W. Hu, M. Hassan, B. Kusy, A. Uddin, and M. Youssef, "Iris: Passive Visible Light Positioning Using Light Spectral Information," *Proceedings of the ACM on Interactive, Mobile, Wearable and Ubiquitous Technologies*, vol. 7, no. 3, pp. 1–27, 2023.

[150] F. Zafari, A. Gkelias, and K. K. Leung, "A survey of indoor localization systems and technologies," *IEEE Communications Surveys & Tutorials*, vol. 21, no. 3, pp. 2568–2599, 2019.

[151] Y. Zhuang, C. Zhang, J. Huai, Y. Li, L. Chen, and R. Chen, "Bluetooth localization technology: Principles, applications, and future trends," *IEEE Internet of Things Journal*, vol. 9, no. 23, pp. 23506–23524, 2022.

[152] J. Singh and P. Li, "Method and system for optical localisation," 2023.
Filed US Patent Application, Application Number: 18/352,987.

[153] PyTorch, "SELU." `https://pytorch.org/docs/stable/generated/torch.nn.SELU.html`, Nov. 2023.
[Last accessed on 10.03.2024].

[154] F. Mahdavi, H. Zayyani, and R. Rajabi, "RSS localization using an optimized fusion of two deep neural networks," *IEEE Sensors Letters*, vol. 5, no. 12, pp. 1–4, 2021.

[155] Albraheem, Lamya and Alawad, Sarah, "A Hybrid Indoor Positioning System Based on Visible Light Communication and Bluetooth RSS Trilateration," *Sensors*, vol. 23, no. 16, p. 7199, 2023.

[156] S. G. Leitch, Q. Z. Ahmed, W. B. Abbas, M. Hafeez, P. I. Laziridis, P. Sureephong, and T. Alade, "On Indoor Localization Using WiFi, BLE, UWB, and IMU Technologies," *Sensors*, vol. 23, no. 20, p. 8598, 2023.

[157] A. Madahian, P. A. Ardakani, J. Abouei, A. Mirvakili, A. Mohammadi, and V. Koomson, "A Hybrid VLC/RF Parking Automation System," *IEEE Access*, 2023.

[158] A. Alizai, M. R. Mousavi, S. Ludwig, and D. Aschenbrenner, "Heterogeneous Communication Networks and Localization for Industry 4.0 Applications in Small and Medium-Sized Enterprises: A Systematic Literature Review," *Procedia CIRP*, vol. 120, pp. 308–313, 2023.

[159] Affan, Affan and Asif, Hafiz M and Tarhuni, Naser, "Machine-Learning-Based Indoor Localization under Shadowing Condition for P-NOMA VLC Systems," *Sensors*, vol. 23, no. 11, p. 5319, 2023.

[160] P. Li, H. Cui, A. Khan, U. Raza, R. Piechocki, A. Doufexi, and T. Farnham, "Wireless Localisation in WiFi using Novel Deep Architectures," in *Proc. of the 25th International Conference on Pattern Recognition (ICPR)*, pp. 6251–6258, 2021.

[161] P. Li, H. Cui, A. Khan, U. Raza, R. Piechocki, A. Doufexi, and T. Farnham, "Deep Transfer Learning for WiFi Localization," in *Proc. of the IEEE RadarConf Conf.*, pp. 1–5, 2021.

[162] M. I. AlHajri, N. T. Ali, and R. M. Shubair, "Indoor Localization for IoT Using Adaptive Feature Selection: A Cascaded Machine Learning Approach," *IEEE Antennas and Wireless Propagation Letters*, vol. 18, no. 11, pp. 2306–2310, 2019.

[163] K. He, X. Zhang, S. Ren, and J. Sun, "Deep Residual Learning for Image Recognition," in *Proceedings of the IEEE conference on computer vision and pattern recognition*, pp. 770–778, 2016.

[164] D. Silver *et al.*, "Mastering Chess and Shogi by Self-play with a General Reinforcement Learning Algorithm," *arXiv preprint 1712.01815*, 2017.

[165] OpenAI, "ChatGPT: Optimizing Language Models for Dialogue." `https://openai.com/blog/chatgpt/`, 2023.
[Last accessed on 10.03.2024].

[166] H. Wen, Y. Li, Z. Zhang, S. Jiang, X. Ye, Y. Ouyang, Y. Zhang, and Y. Liu, "AdaptiveNet: Post-deployment Neural Architecture Adaptation for Diverse Edge Environments," in *Proc. of the 29th MobiCom*, pp. 1–17, 2023.

[167] F. Foukalas, P. Pop, F. Theoleyre, C. A. Boano, and C. Buratti, "Dependable wireless industrial iot networks: Recent advances and open challenges," in *2019 IEEE European Test Symposium (ETS)*, pp. 1–10, IEEE, 2019.

[168] E. C. Strinati and S. Barbarossa, "6G networks: Beyond Shannon towards semantic and goal-oriented communications," *Computer Networks*, vol. 190, p. 107930, 2021.

[169] E. Calvanese Strinati and S. Barbarossa, "6G networks: Beyond Shannon Towards Semantic and Goal-oriented Communications," *Computer Networks*, vol. 190, p. 107930, 2021.

[170] Texas Instruments, "xWR1843 Evaluation Module Single-Chip mmWave Sensing Solution – User's Guide SPRUIM4B." `https://www.ti.com/lit/ug/spruim4b/spruim4b.pdf?ts=1710032740624&ref_url=https%253A%252F%252Fwww.google.com%252F`, 2020.
[Last accessed on 10.03.2024].

[171] P. Zhao, C. X. Lu, J. Wang, C. Chen, W. Wang, N. Trigoni, and A. Markham, "mID: Tracking and Identifying People with Millimeter Wave Radar," in *2019 15th International Conference on Distributed Computing in Sensor Systems (DCOSS)*, pp. 33–40, IEEE, 2019.

[172] H. Cui and N. Dahnoun, "High Precision Human Detection and Tracking Using Millimeter-wave Radars," *IEEE Aerospace and Electronic Systems Magazine*, vol. 36, no. 1, pp. 22–32, 2021.

[173] C. Wu, F. Zhang, B. Wang, and K. R. Liu, "mmTrack: Passive multi-person localization using commodity millimeter wave radio," in *IEEE INFOCOM 2020-IEEE Conference on Computer Communications*, pp. 2400–2409, IEEE, 2020.

[174] P. Balasubramanian and B. Balasubramanian, "Multi-technology based Indoor Localization using UWB and BLE Signals," *Journal of Ambient Intelligence and Humanized Computing*, vol. 12, no. 2, pp. 1247–1260, 2021.

[175] T. Istomin, E. Leoni, D. Molteni, A. L. Murphy, G. P. Picco, and M. Griva, "Janus: Efficient and Accurate Dual-radio Social Contact Detection," *ACM IMWUT*, vol. 5, no. 4, 2021.

[176] D. Gündüz *et al.*, "Beyond Transmitting Bits: Context, Semantics, and Task-Oriented Communications," *IEEE JSAC*, vol. 41, no. 1, pp. 5–41, 2023.

[177] D. B. Kurka and D. Gündüz, "DeepJSCC-f: Deep joint source-channel coding of images with feedback," *IEEE Journal on Selected Areas in Information Theory*, vol. 1, no. 1, pp. 178–193, 2020.

[178] T.-Y. Tung, D. B. Kurka, M. Jankowski, and D. Gündüz, "Deepjscc-q: Channel input constrained deep joint source-channel coding," in *ICC 2022-IEEE International Conference on Communications*, pp. 3880–3885, IEEE, 2022.

[179] E. Erdemir *et al.*, "Generative Joint Source-Channel Coding for Semantic Image Transmission," *IEEE Journal on Selected Areas in Communications*, vol. 41, no. 8, pp. 2645–2657, 2023.

[180] P. Li and A. Aijaz, "Open RAN meets Semantic Communications: A Synergistic Match for Open, Intelligent, and Knowledge-Driven 6G," *arXiv preprint 2310.09951*, 2023.

[181] H. Krim and M. Viberg, "Two decades of array signal processing research: the parametric approach," *IEEE signal processing magazine*, vol. 13, no. 4, pp. 67–94, 1996.

[182] S. Rao, "MIMO Radar." https://www.ti.com/lit/an/swra554a/swra554a.pdf?ts=1709967487283&ref_url=https%253A%252F%252Fdev.ti.com%252F, 2017. [Last accessed on 10.03.2024].

[183] D. P. Kingma and J. Ba, "Adam: A Method for Stochastic Optimization," *arXiv preprint 1412.6980*, 2014.

[184] D. P. Kingma and M. Welling, "Auto-encoding Variational Bayes," *arXiv preprint arXiv:1312.6114*, 2013.

[185] S. Odaibo, "Tutorial: Deriving the Standard Variational Autoencoder (VAE) Loss Function," *arXiv preprint arXiv:1907.08956*, 2019.

[186] P. Li, X. Wang, R. Piechocki, S. Kapoor, A. Doufexi, and A. Parekh, "Variational Autoencoder Assisted Neural Network Likelihood RSRP Prediction Model," in *2022 IEEE 33rd Annual International Symposium on Personal, Indoor and Mobile Radio Communications (PIMRC)*, pp. 554–559, IEEE, 2022.

[187] Silicon Labs, "AN1297: Custom Direction-Finding Solutions using the Silicon Labs Bluetooth Stack." https://www.silabs.com/documents/public/application-notes/an1297-custom-direction-finding-solutions-silicon-labs-bluetooth.pdf. [Last accessed on 10.03.2024].

[188] S. Labs, "Application Development with RTL Library." https://www.silabs.com/documents/public/application-notes/an1296-application-development-with-rtl-library.pdf. [Last accessed on 10.03.2024].

[189] Silicon Labs, "SLTB010A EFR32BG22 Thunderboard Kit." https://www.silabs.com/development-tools/thunderboard/thunderboard-bg22-kit. [Last accessed on 10.03.2024].

[190] A. Reuther, P. Michaleas, M. Jones, V. Gadepally, S. Samsi, and J. Kepner, "Survey of machine learning accelerators," in *Proc. of IEEE HPEC 2020*, pp. 1–12, IEEE, 2020.

[191] NVIDIA, "Advanced AI Embedded Systems." https://www.nvidia.com/en-gb/autonomous-machines/embedded-systems/, 2023.

[Last accessed on 10.03.2024].

[192] NVDIA, "Advanced AI Embedded Systems." https://www.nvidia.com/en-gb/autonomous-machines/embedded-systems/.
[Last accessed on 10.03.2024].

[193] J. Singh, M. Baddeley, C. A. Boano, A. Stanoev, Z. Chai, T. Farnham, Q. Wang, and U. Raza, "BLoB: Beating-based Localization for Single-antenna BLE Devices," in *Proceedings of the* 20^{th} *International Conference on Embedded Wireless Systems and Networks (EWSN)*, ACM, Sept. 2023.

[194] M. Alloulah and H. Huang, "Future millimeter-wave indoor systems: A blueprint for joint communication and sensing," *Computer*, vol. 52, no. 7, pp. 16–24, 2019.

[195] N. Paulino, L. M. Pessoa, A. Branquinho, and E. Gonçalves, "Design and Experimental Evaluation of a Bluetooth 5.1 Antenna Array for Angle-of-Arrival Estimation," in *2022 13th International Symposium on Communication Systems, Networks and Digital Signal Processing (CSNDSP)*, pp. 625–630, IEEE, 2022.

[196] X. Liu, P. Li, and Z. Zhu, "Bayesian optimisation-Assisted Neural Network Training Technique for Radio Localisation," in *2022 IEEE 95th Vehicular Technology Conference:(VTC2022-Spring)*, pp. 1–5, IEEE, 2022.

[197] Wikipedia, "Analytic signal." https://en.wikipedia.org/wiki/Analytic_signal, 2023.
[Last accessed on 10.03.2024].